DOI:10.15774/PPKE.ITK.2022.001

Systematic validation of detailed models of hippocampal neurons based on electrophysiological data

PhD Dissertation

Sára Sáray

Supervisors: Dr. Szabolcs Káli, Dr. Tamás Freund

Pázmány Péter Catholic University

Faculty of Information Technology and Bionics

Roska Tamás Doctoral School of Sciences and Technology

Budapest, 2021

DOI:10.15774/PPKE.ITK.2022.001

DOI:10.15774/PPKE.ITK.2022.001

Contents

Abbreviations 3
1. Introduction 4
1.1. Motivation 4
1.2. Overview of the thesis 6
2. Background 6
2.1. Neurobiological concepts 6
2.1.1. Structure and function of the hippocampus 6
2.1.2. The CA1 pyramidal cell 11
2.2. Multi-compartmental modeling of neurons 27
2.3. The NEURON simulation environment 30
2.4. Hippocampal CA1 pyramidal cell models in the literature 30
3. Methods 31
3.1 Implementation of HippoUnit 31
3.2 Implementation of the tests of HippoUnit 33
3.2.1 The Somatic Features Test 33
3.2.2 The Depolarization Block Test 36
3.2.3 The Back-propagating AP Test 38
3.2.4 The PSP Attenuation Test 39
3.2.5 The Oblique Integration Test 40
3.3 Parallel computing 42
3.4 Classifying the apical sections of pyramidal cells 43
3.5 Models from literature 44
4. Results 45
4.1 The HippoUnit validation suite 45
4.2 Comparison of the behavior of rat hippocampal CA1 pyramidal cell models selected from the literature 47
4.2.1 Somatic Features Test 49
4.2.2 Depolarization Block Test 56
4.2.3 Back-propagating Action Potential Test 58
4.2.4 PSP Attenuation Test 61
4.2.5 Oblique Integration Test 62
4.2.6 Overall characterization and model comparison based on all tests of HippoUnit 66
4.3 Application of HippoUnit to models built using automated parameter optimization within the Human Brain Project 68

DOI:10.15774/PPKE.ITK.2022.001

4.4 Integration of HippoUnit into the Validation Framework and the Brain Simulation Platform of the Human Brain Project 71
4.5 Extending HippoUnit for other important cell types of the hippocampus 73
4.5.1 Back-propagating AP Test Basket Cell 74
4.5.2 AP Propagation Axon Test Basket Cell 75
4.5.3 Back-propagating AP Test CA3 PC 76
5 Discussion 78
5.1 Applications of the HippoUnit test suite 78
5.2 Interpreting the results of HippoUnit 81
5.3 Uniform model formats reduce the costs of validation 82
5.4 Extensibility of HippoUnit 83
5.5 Generalization possibilities of the tests of HippoUnit 84
6 Summary 86
7 The Author's publications 87
7.1 Publications related to the theses: 87
7.1.1 Journal papers: 87
7.1.2 Posters at international conferences: 87
7.1.3 Annual Proceedings of the PPCU Faculty of Information technology and Bionics Doctoral School: 88
7.1.4 Workshop presentation 89
7.2 Publications not related to the theses 89
7.2.1 Conference papers: 89
7.2.2 Posters: 89
Acknowledgements 89
List of Figures 90
List of Tables 95
Bibliography 95
Appendix 107
Example of running the SomaticFeaturesTest of HippoUnit using a Jupyter notebook 107

DOI:10.15774/PPKE.ITK.2022.001

Abbreviations

AHP - after-hyperpolarization

AIS - axon initial segment

AMPA - α-amino-3-hydroxy-5-methyl-4-isoxazolepropionic acid

AP - action potential

bAP - back-propagating action potential

BSP - branch strength potentiation

DG - dentate gyrus

EC - entorhinal cortex

EEG - Electroencephalography

EPSC - excitatory postsynaptic current

EPSP - excitatory postsynaptic potential

GABA - gamma-aminobutyric acid

GUI - graphical user interface

HBP - Human Brain Project

ISI - interspike interval

LEC - lateral entorhinal cortex

LTP - long term potentiation

mACH - muscarinic acetylcholine

MEC - medial entorhinal cortex

NMDA - N-methyl-D-aspartic acid

PC - pyramidal cell

PP - perforant path

PSP - postsynaptic potential

SC - Schaffer-collateral

SD - standard deviation

SPW - sharp wave

SUB - subiculum

Vm - membrane potential

DOI:10.15774/PPKE.ITK.2022.001

1. Introduction

1.1. Motivation

The construction and simulation of anatomically and biophysically detailed models is becoming a standard tool in neuroscience [1]. Such models, which typically employ the compartmental modeling approach and a Hodgkin-Huxley-type description of voltage-gated ion channels, are capable of providing fairly accurate models of single neurons [2]–[10] and (when complemented by appropriate models of synaptic interactions) even large-scale circuits [11]–[14]. However, building such detailed multi-compartmental models of neurons requires setting a large number of parameters (such as the densities of various ion channels in multiple neuronal compartments) that are often not directly constrained by the available experimental data. These parameters are typically tuned (either manually or using automated parameter-search methods [9], [15]–[17]) until the simulated physiological behavior of the model matches some pre-defined set of experimental observations.

For an increasing number of cell types, the available experimental data already provide diverse constraints on the expected physiological behavior of the neuron under a variety of conditions. Based on various (typically small) subsets of the available constraints, a large number of different models of several cell types have been developed to investigate diverse aspects of single-cell behavior, and for inclusion in realistic circuit models. As an example, there are currently 136 different models related to the hippocampal CA1 pyramidal cell (PC) in the ModelDB database [18]. However, even though these models are publicly available, it is still technically challenging to verify their behavior beyond the examples explicitly included with the model, and especially to test their behavior outside the context of the original study, or to compare it with the behavior of other models. This sparsity of information about the performance of detailed models may also be one reason why model re-use in the community is relatively limited, which decreases the chance of spotting errors in modeling studies, and may lead to an unnecessary replication of effort. In addition, even when models are re-used, they are often altered to fit a different subset of the available experimental data, and they may lose their ability to capture the behaviors that were used to constrain the original model. This phenomenon (whereby introducing new features breaks previously correct behavior) is known as a "regression" in software development, and is typically avoided by regularly applying a set of tests that comprehensively verify the correct behavior of the software under various circumstances. Such comprehensive checks are not routinely performed when neural models are developed – and this may be one of the reasons why the development of consensus (community) models, which would aim to capture a wide range of experimental observations by integrating diverse efforts, has rarely been attempted in neuroscience.

A collaborative approach to modeling, and even a systematic comparison of existing models built in different laboratories requires the development of a comprehensive validation suite, a set of automated tests that quantitatively compare various aspects of model behavior with the corresponding experimental data. Such validation suites enable all modeling groups to evaluate their existing and newly developed models according to the same set of well-defined criteria, thus facilitating model comparison and providing an objective measure of progress in matching relevant experimental observations. Applying automated tests also allows researchers to learn more about models published by other groups (beyond the results included in the papers) with relatively little effort, thus facilitating optimal model re-use and co-operative model development. In addition, systematic, automated testing is expected to avoid regressions, aid the identification of problematic aspects of model behavior, and speed up model development in general by allowing researchers to easily evaluate models in relation to the relevant experimental data after every iteration of model adjustment. Finally, a comprehensive evaluation of model behavior appears to be critical for models that are then expected to provide useful predictions in a new context. A prime example of this is detailed single cell models included in network models, where diverse aspects of cellular function such as synaptic integration, intracellular signal propagation, spike generation and adaptation mechanisms all contribute to the input-output function of the neuron in the context of an active network. By comparing multiple different aspects of the behavior of the single cell model with experimental data, one can increase the chance of having a model that also behaves correctly within the network. The technical framework for developing automated test suites for models already exists [19], and is currently used by several groups to create a variety of tests for models of neural structure and function at different scales [20]–[24]. In the current study, our goal was to develop a validation suite for the physiological behavior of one of the most studied cell types of the mammalian brain, the pyramidal cell in area CA1 of the rat hippocampus.

CA1 pyramidal neurons display a large repertoire of nonlinear responses in all of their compartments (including the soma, axon, and various functionally distinct parts of the dendritic tree), which are experimentally well-characterized. In particular, there are detailed quantitative results available on the subthreshold and spiking voltage response to somatic current injections [3], [25]; on the properties of the action potentials back-propagating from the soma into the dendrites [26]–[28], which is a basic measure of dendritic excitability; and on the characteristics of the spread [29] and non-linear integration of synaptically evoked signals in the dendrites, including the conditions necessary for the generation of dendritic spikes [30]–[33].

The test suite that we have developed allows the quantitative comparison of the behavior of anatomically and biophysically detailed models of rat CA1 pyramidal neurons with experimental data in all of these domains.

DOI:10.15774/PPKE.ITK.2022.001

1.2. Overview of the thesis

In the Theoretical background chapter, the most important properties and functions of the hippocampus are briefly discussed, and the characteristic properties and behavior of the CA1 pyramidal cell are described in more detail by reviewing experimental observations available in the literature. The most basic concepts of the computational modeling of neurons are also concisely introduced.

The Methods chapter describes the implementation of the HippoUnit validation suite.

In the Results chapter we show how we used this test suite to systematically compare existing models from six prominent publications from different laboratories. We then show an example of how the tests have been applied to aid the development of new models in the context of the European Human Brain Project (HBP). We describe the integration of our test suite into the general validation framework developed in the HBP. Finally, we show how we extended the test suite for other cell types of the hippocampus, by implementing new tests based on experimental data characterizing the given cell types.

The Discussion contains further interpretation of the results and discussion of several open questions. Finally, in the Summary chapter the results are summarized in the form of thesis points by listing the new scientific contributions of the author.

2. Background

2.1. Neurobiological concepts

2.1.1. Structure and function of the hippocampus

The hippocampus starts in the dorsal-septal part of the cerebral cortex, from where it traverses to the ventral-temporal region of the brain. It got its name from its shape reminiscent of a seahorse (hippocampus - from ancient Greek). As its shape reminds others of the ram's horns, the subregions of the hippocampus (CA1, CA2, CA3) are named from the horns of Ammon (an Egyptian god) as Cornu Ammonis [34]. The hippocampal formation consists of the dentate gyrus (DG), the hippocampus proper (whose sub-fields are the CA3, CA2 and CA1 regions), the subicular complex (containing the subiculum (SUB), the pre-subiculum and the para-subiculum) and the entorhinal cortex (medial and lateral) [35].

The characteristic neural circuit within the hippocampus is referred to as the tri-synaptic loop. The first stage of it are the granule cells of the dentate gyrus that receive sensory information of multiple modalities from the layer II of the entorhinal cortex (EC). The mossy fibers, that are the axons of the granule cells, innervate the proximal dendrites of the pyramidal

DOI:10.15774/PPKE.ITK.2022.001

cells in the CA3 region, which is the second stage of the tri-synaptic loop. In addition, CA3 pyramidal cells receive input directly from layer II of the entorhinal cortex through the so-called perforant path. The axons of CA3 pyramidal cells richly innervate the local cells of the same region by giving rise to recurrent axon collaterals. Those axonal fibers that leave the CA3 region form the Schaffer collaterals and project to the CA1 subfield, which is the third stage of the tri-synaptic loop. In addition to the Schaffer collateral inputs, CA1 pyramidal cells are also innervated by the pyramidal cells of layer III of the entorhinal cortex via the perforant path. The CA1 region is the main output structure of the hippocampus. It projects back to the deep layers of the same column of the entorhinal cortex from where it gets input. The axons of the CA1 pyramidal cells also convey information to the subiculum and they target other limbic cortical areas, the lateral septum, the nucleus accumbens, and the olfactory bulb [36].

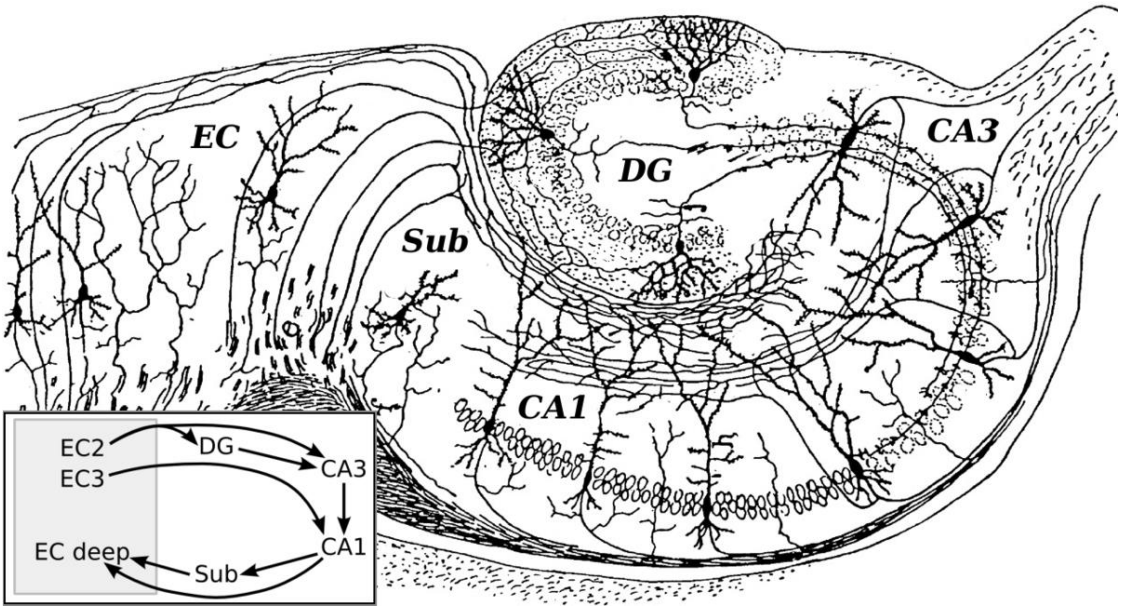

Figure 2.1: Structure of the hippocampal formation. Original drawing of Santiago Ramón y Cajal (1911) of the subregions of the hippocampal formation showing the main cell types and axonal pathways. Inset shows the flow of information in the hippocampus.

As it can be seen from Figure 2.1, the hippocampus proper (from now on referred to as the hippocampus) has a laminar organization. The most conspicuous layer is the pyramidal cell layer (stratum pyramidale) where the somas of the pyramidal cells line up. Below this layer there is the stratum oriens, which is bounded by the alveus that contains fibers entering and leaving the hippocampus. The supra-pyramidal region is the stratum radiatum, where the Schaffer collaterals and their connections are located. The uppermost layer is called the stratum lacunosum-moleculare, that hosts the perforant path fibers [37].

Besides the glutamatergic excitatory principal cells (the pyramidal cells), there are several mostly GABAergic inhibitory interneurons in the hippocampus that contribute to its

DOI:10.15774/PPKE.ITK.2022.001

function. Interneurons can be classified by their morphological, neurochemical or electrophysiological properties.

Among those interneurons that innervate pyramidal cells, two different types can be distinguished morphologically: those that terminate on the perisomatic region of the pyramidal cells and those that terminate on their dendrites. One of the morphological types of the perisomatic inhibitory cells is the basket cell, whose axons terminate on the soma of the pyramidal cells. The other is called the chandelier or axo-axonic cell, and it innervates the axon initial segment (AIS) of the principal cells. Both have dendritic trees that overlap with that of the pyramidal cells, therefore they most probably receive inputs from the same sources as them [36].

Dendritic inhibitory neurons show much more variability in their morphology, axonal and dendritic distribution. The axons of O-LM cells project to the stratum lacunosum-moleculare, thus innervating the same dendrites of the pyramidal cells as the entorhinal afferents. Their dendrites in the CA1 region are limited to the stratum oriens. Bistratified and trilaminar cells are other examples of dendritic inhibitory cells. They innervate the dendrites of pyramidal cells in the strata radiatum and oriens. The location of their dendritic tree suggests that they receive inputs from the Schaffer collaterals and from local recurrent collaterals, which let them function in both feed-forward and feed-back mode. Besides the interneurons that innervate the principal cells, there are other types that terminate on other interneurons [36].

Most of the hippocampal interneurons use GABA as their neurotransmitters, and they often express different neuropeptides such as SOM, CCK, VIP, NPY, etc. - that function as co-transmitters or modulators -, or calcium-binding proteins (PV, BC, CR). This property can be used to further classify and study these cells. For example, it seems that most PV positive GABAergic cells in the hippocampus are basket and chandelier cells, but interestingly not all basket and chandelier cells express PV [36]. Hippocampal interneurons are still under investigation and it is still not completely clear how their neurochemical and morphological properties relate to each other, and how these influence their function.

The hippocampus is known to play a crucial role in learning and memory. A famous early piece of evidence for this is the case of patient H.M., who had his hippocampus resected during a bilateral temporal lobectomy in the 1950s to treat his epilepsy. After the operation he was no longer able to learn new things or create new memories, and he also lost recent memories about events that happened shortly (a few years) before he got into the hospital. However, his early memories remained intact [38]. Magnetic Resonance Imaging studies [39] and postmortem examination of H.M's brain [40] provided more precise insight into the extent of the lesion and the structures affected. According to these results, the medial temporal polar cortex, most of the amygdaloid complex, all of the entorhinal cortex and most of the hippocampus were removed. Moreover, although parts of the posterior hippocampus remained spared (that contained visible

DOI:10.15774/PPKE.ITK.2022.001

portions of the CA regions, the dentate gyrus, and the subiculum), these remained mostly deafferented because of the removal of the whole EC, and thus they probably lost their functionality. The severity of his memory impairment (compared to patients having more selective hippocampal lesions) indicates that his condition was maybe caused by the inclusion of the adjacent cortical structures in the resection in addition to the hippocampus [39], especially the ablation of the entorhinal cortex, that conveys neocortical input to the hippocampus [39], [40]. His case shows that the hippocampus plays a role in memory formation and consolidation, but memory is stored mostly in the much bigger neocortex.

Due to its significant role in cognitive functions, the hippocampus receives much attention in brain research. Animal experiments provide an opportunity to study its structure and function more comprehensively and from different perspectives. Therefore, most of our knowledge on the anatomy, physiology and function of the hippocampus, and its different regions and cell types are mainly based on behavioral, lesion, and electrophysiological experiments on different rodents such as rats and mice.

It has been observed that depending on the actions carried out by the animal, two different activity patterns of the field potential (recorded by extracellular microelectrodes) of the hippocampus can be observed. During exploration of the environment and paradoxical sleep the characteristic pattern is the theta oscillation (4-8 Hz), while during slow wave sleep, awake immobility (resting state), drinking and eating, irregular sharp waves (SPWs) are present in the hippocampal recordings.

According to the two-stage memory model, both states (theta and SPWs) are essential for memory formation [41]. During the theta phase the granule cells of the dentate gyrus fire rhythmically and with high frequency, whereas the pyramidal cells of the CA regions in general show low frequency firing. During exploration, depending on the occurring sensory events, the afferents from entorhinal cortex activate subgroups of granule cells whose high frequency outputs converge on CA3 pyramidal cells that also drive some CA1 pyramidal cells. The activity of CA3 pyramidal cells is suppressed by inhibitory interneurons that are also excited by subcortical input. This prevents the highly synchronous firing of a large set of CA3 PC-s that causes the SPWs to emerge. However, this high frequency input from granule cells is strong enough to trigger a weak and transient synaptic potentiation, which is already a form of a memory trace, even if it is unstable.

At the termination of the theta phase, the CA3 pyramidal cells are temporarily released from the subcortical inhibition, and the previously potentiated cells are able to generate high frequency bursts which, thanks to the recurrent axon collaterals characterizing this subfield, synchronously activate a large number of CA3 PCs, those that are already potentiated and thus carry information. The highly synchronous population bursts, the SPWs, create the appropriate conditions for long term potentiation (LTP) to occur in CA3 PCs and in the Schaffer collateral

synapses of them terminating on CA1 PCs. According to Hebb, long term potentiation (increase in synaptic activity) occurs during the coincident activation of the postsynaptic cell and the correlated activity of a number of its converging afferents. In the CA1 region it generates a sufficiently large depolarization to relieve the Mg^{2+} block of the glutamate activated NMDA channel to let Ca^{2+} enter the postsynaptic cell and trigger Ca^{2+} dependent machineries that strengthen the synapses in different ways [41].

As the CA1 region relays back to the entorhinal cortex, it is suggested that due to the intrahippocampal SPWs, large depolarization is induced in the neurons of the entorhinal cortex sufficient to induce LTP to potentiate the neocortical representation of the memory traces. When the animal is exposed to the same events (e.g., goes to the same part of the maze), the same subsets of the neurons will be reactivated, the memory will be recalled and further potentiated [41].

Another well-known function of the hippocampus is spatial navigation and the representation of the spatial environment in the brain. Already in the 1970s, it was shown that there are cells in the CA regions of the hippocampus that fire only when the animal passes, stays or points in the direction of a particular location of its environment. Therefore, it was suggested that the hippocampus functions as a spatial map [42]. These pyramidal cells are named as place cells and the area where a given cell is most likely to fire action potentials is called its place field. Different place cells fire at different locations in space, representing the entire environment by the activity of the cell population. When the animal is exposed to a new environment, the same pyramidal cells will function as place cells, but the relationship of the developing place fields is different and unpredictable [43].

It has been shown more recently that the entorhinal cortex contains cells that exhibit spatial firing as well. These are called grid cells as, unlike the place cells of the hippocampus (that usually fire at a single location), the firing fields of a grid cell form a triangular matrix that cover the entire environment of the animal. Unlike hippocampal place cells, grid cells and their representation of space remains constant in a new environment. As the pyramidal cells of the hippocampal CA subregions receive numerous afferents from the entorhinal cortex, it is supposed that place field formation may be the result of the summation of convergent inputs arriving from the grid cells to a place cell, but this proposal has not been completely proven [43].

There are several further theories about the function and formation of hippocampal place cells and grid cells of the entorhinal cortex, and their firing fields, but the exact cellular mechanisms are still unknown and under extensive investigation.

DOI:10.15774/PPKE.ITK.2022.001

2.1.2. The CA1 pyramidal cell

As the focus of this dissertation is the validation of CA1 pyramidal cell models, in the following sections the main anatomical and electrophysiological characteristics of this cell type will be described. The goal of this chapter is to review the properties of this cell type that should or could be reproduced by a realistic CA1 pyramidal cell model, and how these properties contribute to the functions of the hippocampus described above. The most important physiological properties of the hippocampal CA1 pyramidal neuron are also summarized in Table 2.1.

As the models investigated in this study were built and tested based on data from *in vitro* experiments in the rat hippocampus, I mainly focus on experimental observations yielded the same way.

2.1.2.1. Morphology and synaptic inputs of CA1 pyramidal cells

The soma of this cell type has pyramidal shape from which two distinct types of dendrite arise: the basal dendrites branch from the base of the pyramid, while the apical dendritic tree originates from the apex. The basal dendrites are located in the stratum oriens, and consist of 2 to 8 dendritic trees, which then branch several more times to form 1 to 20 terminals each. As most branching occur close to the soma, intermediate segments are short, while terminal segments make up 86 % of the total length of the basal dendritic tree. Basal dendrites that have more branches are thicker, but the terminal branches have similar diameter [44].

From the apex of the pyramidal shaped soma the main apical dendrite (trunk) originates which is even thicker than the stem basal dendritic branches. In most CA1 pyramidal cells the trunk is a single dendritic branch traversing the stratum radiatum, but in some cases it bifurcates within the stratum radiatum to form 2 branches. In each case the trunk gives rise to 9-30 trees of radial oblique dendrites in the stratum radiatum. Similarly to basal dendrites, branching of the oblique trees mostly occur close to the soma, therefore the intermediate branches (21 ± 18 μm) are much shorter than the terminal ones (102 ± 45 μm – around 90% of the total length of oblique dendrites); however, the number of terminal branches originating from a single stem oblique dendrite is relatively small, and many of the oblique trees have no branching. In the stratum lacunosum moleculare the trunk divides to form the apical tuft. In the tuft the length of the terminal branches are shorter (only around 66 % of the overall tuft length) relative to the basal and oblique dendrites, consequently the intermediate segments are longer. From the overall dendritic length of CA1 pyramidal cells (10400 to 13300 μm), 47% are the basal, 35% are the trunk and oblique dendrites together, and 19% is the tuft [44].

The dendrites of the CA1 pyramidal cell are covered by dendritic spines, which typically receive excitatory synaptic inputs. Their density varies on the dendritic tree. Terminal oblique

DOI:10.15774/PPKE.ITK.2022.001

and basal dendrites are rich in spines while the intermediate ones are very sparsely covered by spines [45]. The proximal trunk has almost no spines at all, and then the density of the spines increases with distance [46], beginning at around 103 μm from the soma (average: 7.5 ± 1.65 spines / μm). Linear spine density (spine number/μm) seems to be in correlation with branch diameter: thicker dendritic branches have more spines per μm. An exception is the tuft dendrites, which are mostly thicker than the oblique or basal dendrites, but have a smaller number of spines (1.4 ± 0.72 spines / μm). On the basal and oblique dendrites the spine densities are 2.40 ± 0.38 spines / μm and 3.2 ± 0.7 spines / μm, respectively [45].

Distal stratum oriens (basal) and stratum radiatium (oblique, trunk) dendrites receive excitatory inputs on the spines, while inhibitory inputs arrive at the dendritic shaft. Only around 3% of distal inputs are inhibitory while at proximal regions this proportion is 70 to 100 %. The soma and axon initial segment receive only inhibitory inputs. For the stratum lacunosum-moleculare (tuft) dendrites the inhibitory inputs have a ratio of 14 to 17%, and they also arrive at dendritic spines, while excitatory inputs also innervate the dendritic shaft [46].

Distal stratum lacunosum-moleculare dendrites are innervated by the perforant path (PP) from layer III of the entorhinal cortex and get input from subcortical regions such as the nucleus reuniens thalami and the amygdala. Apical dendrites in the stratum radiatum and basal dendrites in the stratum oriens receive inputs from the CA3 region of the hippocampus via the Schaffer collaterals (SC) [46], [47]. Recurrent collaterals from CA1 pyramidal cells innervate the basal dendrites in stratum oriens [46]. These excitatory synapses have AMPA and NMDA receptor components, but their ratio varies even in specific dendritic domains. CA1 pyramidal cells are also innervated by inhibitory interneurons that release the neurotransmitter GABA. Each type of interneurons innervates selectively a specific dendritic type or the soma/axon region, thus each has a different function [47].

From different subcortical nuclei CA1 pyramidal cells receive neuromodulatory inputs, such as cholinergic input from the septum, serotonergic input from the raphe nuclei, dopaminergic afferents from the ventral tegmental area and noradrenergic input from the locus coeruleus. The distribution of the receptor subtypes expressed by CA1 pyramidal cells for these neuromodulators are not uniform, which show that the different neuromodulators may selectively target the inputs from different pathways [47].

From the soma of the CA1 pyramidal cell a single axon originates that extensively branches to form synapses within and outside of the hippocampus. In the CA1 region it mostly targets structures in the stratum oriens. Inside the hippocampus through the alveus CA1 PC axon terminals innervate pyramidal cells of the hippocampus. Via the fimbria CA1 PCs convey information outside the hippocampus. Their target depends on the location of the neuron along the septo-temporal axis [47]. Figure 2.2 shows the target of CA1 PC axon terminals in more detail.

DOI:10.15774/PPKE.ITK.2022.001

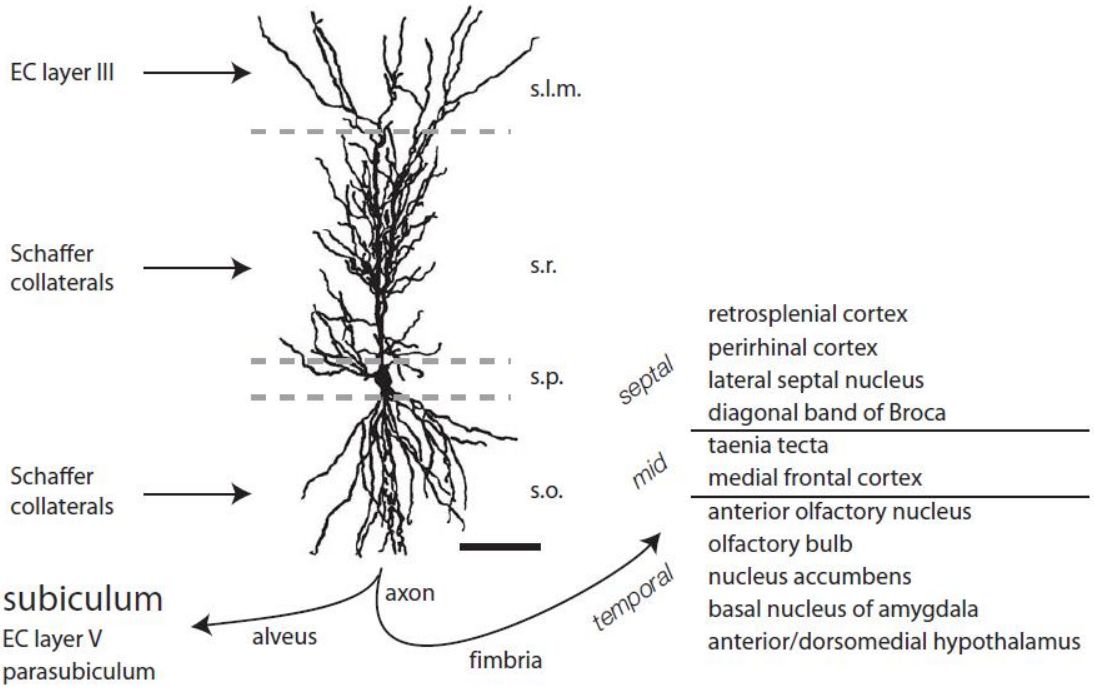

Figure 2.2: The morphology, inputs and outputs of CA1 pyramidal neurons. Drawing of a CA1 pyramidal neuron reconstructed using Camera lucida. The soma is shown in the stratum pyramidale (s.p.), at its base the basal dendrites can be found in the stratum oriens (s.o.), the bifurcating two-branch trunk and the oblique dendrites are in the stratum radiatum (s.r.), and the tuft dendrites are in the stratum lacunosum-moleculare (s.l.m.). The major excitatory inputs of each layer are also indicated along with the most important intra- and extrahippocampal targets of the axonal branches. Extrahippocampal targets depend on the location of the neuron along the septo-temporal axis, which is also indicated on the figure. The figure was adapted from The Hippocampus Book [47].

Although traditionally the pyramidal cells of the hippocampal CA1 region were thought to be morphologically and electrophysiologically homogeneous, there is growing evidence on their heterogeneity, which underlies their computational flexibility and explains how it is possible that a single circuit is capable of performing various functions (such as spatial navigation and processing memories obtained under different conditions) [48].

The hippocampus has a laminar structure that develops in an inside out pattern, meaning that earlier-born cells form the deeper part of the pyramidal cell layer, while the newer cells traverse to the superficial layer. This results in a heterogeneity along the radial axis of the CA1 region in the molecular, anatomical and physiological properties and even in the connectivity of pyramidal cells. Deep cells were reported to have a larger soma and more complex basal dendritic tree, while superficial cells develop a more complex apical dendritic tree. Different parts of the entorhinal cortex convey information to different parts of the CA1 regions in different degree both along the proximodistal and the radial axis. Medial entorhinal cortex (MEC) provides spatial information much more strongly to the proximal CA1 region (closer to

DOI:10.15774/PPKE.ITK.2022.001

CA2), while lateral entorhinal cortex (LEC) conveys mostly non-spatial information more strongly to the distal CA1. In proximal CA1 strong MEC and week LEC projections prefer deep pyramidal cells, while in the distal CA1 weak MEC and strong LEC inputs favour superficial PCs. In accordance with these observations it was shown that deep CA1 PCs are more likely to form place fields [48].

2.1.2.2. Electrophysiological properties and behavior of CA1 pyramidal cells and their functional consequences

According to patch clamp recordings in slice preparation of the rat hippocampal CA1 region, the typical resting membrane potential of CA1 pyramidal neurons is between -64 [49]–[51]and -75 mV [51]. In response to depolarizing somatic current injection they start to fire action potentials with a voltage threshold in the range of -46 to -56 mV [49], [51]–[54]. Single spikes elicited by brief current injection are followed by after-hyperpolarization (AHP) that consists of three stages: the fast AHP lasts for 2-5 ms, the medium AHP for 50-100 ms and the slow AHP for more than a second [47], [55]. The fast AHP is mediated by the fast-activating, large-conductance Ca^{2+} dependent K^+ channels (BK) [56]. There are two conductances contributing to the medium AHP: voltage gated muscarine-sensitive K^+ current (I_M) by M-type potassium channel, and the hyperpolarization-activated current (I_h). Contrary to earlier reports [55], medium AHP is not affected by Ca^{2+}-activated K^+ channels[57]. Opposing earlier experimental results suggesting that the slow AHP is mediated by the slowly activating, small-conductance Ca^{2+}-dependent K^+ (SK) channels, a more recent study reports that these are the intermediate-conductance Ca^{2+}-dependent K^+ (IKCa) channels that are responsible for the generation of the slow AHP [58], [59].

In many experimental recordings it has been observed that in response to somatic current injection the first spike is fired with a latency. However different studies report different length of this delay from a few milliseconds to seconds [60]. It is known that the latency to first spike decreases with increasing current intensity [61], but it also depends on the intrinsic properties of the cell. In relation to which mechanisms control this property, there are different experimental observations, therefore it is likely that multiple currents take part in the mediation of spike latency [60].

In response to prolonged somatic current injection under normal in vitro conditions (without any pharmacological manipulation), the majority of CA1 pyramidal cells fire regular trains of action potentials [25], [49], [62], while a small portion (16%) of these cells may exhibit burst firing [62]. The number of spikes in the regular train, and therefore the spike frequency, depends on the nature of the stimulus and increases with increasing stimulus strength (in a moderate range).

DOI:10.15774/PPKE.ITK.2022.001

A characteristic property of CA1 pyramidal cells is that they exhibit spike frequency adaptation (accommodation) [25], [60], [63], meaning that the inter-spike intervals increase (the firing frequency decreases) with time in the action potential train during the current injection. Spike adaptation can be divided into two phases: an early and a late phase. The early one is mediated by the same ion channels as the medium AHP while the late one is mediated by the ion channels that contribute to the slow AHP [57].

It has also been reported that the frequency adaptation can be so strong that the slowed action potential train even stops while the depolarizing current injection is still upheld, which is due to the activity of a calcium-activated potassium current and the M-type potassium current. In this study they observed this silent period after the action potential train but during the current input in most of the studied cells (135/141) even at moderate current intensity [63].

A more recent study analyzed this behavior of the CA1 pyramidal cells further. They found that as a response to prolonged (1s) somatic current injection of moderate intensity, the cells fire a regular, weakly adapting action potential train until the end of the stimulus. Although the AP train shows frequency adaptation, the number of spikes elicited during the 1sec stimulus, and therefore the overall mean frequency, increases with increasing current intensity below a threshold current intensity. When the amplitude of the injected current is increased further above this threshold, the overall spike number decreases with increasing current intensity, because after some action potentials, the cell stops firing during the current step stimulus, enters a depolarization block, and the membrane potential reaches an equilibrium value between -40 and -35 mV [25]. Using a modeling approach it has been shown that the key mechanisms behind depolarization block are the sodium and the delayed-rectifier potassium currents, and the appropriate relation between their activation curve. The M-type potassium current affects the value of the equilibrium potential during depolarization block. Mimicking background synaptic activity in the gamma range on the model, they also showed that depolarization block may occur under in vivo conditions [25]. Another recent study suggests that besides the M-type potassium channel, the SK channel also plays an important role in depolarization block, and that pyramidal cells located at the more dorsal part of the CA1 region, are more likely to enter depolarization block [64]. Although, depolarization block is still rarely studied, it may play an important role in network activity, as it modulates the firing activity and properties of CA1 pyramidal cells. Its main role can be to prevent the cell from firing at too high frequencies and therefore potentially initiating or promoting the spread of epileptic seizures [25], [64].

As it was mentioned above, in a small portion of the CA1 pyramidal cells somatic current injection evokes burst firing. This occurs when the afterdepolarization following the first spike is able to depolarize the membrane to such an extent that its voltage reaches the spiking threshold to elicit a second spike [62]. The afterdepolarization is the result of the activation of the dendritic L- and T-type calcium channels by the back-propagation of the first action

DOI:10.15774/PPKE.ITK.2022.001

potential, which leads to the formation of a prolonged dendritic Ca^{2+} spike that propagates to the soma [65]. This process is enhanced if the density of the A-type potassium channel is lowered at the distal dendrites (either artificially by blockers, or naturally by neuromodulatory substances or by plasticity events related with synaptic activity), as under this condition the action potentials are able to backpropagate to the dendrites more actively.[65]

In the absence of experimental data, the dendrites of neurons have long been thought of as a passive cable whose function is to transmit the synaptic signal to the cell body. The behavior of such dendrites is described by cable theory. Accordingly, the extent to which an input contributes to the development of dendritic or somatic excitatory postsynaptic potential (EPSP) depends largely on which location in the dendritic tree the synapse is at. At the end of the dendrites - where due to the rather small diameter of the dendrites and the proximity of a closed end, the input resistance is much higher than at the origin of the dendrites - the synaptic input causes greater depolarization than at locations close to the origin of the dendrite or the soma [66], [67]. Furthermore, the attenuation of the signals is asymmetric, so that the amplitude of the signal decreases less as it spreads to the more distant regions than to the proximal regions, therefore the signal is greatly attenuated by the time it reaches the soma from the distal dendritic sites, mainly due to dendritic filtering. Distant synapses thus elicit a larger dendritic signal but are expected to contribute much less to the formation of somatic EPSP than proximal inputs, which in turn result in smaller amplitude dendritic EPSPs [66], [68].

However, it has been shown experimentally that although the local amplitude of the synaptically induced EPSPs increase significantly with the distance of the synapse from the soma, the corresponding somatic EPSPs have nearly the same amplitude, which is not dependent on the synaptic location on the dendrite. When dendritic EPSPs were evoked by current injection (instead of synaptic input), the efficacy of the inputs became location dependent, meaning that the amplitude of the triggered somatic EPSP decreased as the distance of the input increased. From these observations it was concluded that it is the increasing synaptic conductance with increasing distance from the soma (and not other dendritic mechanisms), that counterbalances the dendritic filtering [29]. Further cellular and computational study [67] suggested that at least in the stratum radiatum the expression of AMPA receptors increases on the dendrites with increasing distance from the soma [69] and that synaptic strength increases with distance on the apical trunk and along the somato-dendritic axis on the origin of the oblique dendrites but decreases along the length of the obliques [68].

In a passive dendritic tree, the inputs to different dendritic locations are summed linearly. However, when multiple inputs arrive on a single dendritic location, close to each other in space and time, summation is sublinear due to decreasing driving force and shunt current activation [67]. However, by now it has been shown in several studies, that the dendrites of CA1 pyramidal cells are able to generate different types of dendritic spikes (depending on their

DOI:10.15774/PPKE.ITK.2022.001

spatiotemporal pattern) , thus exhibiting supralinear summation of the incoming signal [31], [33], [53], [67], [70]. This is strong evidence that the dendrites of CA1 pyramidal cells are not passive cables, but they have various active membrane mechanisms, which make them function as independent computational units. Thus, another way to compensate for the dendritic filtering is that synaptic inputs activate voltage-gated ion channels in the dendritic branch, which may result in the generation of dendritic spikes. These spikes can propagate more effectively to the soma enhancing the contribution of distal synapses to the somatic EPSP. This is called the two-stage integration mode, as inputs are first summed in the dendritic branch to generate dendritic spikes, then the output of several branches are summed at the soma [66], [68]. Taking into account that dendritic spikes are easier to trigger at the distal end of the dendritic branches (because of the high input impedance there), and also the previous suggestions on the differences in synaptic conductance along the dendrite, it has been proposed that synaptic strength increases along the somato-dendritic axis of the neuron but decreases from the origin of each oblique dendritic branch to its end [68].

Another, even earlier piece of evidence supporting that the dendrites of CA1 pyramidal cells express various types of voltage gated ion channels is that action potentials initiated at the axon are able to invade the dendritic tree and actively back-propagate in the main apical dendrite (trunk) [26], [27]. Experiments have shown that when sodium channels are pharmacologically blocked, the amplitude of the back-propagating action potentials decrease significantly. They thus propagate regeneratively up to a certain distance from the soma due to the activity of Na^+ channels [26]. However, due to the increasing density of the A-type potassium channels towards the end of the dendrites, the back-propagating action potentials are not fully regenerative, but their amplitude decreases with distance [71]. Above 300 μm on the apical trunk from the soma, their amplitude decreases significantly. It has been shown that CA1 pyramidal cells can be divided into two populations; in one of them the amplitude of the first back-propagating action potential in a train decreases to the same extent above 300 μm as below, while in the other group the decrease in the amplitude is much stronger. This shows that there is a great variability in the density and distribution of the ion channels that affect back-propagation among these cells [27].

In distal parts of the main apical dendrite, action potential trains propagate in an activity-dependent manner, with the first few action potentials of the train propagating actively, while the others are no longer able to actively regenerate. This is mainly due to the fact that repetitive firing causes prolonged inactivation of Na^+ channels from which they return relatively slowly [72]. In the case of the attenuation of the last action potentials of the train, which underwent activity-dependent attenuation, there was no evidence for observable dichotomy in the population [27].

Measuring calcium and voltage signals using confocal and two-photon imaging in *in vitro* slices, it has been shown that the action potentials generated at the soma/axon region back-

propagate not only into the main apical trunk but from there also to the thin oblique dendrites [28]. As the action potential propagates into the oblique branch, initially its amplitude and the associated Ca^{2+} signal is increased compared to the value measured on the apical trunk, then as it propagates further towards the end of the oblique dendrite, the signals attenuate. Before the bAP starts to attenuate, its value remains constant within a branch, and the length of this section depends on the distance of the branching point from the soma. For more distant oblique branches the propagation is weaker, therefore the length for which the bAP amplitude remains constant decreases with distance from the soma. This relation also holds for the Ca^{2+} associated signal, and is mediated by the A-type potassium current. On the other hand, the bAP amplitude and the strength of the Ca^{2+} signal increases when the membrane of the oblique branch is depolarized by synaptic inputs, overcoming the inhibitory effect of the potassium channels by its voltage-dependent inactivation [28].

Action potentials also back-propagate into the distal tuft region of the apical dendritic tree, and as it was mentioned before, the depolarization caused by them activates calcium channels, which induces the generation of Ca^{2+} spikes or plateau potentials. The efficacy of this process is reported to be dependent on the activity of the A-type potassium channel, the same way as in the case of the oblique dendrites [65]. Besides regulating the action potential output of the cell, by inducing burst firing in the soma [65], the Ca^{2+} influx created by the back-propagating action potentials may cause long term potentiation (LTP) or depression (LTD) at the synapses of distal dendrites by acting on biochemical signaling pathways to modulate the properties and densities of the various ion channels and receptors [28]. Back-propagating action potentials can also induce NMDA-dependent synaptic plasticity by unblocking the NMDA receptor that is activated by a coincident synaptic input, thus allowing a large Ca^{2+} influx through the NMDA receptor [28].

As it was mentioned before, due to the activity of the various types of voltage-gated ion channels present in their membrane, the dendrites of CA1 pyramidal cells are able to generate dendritic action potentials (dendritic spikes), and therefore influence synaptic integration [66].

Depending on the type of mechanism that generates them, the dendritic spikes of CA1 pyramidal cells can be divided into three categories. Sodium spike is the narrowest type of dendritic spikes; however, it is often coupled with an NMDA component, that shapes its duration due to the coincident activation of these receptors [31], [33], [53]. Although their threshold (on the trunk) is about 10 mV higher than on the soma [53] fast sodium spikes can be also generated on the main apical dendrite and on the oblique and basal dendrites [30], [31], [33], [53], [73]. Depending on their amplitude and the reliability of their forward propagation, spreading from the trunk to the soma, sodium spikes can cause rapid and sufficiently large depolarization to generate a single precisely timed action potential [30], [73]. Calcium spikes are longer-lasting spikes that are more characteristic of the distal trunk and the apical tuft region

DOI:10.15774/PPKE.ITK.2022.001

and that are formed through the activity of calcium channels [32], [65], [74]. These spikes, when they spread to the soma, cause prolonged depolarization often resulting in high-frequency re-firing, called "burst" firing [65]. Small-diameter, terminal apical and basal dendrites are able to generate NMDA spikes when they are depolarized effectively enough that the voltage-dependent magnesium block of the NMDA receptor is relieved. These spikes are even longer in duration than the Ca^{2+} spikes, but they are unable to propagate far from the site of the synapse, as the glutamate neurotransmitter is also required to activate NMDA receptors [66], [70], [75]. Under *in vivo* conditions, when the pyramidal cell is sufficiently depolarized, synchronous synaptic activation of Ca^{2+} channels and NMDA receptors results in the emergence of multi-dendrite Ca^{2+} spikes on basal and apical dendrites which leads to the generation of complex-spike bursts output [76]. Complex-spike bursts occur spontaneously during the non-theta state of the hippocampus *in vivo*, associated with feeding and slow wave sleep [77].

On the distal main apical dendrite and the proximal tuft region of the CA1 pyramidal cells it has been shown how the formation of dendritic spikes and the form of dendritic integration depend on the spatial and temporal pattern of inputs. Because dendritic spikes have a relatively high voltage threshold, rapid and large depolarization is required for their formation. This can be achieved if several inputs arrive at the dendrites very close to each other in time [53]. Glutamate uncaging experiments have shown that when the inputs arrive at the apical trunk synchronously, within 3 ms, a dendritic spike is generated, resulting in the supralinear summation of the incoming signals. However, the amplitude of the spike and the degree of supralinearity are also greatly influenced by the spatial arrangement of the inputs. If the synapses are farther apart, scattered over a 150 μm long section of dendrites, the spike amplitude and the degree of supralinearity decrease compared to the clustered case, when the inputs arrive at a short section of only 25 μm. If the synapses are activated asynchronously within 50 ms, no spike is generated on the dendrites, and the summation remains linear regardless of the spatial arrangement [30].

It has been shown by pharmacological means that the dendritic spikes described above are mediated by the activity of sodium channels, while A-type potassium channels greatly influence the form of dendritic integration. Blocking the latter one, the voltage threshold of the dendritic spike decreases, and its amplitude increases. Blockade of calcium channels had no significant effect on spike formation and amplitude. These spikes are thus very different from the calcium spikes observed in tuft dendrites [53].

The distal trunk and proximal tuft region are thus capable of two forms of signal integration that determine the somatic output of the CA1 pyramidal cell. In the case of supralinear integration caused by temporally synchronous and spatially clustered inputs, a single, precisely timed somatic action potential is generated due to the rapid depolarization caused by the dendritic spike. The number of inputs required to generate somatic action

DOI:10.15774/PPKE.ITK.2022.001

potential, however, increases when the input pattern is less synchronous. Distributing the synchronous inputs lowers their efficacy to generate somatic output. Furthermore, in the case of linear integration mode the precision of the timing of the action potential output decreases, the delay of the first spike is highly variable, and the number of evoked somatic action potentials increases with the number of inputs. In conclusion it can be said that CA1 pyramidal neurons are able to detect the pattern of incoming signals and respond accordingly [30].

This seems consistent with observations about the behavior and function of these cells during the two different behavioral states characteristic of the hippocampus, and it can be hypothesized that these cells are able to shift the mode of dendritic integration according to the behavioral state. Asynchronous inputs characterize the theta phase, when the animal is actively exploring the environment. This results in linear summation of the signals and therefore somatic action potential output whose rate and timing depends on the number of inputs, as this usually occurs in the behaving animal while sequences of episodes are stored during exploration. Also, as the animal approaches the cell's place field, more and more synaptic inputs arrive at the cell, which increases the firing rate of the cell as well. By contrast, during sharp wave ripples these cells receive highly synchronous inputs from groups of CA3 pyramidal cells and will respond with a precisely timed single action potential to only those inputs that are also spatially clustered, making possible the rapid replay of the stored information and saving them to higher cortical areas [30].

According to glutamate uncaging experiments in rat hippocampal slices, nonlinear summation of incoming signals can also be observed on the radial oblique dendrites of CA1 pyramidal cells. Due to the small diameter and poor accessibility of these dendrites, their local voltage response could not be directly recorded, therefore the voltage response of the cell to the synaptic inputs could be obtained only by somatic recordings. The local effect of the inputs could be observed by the two-photon calcium imaging method, which, however is difficult to calibrate to obtain voltage values, and its temporal resolution is poor. Based on somatic voltage responses, it was observed that when an increasing number of inputs arrive at an oblique dendritic branch synchronously (in every 0.1 ms) the incoming signals are always summed according to a supralinear function that has a kind of sigmoidal shape. At a certain input level a disproportionately large increase is observed in the amplitude of the voltage response. This step-like increase is reported to be the result of the generation of a dendritic sodium spike, which greatly increases the slope of the rising phase of the somatic EPSP. This is the fast component of the somatic EPSP, which thus also causes a sharp increase in the maximum value of the first temporal derivative of the somatic voltage at the given input level. Although the dendritic spike shown here is the result of the activity of sodium channels, it contributes to the formation of the subsequent slow component. The slow component of the somatic EPSP and thus the overall amplitude of the voltage response is shaped by the activity of NMDA receptors - and not

DOI:10.15774/PPKE.ITK.2022.001

voltage-gated Ca^{2+} channels - which also contributes greatly to the supralinearity of signal integration [33]. However, it seems that the local calcium signal is mediated mainly by the activity of the voltage gated calcium channels.

In calcium imaging experiments, the calcium signal showed similar characteristics as the somatic voltage response they were associated with. It also increased linearly for small inputs and had a sharp increase at the same input level as the somatic voltage response [33].

In contrast to the observations about the apical trunk, on the oblique dendrites the described behavior does not depend on the spatial pattern of the inputs. As long as the appropriate number of inputs arrive synchronously at a single oblique branch, it is able to produce dendritic spikes even if the synapses are distributed. However again contrary to the dendritic spikes generated on the trunk, spikes from the oblique dendrites are unable to spread to the soma effectively enough to trigger action potential output there. On the other hand, when inputs arrive asynchronously (> 1 ms between the inputs), similarly to the trunk, oblique branches are also unable to produce dendritic spikes, because the membrane potential is depolarized too slowly, thus the mode of signal integration is linear [30], [33].

By blocking A-type potassium channels, it has been shown that, similarly to the trunk, these channels play an important role in signal integration on the radial oblique dendrites as well. In the synchronous case, the block of A-type K^+ channels resulted in higher amplitude somatic EPSPs and increased the slope of the fast component, which is probably due to the facilitation of signal propagation. In the asynchronous case, the voltage threshold for sodium spike generation decreased, so that the input-output curve changed from linear to supralinear [33].

When inputs are synchronously activated on multiple oblique dendrites, the summation becomes significantly sublinear, probably due to the additional activation of A-type potassium channels at the branching point where these oblique dendrites converge. The extent of sublinearity increases with the number of branches receiving the inputs. [78].

These results support the assumption previously shown by modeling studies that thin dendrites are capable of functioning as computational subunits with a sigmoidal input-output curve. The outputs of the subunits add up linearly on the soma and, if appropriate, can result in an action potential output, so that the cell can function as a two-layer neural network [6], [79]. Moreover, it can be seen that oblique branches, like the main apical dendrite, are also able to switch their mode of integration depending on the spatiotemporal pattern of the input, thus performing the computation best suited for the behavioral state. Furthermore, the coincident activation of NMDA receptors and the generation of dendritic spikes causes large amplitude NMDA-mediated signals that have important roles in several forms of synaptic plasticity [33], [80], [81].

Using focal synaptic stimulation and glutamate uncaging methods to activate inputs on basal dendrites it has been shown that these dendrites are also capable of generating dendritic spikes that are composed of an early fast sodium spike and a late, slow NMDA spike in response to synchronous and clustered inputs. In contrast to the oblique dendrites, however, the amplitude of the basal spikes is mostly dominated by the fast and not the slow component and are able to effectively propagate to the soma. Fast basal spikes trigger precisely timed axonal action potential output, similarly to what has been observed on the apical trunk. Asynchronous or distributed inputs to the basal dendrites lead to linear or in some cases even to sublinear summation of the individual EPSPs. These results suggest that basal dendrites are capable of acting as coincidence detectors and convert the simultaneously received signal into a precisely timed, reliable AP output. [31]. On the other hand, it has been shown that similarly to oblique dendrites, when inputs are synchronously activated on multiple basal dendrites the summation is significantly sublinear [78].

While previous experiments showed that dendritic spikes of the oblique dendrites are unable to effectively propagate to the soma to trigger action potential output [33], further studying the signal integration of the oblique and basal dendrites, it was found that most of the proximal (branching point > 40 μm from the soma) primary branches, while only a small proportion of the terminal branches, generate strongly propagating dendritic APs. This increases the amplitude of the fast component of somatic EPSP and in many cases can also induce precisely timed somatic APs. Furthermore, highly synchronous inputs arriving at a weakly propagating branch, triggering repetitive local spiking, together with mACH receptor activation or backpropagating action potentials, could permanently increase the coupling strength of the specific branch, by triggering NMDA receptor-dependent signaling pathways. This form of dendritic plasticity was named branch strength potentiation (BSP). In addition to its NMDA dependence, BSP is also mediated by the A-type potassium channels. BSP might be a way of information storage as the enhancement of coupling strength occurs only in the case of a unique pattern of synaptic inputs [82].

Branch strength potentiation occurs naturally in rats that have been exposed to a socially and spatially enriched environment for a few days before the *in vitro* experiment. It has been shown that the number of strongly propagating terminal oblique dendrites was much higher in enriched pyramidal cells than in the control group. Thus, enrichment created dendritic domains that consist of a very strong parent branch and strong daughter dendrites. This shows that electrical properties of dendritic branches may be altered in behaving animals. This kind of plasticity is triggered by the highly correlated input pattern during sharp waves and seems to take place as a storage process during learning of a rich environment [83].

In contrast to BSP, on basal dendrites it has been shown that when dendritic spikes are triggered on the same branch with a frequency between 5 and 10 Hz (which characterizes the

DOI:10.15774/PPKE.ITK.2022.001

theta behavioral phase of the hippocampus) the amplitude of the consecutive spikes decreases until the branch even fails to produce a dendritic spike. This activity-dependent attenuation affects the strongly coupled branches more significantly and converts the mode of signal integration into linear in the specific branch. This modified behavior lasts for several hundreds of milliseconds. Moreover, bursts of backpropagating action potentials (that arrive prior to the dendritic input and not coincidentally with the peak of the dendritic spike as in the case of BSP) globally reduced the dendritic excitability and prevented supralinear dendritic integration in most of the basal branches. These results show that the mode of signal integration in basal dendrites depends on the past activity of the cell [84]. Similarly to the activity-dependent attenuation of back-propagating action potentials [72], spike attenuation on basal dendrites is caused by the prolonged inactivation of Na^+ channels due to previous activity. These data suggest that information storage during sharp wave ripples is more effective when neural activity is rather sparse, thus there is a "speed limit" for information storage [84].

To test whether the tuft dendrites, which get input through the perforant path, are able to generate dendritic spikes and somatic action potential output, the perforant path was activated by a stimulating electrode placed in the stratum lacunosum-moleculare of the hippocampal slice [85]. As stimulus intensity was increased, the somatic EPSP increased, but it never reached the threshold for action potential generation. Using bursts of high frequency pulses (5-10 pulses at 100 Hz) spikelets (small spikes) were observed in the somatic voltage response, that are the sign of dendritic spikes generated by the inputs which however propagated unreliably to the soma [81], [85], and were able to trigger somatic action potential only in response to 10 input pulses. However, even a moderate input to the distal apical trunk by the activation of the Schaffer collaterals can facilitate the propagation of the spikes generated in the tuft region by PP input and increased the frequency of the spikelets [85]. It seems that the only way tuft dendrites can have an impact on the neuronal output is by generating dendritic spikes.

In another experiment, the Schaffer collaterals and the perforant path were activated with a moderate intensity separately and simultaneously in a manner that mimics theta activity. When synapses on the trunk were activated through the stimulation of the Schaffer collaterals, the generated summed EPSP produced a small number of somatic action potentials in some cases, but mostly remained subthreshold. When the trunk region was activated through the perforant path, low amplitude and short duration plateau potentials could be observed at the distal trunk region, and brief burst of action potentials on the soma. Simultaneous activation of both pathways, however, resulted in supralinear summation of the signals by the generation of high amplitude and long duration plateau potentials at the recording site on the distal trunk, and high frequency burst firing in the soma. This activity was associated with high level dendritic Ca^{2+} influx. The duration of the plateau potential decreased with increasing delay between the stimulation of the two pathways, and plateau generation failed if the Schaffer collateral input

was delayed by more than 150 ms [32]. These plateau potentials are formed by NMDA, voltage gated Ca^{2+} dependent mechanisms [32], [62], [65], and back-propagating action potentials play an important role in their generation as well [32]. Plateau potentials propagate to the soma/axon region where they appear in the form of strong after-depolarizing potentials, which switch the mode of neuronal output from single AP or regular trains of APs to burst firing.

This functionality makes the cell behave as a coincident detector as it provides a unique output when the CA3 pyramidal cells give input to them through the SC coincidently with inputs from the entorhinal cortex via the PP. Entorhinal cortex and the CA3 region are hypothesized to be activated together during context-dependent memory retrieval [32].

Already from the experiments described above it can be seen that in contrast to the basal and oblique dendrites, tuft dendrites are capable of the supralinear integration of incoming signals even when inputs are received at multiple tuft branches, as in the studies described above synapse activation was done through the stimulation of the perforant path, which projects to multiple dendritic branches of the same neuron. However, it has been specifically tested and shown that multibranch integration of tuft dendrites is just as supralinear as single branch integration. This suggests that multibranch integration may better store information that is transmitted by spike timing, while single branch integration respond more effectively to spike rate [78].

Dendritic plateau potentials and the generated burst firing are very effective in inducing long term potentiation (LTP) in the synapses of distal dendrites where the back-propagating action potentials cannot propagate effectively enough to provide the sufficient depolarization [32], [81]. The NMDA and voltage gated Ca^{2+} dependent long-lasting plateau potentials provide the sufficient depolarization and calcium influx for plasticity mechanisms to occur. As the propagation of dendritic spikes in the dendritic tree is limited, it is likely that the type of LTP described here will be induced in smaller dendritic domains than those mediated by bAP that is able to spread to most of the dendritic tree [81]. On the other hand, NMDA receptors and voltage-gated Ca^{2+} channels are known to be strongly voltage dependent, thus it is likely that their activity is triggered by fast sodium spikes. A more recent study reported that it is the fast sodium spike that activates calcium permeable channels and triggers the brief, but strong calcium influx that induces LTP, rather than the accompanying long-lasting calcium plateau. Furthermore, they suggest that the NMDA-dependent depolarization is neither sufficient nor necessary for LTP induction on distal dendrites [80].

One of the most important functions of the hippocampus is spatial representation and memory. Through the activity of place cells, the hippocampus is thought to form a cognitive map of places to help navigation. Each place cell is active at a particular location of the environment, which is called the neuron's place field. Around 25% of the pyramidal cells of the CA1 region function as place cells in an environment [86]. In a new environment another

DOI:10.15774/PPKE.ITK.2022.001

random 25% of the population (which naturally may be overlapping with the previous group) will show place cell firing.

There are instant place cells that fire already at the first time the animal crosses their place field, while delayed place cells start to fire only if the animal traverses their place field multiple times. In both types, dendritic active mechanisms, and different types of dendritic spikes play crucial roles in place field formation. In instant place cells the sensory input at a location of the new environment arrives in a configuration and to already strong synapses that is sufficient to generate plateau potentials to drive somatic burst firing or sums strongly enough to induce regular firing in the soma. Burst firing may initiate plasticity events that further increase the precision of the place field [86].

Delayed place cells receive sensory input when the animal crosses the future place field, that activate many synapses at the dendrites of CA1 pyramidal cells, but they do not sum strongly enough to elicit action potential output. However, it may occur that afferents innervating the same dendritic branch are coactivated at the same location. This leads to a clustered and synchronous input pattern that induces NMDA or other Ca^{2+} dependent local spike leading to potentiation of the synapses. Traversing the same location multiple times leads to further strengthening of these synapses, or the same process may happen at other dendritic branches. Finally, the synapses are strong enough that the sum of the synaptic inputs is able to trigger somatic action potential output, and the new place field is generated [86].

Recently it has been shown that place field formation can be induced by behavioral time scale synaptic plasticity, where plateau potentials or complex spiking drives the potentiation of synaptic inputs that were active (in many cases even remaining subthreshold) seconds before or after the more global plateau signals. This means that the events of a much longer time scale can be rapidly stored, than in the conventional Hebbian plasticity rules, where the firing of the pre- and postsynaptic cell must occur within tens of milliseconds for potentiation to take place [87].

As we have seen, the different dendritic types of the dendritic tree of CA1 pyramidal cells, a dendritic subtree or even a single dendritic branch is capable of behaving as an independent computational subunit. Dendritic active mechanisms make these subunits capable of coincidence detection, pattern recognition and inducing synaptic plasticity, and thereby shaping the axonal output of the cell. These properties of the CA1 pyramidal cells play essential roles in the function of the hippocampal circuit.

DOI:10.15774/PPKE.ITK.2022.001

	Observed property or behavior	Underlying mechanisms
Somatic spiking	Voltage threshold of APs is in the range of -46 to -56 mV [49], [51]–[54].	Activity of voltage-gated Na^+ and voltage-gated K^+ channels [52].
	Spikes are followed by after-hyperpolarization (AHP): the fast AHP lasts for 2-5 ms, the medium AHP for 50-100 ms, and the slow AHP for more than a second [47], [55].	 Activity of fast-activating, large-conductance Ca^{2+} dependent K^+ channels (BK) [56]; voltage gated muscarine-sensitive K^+ current (IM) by M-type potassium channel, and the hyperpolarization-activated current (Ih) [57]; intermediate-conductance Ca^{2+}-dependent K^+ (IKCa) [58], [59].
	First spike is fired with latency [60], [61]	Most likely caused by the activity of multiple currents [60].
	Spike frequency adaptation [25], [60], [63].	Activity of M-type K^+ channels, the hyperpolarization-activated current (Ih) and intermediate-conductance Ca^{2+}-dependent K^+ (IKCa) [57], [63].
	Depolarization block [25], [64]	Inactivation of Na^+ channels, activity of M-type K^+ channels, delayed rectifier K^+ channels (KDR), small-conductance Ca^{2+} - dependent K^+ (SK) channels [25], [64].
	Burst firing [62], [65]	Activity of dendritic L-, R-, and T-type Ca^{2+} channels activated by back-propagating action potentials or synaptic inputs [65].
Dendritic	Somatic EPSP amplitude is independent of the distance of the synaptic location [29].	Increasing synaptic conductance with increasing distance from the soma - in the stratum radiatum the expression of AMPA receptors increases [29],[68],[69].
	Action potentials are able to back-propagate to the dendrites [26], [27]	Activity of Na^+ channels on the dendrites [26], [27].
	At distal dendrites AP back-propagation is not fully regenerative [71].	Increasing density of the A-type K^+ channels towards the end of the dendrites [71].
	Activity-dependent back-propagation of AP trains [72].	Prolonged inactivation of Na^+ channels [72].
	Back-propagating APs induce the generation of Ca2+ spikes or plateau potentials in tuft dendrites which causes burst firing in the soma [65].	Activity of (primarily T and R type) Ca^{2+} channels. Efficacy depends on the activity of the A-type K^+ channels [65].
	Synchronous synaptic input to the distal trunk leads to the generation of dendritic Na^+ spikes and the supralinear integration of the incoming signal [53], [30].	Activity of Na^+ channels, also influenced by the activity of A-type K^+ channels [30]
	Synchronous synaptic input to the oblique dendrites leads to the generation of local dendritic Na^+ spikes and the supralinear integration of the incoming signal [33].	Activity of Na^+ channels and NMDA receptors, also influenced by the activity of A-type K^+ channels [33].
	A portion of the oblique dendrites generates strongly propagating dendritic APs that in many cases can also induce precisely timed somatic APs. [82]	Branch strength potentiation – induced by the activity of NMDA channels, mediated by the activity of A-type K^+ channels [82].
	Synchronous and spatially clustered synaptic input to the basal dendrites leads to the generation of local dendritic Na^+ spikes and the supralinear integration of the incoming signal [31].	Activity of Na^+ channels and NMDA receptors [31].
	Basal dendrites show activity dependent attenuation in the amplitude of the dendritic spike [84].	Prolonged inactivation of Na^+ channels due to previous activity [84].
	Simultaneous stimulation of the trunk dendrites via the Schaffer collaterals and the tuft dendrites via the perforant path results in supralinear summation of the signals by the generation of high amplitude and long duration plateau potentials on the distal trunk, and high frequency burst firing in the soma [32].	Formed by NMDA, voltage gated Ca^{2+} dependent mechanisms (mostly R-type), and back-propagating action potentials play an important role in their generation as well [32], [62], [65].

Table 2.1: Summary of the most important physiological properties of the hippocampal CA1 pyramidal cell, and the main mechanisms underlying them.

DOI:10.15774/PPKE.ITK.2022.001

2.2. Multi-compartmental modeling of neurons

Mathematical and computer modeling are the basic tools used in theoretical and computational neuroscience to understand the behavior and function of the nervous system and the neurons that make it up. The basis of modeling the nervous system and neurons is the mathematical description of the biophysical processes taking place in neurons. In this section, the most important concepts of single cell neural modeling will be described.

The processes of a neuron, the axon and the dendrites, are best approximated by considering them as elongated cylindrical structures, in which the membrane potential is not uniform, but its value varies along the longitudinal axis of the cylinder. The electrical signal generated during synaptic interaction is strongly attenuated as it propagates over long, thin, cable-like dendrites. The mathematical analysis of voltage signal propagation in neurons is called cable theory. Understanding signal propagation and understanding how cell geometry affects it can be important in determining whether a particular synaptic input triggers an action potential output, and if so, when. Dendrites and the axon are typically so thin structures that the axial and radial changes in the potential on them are negligible compared to the longitudinal change. Therefore, on neural cables, the membrane potential can be expressed by the function V(x, t), where x is the longitudinal coordinate and t is time. The cable equation is a differential equation that describes how the membrane potential, V(x, t) depends on the currents flowing in, into and out of the cell. The cable equation can therefore be written as:

$$c_m \frac{\partial V}{\partial t} = \frac{1}{2ar_L} \frac{\partial}{\partial x}\left(a^2 \frac{\partial V}{\partial x}\right) - i_m + i_e, \tag{2.1}$$

where c_m is the specific membrane capacity, V=V(x,t) is the membrane potential, a a is the radius of the cable, r_L is the intracellular resistance, i_m is the current flowing through the ionic and synaptic channels in the unit membrane area, and i_e is the current flowing to the given region through the electrode divided by the surface of the region [88].

The analytical solution of the cable equation requires the introduction of two harsh simplifications: ignoring synaptic currents and considering the membrane current as a linear function of the membrane potential. This method is called linear cable theory. The solution can be further simplified by keeping the intensity of the current injection at a constant value. The membrane potential then sets to a steady state, where it depends only on the longitudinal coordinate, not on time. Then the cable equation is simplified to an ordinary differential equation. However, this can only be used in simple cases, for more complex models, employing realistic membrane conductances, the membrane potential must be computed numerically. For this purpose, the processes of the cell model are divided into separate compartments. In this case, it is assumed that the compartments are short enough that the longitudinal membrane

DOI:10.15774/PPKE.ITK.2022.001

potential change in them is negligible. Therefore, the continuous membrane potential can be approximated by a set of discrete values, which represent the membrane potential of each compartment (V_μ). In addition, each compartment has its membrane current (i_m^μ), determined by its voltage-gated ion channels. In a single, independent compartment the membrane potential can be given by the following differential equation:

$$c_m \frac{dV}{dt} = -i_m + \frac{I_e}{A} \tag{2.2}$$

However, the compartments of the long neural processes have neighboring compartments, that must be taken into account. Therefore, for a non-branching axon or dendrite, the membrane potential of each compartment is given by the equation:

$$c_m \frac{dV_\mu}{dt} = -i_m^\mu + \frac{I_e^\mu}{A_\mu} + g_{\mu,\mu+1}\left(V_{\mu+1} - V_\mu\right) + g_{\mu,\mu-1}\left(V_{\mu-1} - V_\mu\right) \tag{2.3}$$

where I_e^μ is the electrode current in compartment μ, A_μ is the surface of the compartment, and the $g_{\mu,\mu'}$ constant gives the coupling between the neighboring compartments. The value of the latter is the current flow from one compartment to another calculated according to Ohm's law [88].

Nonlinearities in the change of membrane potential, caused by active membrane conductances, determine most of the electrical properties of neurons, including action potential firing and propagation. Voltage-dependent ion channels, which provide a significant portion of membrane conductance, are often described using the Hodgkin-Huxley model.

According to the Hodgkin-Huxley model, the channels of persistent, non-inactivating conductances, such as the delayed rectifier potassium current, are modelled as having a number of equivalent gates. Activation of the conductance is the result of opening the gates, while the closing of them is called the deactivation. In these channels, depolarization of the membrane increases the probability that the channel is open (P), and with hyperpolarization the probability decreases. If n is the probability that a given gate undergoes a conformational change to open, and there are k gates that open independently of each other, then $P = n^k$. The value of the gating variable n is between 0 and 1. In general, n is the probability that a given subunit is open, then 1-n is the probability that it is closed. The probability of the transition from open to closed and from closed to open is voltage dependent. These are described by the α (V) and β (V) rates respectively. From the difference of the probability of opening and closing, we get how the probability that a given gate is open changes:

$$\frac{dn}{dt} = \alpha_n(V)(1-n) - \beta_n(V)n \tag{2.4}$$

DOI:10.15774/PPKE.ITK.2022.001

The rate functions $\alpha_n(V)$, $\beta_n(V)$ are usually set based on experimental data, and different models use different forms of equations to describe them. An example of $\alpha_n(V)$ is the following:

$$\alpha_n(V) = A_\alpha \, exp\left(-\frac{qB_\alpha V}{k_B T}\right) = A_\alpha \, exp\left(-\frac{B_\alpha V}{V_T}\right) \tag{2.5}$$

where A_α is a constant, qB_α describes the movement of charges, $qB_\alpha V$ is the energy needed for this. The B_α constant reflects the amount of moving charges and the distance they make. The probability that enough energy is generated to overcome this energy barrier is proportional to the Boltzmann factor [88]:

$$exp\left(-\frac{qB_\alpha V}{k_B T}\right). \tag{2.6}$$

The channels of transient conductances, such as sodium conductance, are regulated by two different voltage-dependent gates. The probability that the swinging gate is open is m^k, where m is the activation variable and k is an integer. The probability that the second gate, which is able to inactivate the channel, is not blocking it at the moment is h. This is the inactivation variable. The two variables have different voltage dependencies. With depolarization, m increases and h decreases. For current to flow through the channel, both channels must be open. The probability of this is $P = m^k h$. The rate functions of such channels are α_m, β_m, and α_h, β_h. These can be given similarly to α_n, β_n described above [88].

The conductance of the "j" type ion channel per unit area is denoted as g_j. At a given time, the value of g_j is obtained as the product of three factors, which are the conductance of a single open channel, the channel density in the membrane, and the ratio of open channels. The product of the channel density and the conductance of a channel is a constant value, the maximum conductance ($\overline{g_j}$), which is the conductance per unit area if all channels from the given channel type (j) are open. P_j is the probability that a particular channel is currently open, therefore $g_j = \overline{g_j} P_j$. The change in P_j is determined by the voltage-dependent change in conductances described above [88].

The membrane current due to the activity of a particular channel type is given by the following equation:

$$i = g(V - E), \tag{2.7}$$

where g is the conductance of the channel, V is the membrane potential, and E is the reversal potential of the given channel. The total membrane current is obtained by summing the different channel currents [88]:

$$I = \sum_j g_j \left(V - E_j\right) \tag{2.8}$$

Synaptic conductances also contribute to the total membrane current, which can be given by multiplying the maximum conductance ($\overline{g_s}$) of the given channel and the probability

(P) that the channel is open: $g_s=\overline{g_s}P$. P is derived from the product of two probability components: $P = P_sP_{rel}$, where P_{rel} is the probability that neurotransmitters are released from the presynaptic terminal when an action potential reaches that region, and P_s is the probability that the postsynaptic ion channel is open when transmitter is released [88].

2.3. The NEURON simulation environment

The NEURON simulation environment is a free, actively developed and supported software tool that was developed to aid the building of neuron models and neural network models and running simulations on them. It can be used to conveniently construct computationally efficient neural models based on experimentally determined biophysical and anatomical properties. When modeling a dendritic tree, the user does not have to bother writing and calculating cable equations. In NEURON, a neuron can be defined by its morphology and active and passive mechanisms. The dendritic and axonal tree, and even the soma of the model are split into short segments, so that the differential equations can be solved during the simulation numerically using the method of spatial and temporal discretization [89].

In NEURON, programming is done using the HOC programming language. Its syntax is similar to that of the widely used C-type languages, but it is extended with functions that are useful for neural and neuronal modeling and that help with the usage of its graphical user interface as well as allowing the creation of new graphical user interfaces [89]. In addition to the HOC programming language, all NEURON functions and variables are also available from Python [90].

In the NEURON simulator, the equations describing the kinetics and other properties of various mechanisms such as voltage-gated ion channels or synaptic receptors are included in MOD files, which are written in the NMODL programming language. These can be added to the model defined in the HOC file [89].

Each model tested in this study was built in the NEURON simulator.

2.4. Hippocampal CA1 pyramidal cell models in the literature

Numerous laboratories and research groups worldwide are involved in modeling hippocampal CA1 pyramidal cells. Models are usually developed specifically to reproduce only a few, or sometimes even only a single property of the real cell. New CA1 pyramidal cell models are often built by upgrading or further developing older ones, or by merging two models and modifying it to show the desired behavior. As a result, currently there are 136 models on ModelDB [18] related to the CA1 pyramidal cell, that may differ in their biophysical or anatomical complexity and were developed using different simulators and for different scientific

DOI:10.15774/PPKE.ITK.2022.001

purposes. The oldest CA1 PC model on ModelDB is the Migliore 1996 model [91], that was developed to study the mechanisms behind AP attenuation on the dendrites. The model was built in the NEURON simulator. It has a simplified morphology containing 16 compartments and involves only the main conductances that play a role in the shape and timing of action potentials (g_{Na}, g_{KDR}, g_h, g_{KM}). The author of this model and his group keep building models for different studies even today, typically by modifying and improving the previous ones. Moreover, other modeling groups also develop models based on these models or use parts of them (e.g., the implementation of different ion channels).

Nevertheless, there exist even older CA1 PC models in the literature. One of the earliest single-cell models of this cell type is the Traub & Llinás 1979 model [92] whose purpose was to integrate the basic knowledge of that time on the membrane behavior and electrophysiological properties of CA1 PCs in a model and make predictions on the mechanism of hippocampal epileptic seizures.

While most of the CA1 PC models concentrate on the reproduction of the real cell on the level of its membrane behavior and electrophysiological properties (these models are the focus of this dissertation, and will be discussed in detail in the following chapters), there are an increasing number of studies dealing with subcellular signaling pathways [93], [94], and modelling the CA1 region on a network level [95]–[97].

3. Methods

3.1 Implementation of HippoUnit

HippoUnit is a Python test suite based on the SciUnit [19] framework, which is a Python package for testing scientific models, and during its implementation the NeuronUnit package [20] was taken into account as an example of how to use the SciUnit framework for testing neuronal models. In SciUnit tests usually four main classes are implemented: the test class, the model class, the capabilities class and the score class. HippoUnit is built in a way that keeps this structure. The key idea behind this structure is the decoupling of the model implementation from the test implementation by defining standardized interfaces (capabilities) between them, so that tests can easily be used with different models without being rewritten, and models can easily be adapted to fit the framework.

Each test of HippoUnit is a separate Python class that, similarly to other SciUnit packages, can run simulations on the models to generate model *predictions,* which can be compared with experimental *observations* to yield the final score, provided that the model has the required capabilities implemented to mimic the appropriate experimental protocol and produce the same type of measurable output. All measured or calculated data that contribute to

the final score (including the recorded voltage traces, the extracted features and the calculated feature scores) are saved in JSON or pickle files (or, in many cases, in both types of files). JSON files are human readable, and can be easily loaded into Python dictionaries. Data with a more complex structure are saved into pickle files. This makes it possible to easily write and read the data (for further processing or analysis) without changing its Python structure, no matter what type of object or variable it is. In addition to the JSON files a text file (log file) is also saved, that contains the final score and some useful information or notes specific to the given test and model. Furthermore, the recorded voltage traces, the extracted features and the calculated feature scores are also plotted for visualization.

Similarly to many of the existing SciUnit packages the implementations of specific models are not part of the HippoUnit package itself. Instead, HippoUnit contains a general `ModelLoader` class. This class is implemented in a way that it is able to load and deal with most types of models defined in the HOC language of the NEURON simulator (either as standalone HOC models or as HOC templates) [89]. It implements all model-related methods (capabilities) that are needed to simulate these kinds of neural models in order to generate the prediction without any further coding required from the user.

For the smooth validation of the models developed using parameter optimization within the HBP there is a child class of the `ModelLoader` available in HippoUnit that is called `ModelLoader_BPO`. This class inherits most of the functions (especially the capability functions) from the `ModelLoader` class, but it implements additional functions that are able to automatically deal with the specific way in which information is represented and stored in these optimized models. The role of these functions is to gather all the information from the metadata and configuration files of the models that are needed to set the parameters required to load the models and run the simulations on them (such as path to the model files, name of the model template or the simulation temperature (the `celsius` variable of Neuron)). This enables the validation of these models without any manual intervention needed from the user. The section lists required by the tests of HippoUnit are also created automatically using the morphology files of these models (for details see the “Classify apical sections of pyramidal cells” subsection). For neural models developed using other software and methods, the user needs to implement the capabilities through which the tests of HippoUnit perform the simulations and recordings on the model.

The capabilities are the interface between the tests and the models. The `ModelLoader` class inherits from the capabilities and must implement the methods of the capability. The test can only be run on a model if the necessary capability methods are implemented in the `ModelLoader`. All communication between the test and the model happens through the capabilities.

DOI:10.15774/PPKE.ITK.2022.001

The methods of the score classes perform the quantitative comparison between the *prediction* and the *observation*, and return the score object containing the final score and some related data, such as the paths to the saved figure and data (JSON) files and the prediction and observation data. Although SciUnit and NeuronUnit have a number of different score types implemented, those typically compare a single *prediction* value to a single *observation* value, while the tests of HippoUnit typically extract several features from the model's response to be compared with experimental data. Therefore, each test of HippoUnit has its own score class implemented that is designed to deal with the specific structure of the output *prediction* data and the corresponding *observation* data. For simplicity, we refer to the discrepancy between the target experimental data (*observation*) and the models' behavior (*prediction*) with respect to a studied feature using the term feature score. In most cases, when the basic statistics (mean and standard deviation) of the experimental features (typically measured in several different cells of the same cell type) are available, feature scores are computed as the absolute difference between the feature value of the model and the experimental mean feature value, divided by the experimental standard deviation (absolute Z-score) [98]:

$$\text{absolute Z-score} = \text{abs}(\text{p - m\_o})/\text{SD\_o}, \tag{3.1}$$

where p is the prediction (feature value of the model), m_o is the mean of the observation (experimental mean feature value) and SD_o is the standard deviation of the observation.
The final score of a test achieved by a model is given by the average (or, in some cases, the sum) of the feature scores for all the features evaluated by the test:

$$final\ score = avg(s_1, s_2, \dots, s_n) \tag{3.2}$$

where s_i indicate the feature scores and n is the number of the features evaluated by the given test.

3.2 Implementation of the tests of HippoUnit

3.2.1 The Somatic Features Test

The Somatic Features Test uses the Electrophys Feature Extraction Library (eFEL) [99] to extract and evaluate the values of both subthreshold and suprathreshold (spiking) features from voltage traces that represent the response of the model to somatic current injections of different positive (depolarizing) and negative (hyperpolarizing) current amplitudes. Spiking features describe action potential shape (such as AP width, AP rise/fall rate, AP amplitude, etc.) and timing (frequency, inter-spike intervals, time to first/last spike, etc.), while some passive features (such as the voltage base or the steady state voltage), and subthreshold features for negative current stimuli (voltage deflection, sag amplitude, etc.) are also examined. In Figure 3.1 the meaning of some important eFEL features are illustrated.

DOI:10.15774/PPKE.ITK.2022.001

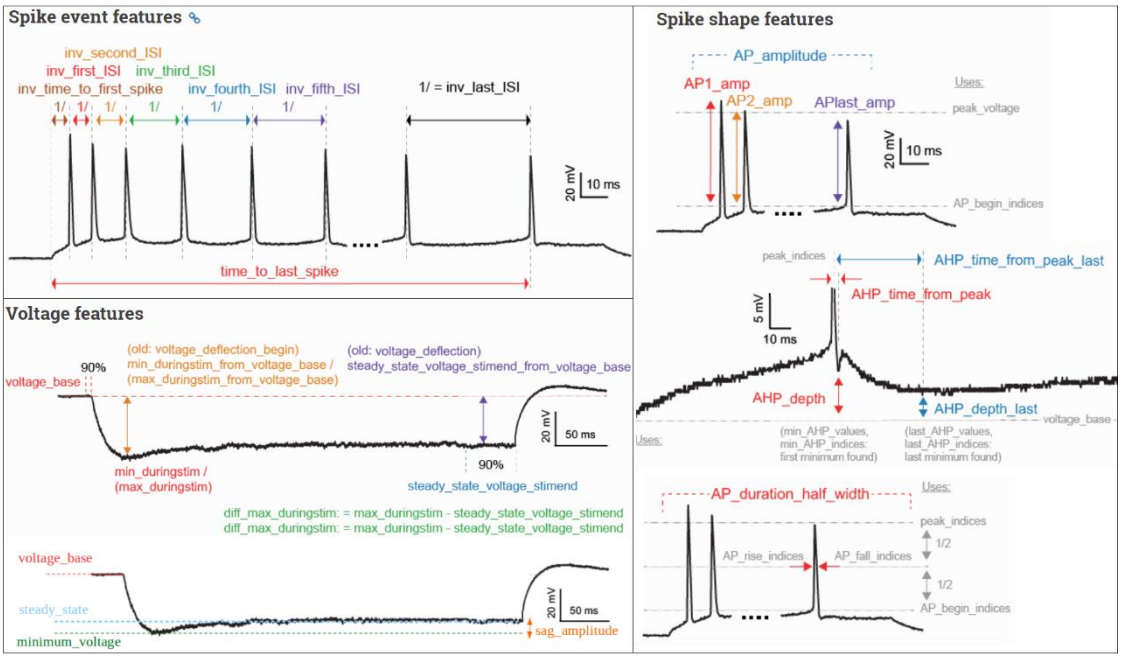

Figure 3.1: Illustration of the meaning of some important eFEL features. The figures were adapted from the documentation of eFEL: https://efel.readthedocs.io/en/latest/eFeatures.html.

In this test step currents of varying amplitudes are injected into the soma of the model and the voltage response is recorded. The simulation protocol is set according to an input configuration JSON file, which contains all the current amplitudes, the delay and the duration of the stimuli, and the stimulation and recording positions. Simulations using different current amplitudes are run in parallel if this is supported by the computing environment.

As the voltage responses of neurons to somatic current injections can strongly depend on the experimental method, and especially on the type of electrode used, target values for these features were extracted from two different datasets. One dataset was obtained from sharp electrode recordings from adult rat CA1 neurons (this will be called the sharp electrode dataset) [3], and the other dataset is from patch clamp recordings in rat CA1 pyramidal cells (data provided by Judit Makara, which will be referred to as the patch clamp dataset). For both of these datasets we had access to the recorded voltage traces from multiple neurons, which made it possible to perform our own feature extraction using eFEL. This ensures that the features are interpreted and calculated the same way for both the experimental data and the models' voltage response during the simulation. Furthermore, it allows a more thorough comparison against a large number of features extracted from experimental recordings yielded using the exact same protocol, which is unlikely to be found in any paper of the available literature. However, to see how representative these datasets are of the literature as a whole we first compared some of the features extracted from these datasets to data available on Neuroelectro.org [100] and on Hippocampome.org [101]. The features we compared were the following: resting potential, voltage threshold, after-hyperpolarization (AHP) amplitudes (fast, slow), action potential width

DOI:10.15774/PPKE.ITK.2022.001

and sag ratio. Although these databases have mean and standard deviation values for these features that are calculated from measurements using different methods, protocols and from different animals, we found that most of the feature values for our two experimental datasets fall into the ranges declared as typical for CA1 PCs in the online databases. The only conspicuous exception is the fast AHP amplitude of the patch clamp dataset used in this study, which is 1.7 ± 1.5 mV, while the databases cite values between 6.8 and 11.64 mV. This deviation could possibly stem from a difference in the way that the fast AHP is measured. However, we note that during the patch clamp recordings some of the cells were filled with a high-affinity Ca^{2+} sensor, which may have affected several Ca-sensitive mechanisms (such as Ca-dependent potassium currents) in the cell, and therefore may have influenced features like the AP width and properties of the spike after-hyperpolarization.

We also performed a more specific review of the relevant literature to compare the most important somatic features of the patch clamp dataset to results from available patch clamp recordings (Table 1). Our analysis confirmed that the values of several basic electrophysiological features such as the AP voltage threshold, the AP amplitude, the AP width, and the amplitude of the hyperpolarizing sag extracted from our patch clamp dataset fall into the range observed experimentally. We conclude that the patch clamp dataset is in good agreement with experimental observations available in the literature, and will be used as a representative example in this study.

Feature *(eFEL feature name)*	**Value in literature**	**Value in patch clamp dataset**
AP voltage threshold *(AP_begin_voltage)*	-46 - -53 mV [49], [51], [52], [54]	-51.13±0.97 mV (0.15 nA current step) -50.14±1.97 mV (0.2 nA current step) -49.36±2.02 mV (0.25 nA current step)
AP amplitude (*AP_amplitude_from_voltagebase)*	71 - 112 mV [49], [54], [102]	98.36±5.82 mV (0.15 nA current step) 96.83±5.66 mV (0.2 nA current step) 95.99±5.22 mV (0.25 nA current step)
AP width at half amplitude *(AP_duration_half_width)*	0.8 - 1.29 ms [49], [52], [54], [102]	1.23±0.096 ms (0.15 nA current step) 1.25±0.11 ms (0.2 nA current step) 1.32±0.086 ms (0.25 nA current step)
sag ratio *(sag_ratio2)*	0.84±0.02 [102], 0.83±0.01 [103]	0.79±0.023 (-0.05 nA current step) 0.81±0.03 (-0.1 nA current step) 0.81±0.027 (-0.15 nA current step) 0.81±0.03 (-0.2 nA current step) 0.80±0.03 (-0.25 nA current step)

DOI:10.15774/PPKE.ITK.2022.001

Table 3.1: Comparison of the most important somatic features extracted using eFEL from the patch clamp dataset (used as target data in the Somatic Features Test) to results from patch clamp recordings available in the literature. [Th1]

The *observation* data are loaded from a JSON file of a given format which contains the names of the features to be evaluated, the current amplitude for which the given feature is evaluated and the corresponding experimental mean and standard deviation values. The feature means and standard deviations are extracted using BluePyEfe [104] from a number of voltage traces recorded from several different cells. Its output can be converted to stimulus and feature JSON files used by HippoUnit using the script available here: https://github.com/sasaray/HippoUnit_demo/blob/master/target_features/Examples_on_creating_JSON_files/Somatic_Features/convert_new_output_feature_data_for_valid.py. Setting the `specify_data_set` parameter it can be ensured that the test results against different experimental data sets are saved into different folders.

For certain features eFEL returns a vector as a result; in these cases, the feature value used by HippoUnit is the average of the elements of the vector. These are typically spiking features for which eFEL extracts a value corresponding to each spike fired. For features that use the '*AP_begin_time*' or '*AP_begin_voltage*' feature values for further calculations, we exclude the first element of the vector output before averaging because we discovered that these features are often incorrectly detected for the first action potential of a train.

The score class of this test returns as the final score the average of *Z-scores* for the evaluated eFEL features achieved by the model. Those features that could not be evaluated (e.g., spiking features from voltage responses without any spikes) are listed in a log file to inform the user, and the number of successfully evaluated features out of the number of features attempted to be evaluated is also reported.

3.2.2 The Depolarization Block Test

This test aims to determine whether the model enters depolarization block in response to a prolonged, high intensity somatic current stimulus. For CA1 pyramidal cells, the test relies on experimental data from Bianchi et al. [25]. According to these data, rat CA1 PCs respond to somatic current injections of increasing intensity with an increasing number of action potentials until a certain threshold current intensity is reached. For current intensities higher than the threshold, the cell does not fire over the whole period of the stimulus; instead, firing stops after some action potentials, and the membrane potential is sustained at some constant depolarized level for the rest of the stimulus (see Figure 4.5A,B). This phenomenon is termed depolarization block [25].

DOI:10.15774/PPKE.ITK.2022.001

This test uses the same capability class as the Somatic Features Test for injecting current and recording the somatic membrane potential (see the description above). Using this capability, the model is stimulated with 1000 ms long square current pulses increasing in amplitude from 0 to 1.6 nA in 0.05 nA steps, analogous to the experimental protocol. The stimuli of different amplitudes are run in parallel. Somatic spikes are detected and counted using eFEL [99].

From the somatic voltage responses of the model, the following features are evaluated. I_{th} is the threshold current to reach depolarization block; experimentally, this is both the amplitude of the current injection at which the cell exhibits the maximum number of spikes, and the highest stimulus amplitude that does not elicit depolarization block. In the test two separate features are evaluated for the model and compared to the experimental I_{th}: the current intensity for which the model fires the maximum number of action potentials (*I_maxNumAP*), and the current intensity one step before the model enters depolarization block (*I_below_depol_block*). If these two feature values are not equal, a penalty is added to the score. The model is defined to exhibit depolarization block if *I_maxNumAP* is not the highest amplitude tested, and if there exists a current intensity higher than *I_maxNumAP*, for which the model does not fire action potentials during the last 100 ms of its voltage response.

In the experiment the V_{eq} feature is extracted from the voltage response of the pyramidal cells to the current injection one step above I_{th} *(or I_max_num_AP* in the test). Both in the experiment and in this test this is calculated as the mean voltage over the last 100 ms of the voltage trace. However, in the test, before calculating this value it is examined whether there are any action potentials during this period. The presence of spikes here means that the model did not enter depolarization block prior to this period. In these cases the test iterates further on the voltage traces corresponding to larger current steps to find if there is any where the model actually entered depolarization block; if an appropriate trace is found, the value of V_{eq} is extracted there. This trace is the response to the current intensity one step above *I_below_depol_block.*

If the model does not enter depolarization block, a penalty is applied, and the final score gets the value of 100. Otherwise, the final score achieved by the model on this test is the average of the feature scores (Z-scores) for the features described above, plus an additional penalty if *I_maxNumAP* and *I_below_depol_block* differ. This penalty is 200 times the difference between the two current amplitude values (in pA – which in this case is 10 times the number of examined steps between them).

$$final\ score = avg\left(s_{I\_maxNumAP},\ s_{I\_below\_depol\_block},\ s_{Veq}\right) + 200 * I\_diff\_penalty \quad (3.3)$$

where $s_{I\_maxNumAP}$, $s_{I\_below\_depol\_block}$, s_{Veq} are the feature scores of the investigated features and

$$\text{I\_diff\_penalty} = \text{abs}(I\_maxNumAP - I\_below\_depol\_block). \quad (3.4)$$

DOI:10.15774/PPKE.ITK.2022.001

3.2.3 The Back-propagating AP Test

This test evaluates the strength of action potential back-propagation in the apical trunk at locations of different distances from the soma. The observation data for this test were yielded by the digitization of Fig 1B of [27] (see Figure 4.6B), using the DigitizeIt software [105]. The values were then averaged over distances of 50, 150, 250, 350 ± 20 μm from the soma to get the mean and standard deviation of the features. The features tested here are the amplitudes of the first and last action potentials of a 15 Hz spike train, measured at the 4 different dendritic locations.

The test automatically finds current amplitudes for which the soma fires, on average, between 10-20 Hz and chooses the amplitude that leads to firing nearest to 15 Hz. For this task, the following algorithm was implemented. Increasing current step stimuli of 0.0 - 1.0 nA amplitude with a step size of 0.1 nA are applied to the model and the number of spikes is counted for each resulting voltage trace. If spontaneous spiking occurs (i.e., if there are spikes even when no current is injected) or if the spiking rate does not reach 10 Hz even for the highest amplitude, the test quits with an error message. Otherwise the amplitudes for which the soma fires between 10 and 20 Hz are appended to a list and (if the list is not empty) the one providing the spiking rate nearest to 15 Hz is chosen. If the list is empty because the spiking rate is smaller than 10 Hz for a step amplitude but higher than 20 Hz for the next step, a binary search method is used to find an appropriate amplitude in this range.

This test uses a trunk section list (or generates one if the `find_section_lists` variable of the `ModelLoader` is set to True – see the section 'Classifying the apical sections of pyramidal cells' below) to automatically find the dendritic locations for the measurements. The desired distances of the locations from the soma and the distance tolerance are read from the input configuration file, and must agree with the distances and the tolerance over which the experimental data were averaged. All the trunk dendritic segments whose distance from the soma falls into one of the distance ranges are selected. The locations and also their distances are then returned in separate dictionaries.

Then the soma is stimulated with a current injection of the previously chosen amplitude and the voltage response of the soma and the selected dendritic locations are recorded and returned.

The test implements its own function to extract the amplitudes of back-propagating action potentials, but the method is based on eFEL features. This is needed because eFEL's spike detection is based on a given threshold value for spike initiation, which may not be reached by the back-propagating signal at more distant regions. First the maximum depolarization of the first and the last action potentials are calculated. This is the maximum value of the voltage trace in a time interval around the somatic action potential, based on the start time of the spike (using

the *AP_begin_time* feature of eFEL) and the inter-spike interval to the next spike recorded at the soma. Then the amplitudes are calculated as the difference between this maximum value and the voltage at the begin time of the spike (on the soma) minus 1 ms (which is early enough not to include the rising phase of the spike, and late enough in the case of the last action potential not to include the afterhyperpolarization of the previous spike).

To calculate the feature scores the amplitude values are first averaged over the distance ranges to be compared to the experimental data and get the feature Z-scores. The final score here is the average of the Z-scores achieved for the features of first and last action potential amplitudes at different dendritic distances. In the result it is also stated whether the model is more like a strongly or a weakly propagating cell in the experiment, where they found examples of both types [27].

3.2.4 The PSP Attenuation Test

The PSP Attenuation test evaluates how much the post-synaptic potential attenuates as it propagates from different dendritic locations to the soma in rat CA1 pyramidal cell models. The *observation* data for this test were yielded by the digitization of Figure 1E (see Figure 4.7B) and Figure 2B of Magee and Cook, 2000 [29] using the DigitizeIt software [105]. The somatic and dendritic depolarization values were then averaged over distances of 100, 200, 300 ± 50 µm from the soma and the soma/dendrite attenuation was calculated to get the mean and standard deviation of the attenuation features at the three different input distances. The digitized data and the script that calculates the feature means and standard deviations, and creates the JSON file are available here: https://github.com/sasaray/HippoUnit_demo/tree/master/target_features/Examples_on_creating_JSON_files/Magee2000-PSP_att/.

In this test the apical trunk receives excitatory post-synaptic current (EPSC)-shaped current stimuli at locations of different distances from the soma. The maximum depolarization caused by the input is extracted at the soma and divided by the maximum depolarization at the location of the stimulus to get the soma/dendrite attenuation values that are then averaged in distance ranges of 100, 200, 300 ± 50 µm and compared to the experimental data. The distances and tolerance are defined in the configuration file and must agree with how the *observation* data were generated.

The test uses a trunk section list, which needs to be specified in the NEURON HOC model (or the test generates one if the `find_section_lists` variable of the `ModelLoader` is set to True – see the section 'Classify apical sections of pyramidal cells' below) to find the dendritic locations to be stimulated. Randomly selected dendritic locations are used because the distance ranges that are evaluated cover almost the whole length of the trunk of a pyramidal cell.

DOI:10.15774/PPKE.ITK.2022.001

The probability of selecting a given dendritic segment is set to be proportional to its length. The number of dendritic segments examined can be chosen by the user by setting the `num_of_dend_locations` argument of the test. The random seed (also an argument of the test) must be kept constant to make the selection reproducible. If a given segment is selected multiple times (or it is closer than 50 μm or further than 350 μm), a new random number is generated. If the number of locations to be selected is more than the number of trunk segments available in the model, all the segments are selected.

The *Exp2Syn* synaptic model of NEURON with a previously calculated weight is used to stimulate the dendrite. The desired EPSC amplitude and time constants are given in the input configuration file according to the experimental protocol. To get the proper synaptic weight, first the stimulus is run with weight = 0. The last 10% of the trace is averaged to get the resting membrane potential (Vm). Then the synaptic weight required to induce EPSCs with the experimentally determined amplitude is calculated according to Equation 3.1:

$$\text{weight} = - \text{EPSC\_amp} / \text{Vm} \tag{3.1}$$

where EPSC_amp is read from the config dictionary, and the synaptic reversal potential is assumed to be 0 mV.

To get the somatic and dendritic maximum depolarization from the voltage traces, the baseline trace (weight = 0) is subtracted from the trace recorded in the presence of the input. To get the attenuation ratio the maximum value of the somatic depolarization is divided by the maximum value of the dendritic depolarization.

To calculate the feature scores the soma/dendrite attenuation values are first averaged over the distance ranges to be compared to the experimental data to get the feature Z-scores. The final score is the average of the feature scores calculated at the different dendritic locations.

3.2.5 The Oblique Integration Test

This test evaluates the signal integration properties of radial oblique dendrites, determined by providing an increasing number of synchronous (0.3 ms between inputs, as in the glutamate uncaging experiment, 0.2 ms long laser pulses are used with 0.1 ms interval between them) or asynchronous (2.2 ms between inputs) clustered synaptic inputs. The experimental mean and standard error (SE) of the features examined are available in the paper of Losonczy and Magee [33] and are read from a JSON file into the *observation* dictionary of the test. The SE values are then converted to standard deviation values. The following features are tested: voltage threshold for dendritic spike initiation (defined as the expected somatic depolarization at which a step-like increase in peak dV/dt occurs); proximal threshold (defined the same way as above, but including only those results in the statistics where the proximal part of the examined dendrite was stimulated); distal threshold; degree of nonlinearity at threshold;

suprathreshold degree of nonlinearity; peak derivative of somatic voltage at threshold; peak amplitude of somatic EPSP; time to peak of somatic EPSP; degree of nonlinearity in the case of asynchronous inputs.

The test automatically selects a list of oblique dendrites that meet the criteria of the experimental protocol, based on a section list containing the oblique dendritic sections (this can either be provided by the HOC model, or generated automatically if the `find_section_lists` variable of the `ModelLoader` is set to True – see the section 'Classify apical sections of pyramidal cells' below). For each selected oblique dendrite a proximal and a distal location is examined. The criteria for the selection of dendrites, which were also applied in the experiments, are the following. The selected oblique dendrites should be terminal dendrites (they have no child sections) and they should be at most 120 μm from the soma. This latter criterion can be changed by the user by changing the value of the `ModelLoader`'s *`max_dist_from_soma`* variable, and it can also increase automatically if needed. In particular, if no appropriate oblique is found up to the upper bound provided, the distance is increased iteratively by 15 μm, but not further than 190 μm.

Then an increasing number of synaptic inputs are activated at the selected dendritic locations separately, while recording the local and somatic voltage response. HippoUnit provides a default synapse model to be used in the `ObliqueIntegrationTest`. If the `AMPA_name`, and *`NMDA_name`* variables are not set by the user, the default synapse is used. In this case the AMPA component of the synapse is given by the built-in `Exp2Syn` synapse of NEURON, while the NMDA component is defined in an NMODL (.mod) file which is part of the HippoUnit package. This NMDA receptor model uses a Jahr-Stevens voltage dependence [106] and rise and decay time constants of 3.3 and 102.38 ms, respectively. The time constant values used here are temperature- (Q10-) corrected values from [54]. Q10 values for the rise and decay time constants were 2.2 [107] and 1.7 [108], respectively. The model's own AMPA and NMDA receptor models can also be used in this test if their NMODL files are available and compiled among the other mechanisms of the model. In this case the `AMPA_name`, and `NMDA_name` variables need to be provided by the user. The time constants of the built-in Exp2Syn AMPA component and the AMPA/NMDA ratio can be adjusted by the user by setting the *AMPA_tau1, AMPA_tau2* and `AMPA_NMDA_ratio` parameter of the `ModelLoader`. The default AMPA/NMDA ratio is 2.0 from [54], and the default AMPA_tau1 and AMPA_tau2 are 0.1 ms and 2.0 ms, respectively [29], [30].

To test the Poirazi et al. 2003 model using its own receptor models, we also had to implement a modified version of the synapse functions of the ModelLoader that can deal with the different (pointer-based) implementation of synaptic activation in this model. For this purpose, a child class was implemented that inherits from the ModelLoader class. This modified

version is not part of the official HippoUnit version, because this older, more complicated implementation of synaptic models is not generally used anymore; however, this is a good example on how one can modify the capability methods of HippoUnit to match their own models or purposes. The code for this modified ModelLoader is available here: https://github.com/KaliLab/HippoUnit_demo/blob/master/ModelLoader_Poirazi_2003_CA1.py.

The synaptic weights for each selected dendritic location are automatically adjusted by the test using a binary search algorithm so that the threshold for dendritic spike generation is 5 synchronous inputs – which was the average number of inputs that had to be activated by glutamate uncaging to evoke a dendritic spike in the experiments [33]. This search runs in parallel for all selected dendritic locations. The search interval of the binary search and the initial step size of the searching range can be adjusted by the user through the `c_minmax` and `c_step_start` variables of the `ModelLoader`. During the iterations of the algorithm the step size may decrease if needed; a lower threshold for the step size (`c_step_stop` variable of the `ModelLoader`) must be set to avoid infinite looping. Those dendritic locations where this first dendritic spike generates a somatic action potential, or where no dendritic spike can be evoked, are excluded from further analysis. To let the user know, this information is displayed on the output and also printed into the log file saved by the test. Most of the features above are extracted at the threshold input level (5 inputs).

The final score of this test is the average of the feature scores achieved by the model for the different features; however, a T-test analysis is also available as a separate score type for this test.

3.3 Parallel computing

Most of the tests of HippoUnit require multiple simulations of the same model, either using stimuli of different intensities or at different locations in the cell. To run these simulations in parallel and save time, the Python `multiprocessing.Pool` module is used. The size of the pool can be set by the user. Moreover, all NEURON simulations are performed in multiprocessing pools to ensure that they run independently of each other, and to make it easy to erase the models after the process has finished. This is especially important in the case of HOC templates in order to avoid previously loaded templates running in the background and the occurrence of 'Template cannot be redefined' errors when the same model template is loaded again.

DOI:10.15774/PPKE.ITK.2022.001

3.4 Classifying the apical sections of pyramidal cells

Some of the validation tests of HippoUnit require lists of sections belonging to the different dendritic types of the apical tree (main apical trunk, apical tuft dendrites, and radial oblique dendrites). To classify the dendrites NeuroM [109] is used as a base package. NeuroM contains a script that, starting from the tuft (uppermost dendritic branches in Fig 1) endpoints, iterates down the tree to find a single common ancestor. This is considered as the apical point. The apical point is the upper end of the main apical dendrite (trunk), from where the tuft region arises. Every dendrite branching from the trunk below this point is considered an oblique dendrite.

However, there are many CA1 pyramidal cell morphologies where the trunk bifurcates close to the soma to form two or even more branches. In these cases the method described above finds this proximal bifurcation point as the apical point (see Figure 3.2A). To overcome this issue, we worked out and implemented a method to find multiple apical points by iterating the function provided by NeuroM. In particular, if the initial apical point is closer to the soma than a pre-defined threshold, the function is run again on subtrees of the apical tree where the root node of the subtree is the previously found apical point, to find apical points on those subtrees (see Figure 3.2B). When (possibly after multiple iterations) apical points that are far enough from the soma are found, NeuroM is used to iterate down from them on the parent sections, which will be the trunk sections (blue dots in Figure 3.2C). Iterating up, the tuft sections are found (green dots in Figure 3.2C), and the other descendants of the trunk sections are considered to be oblique dendrites (yellow dots in Figure 3.2C). Once all the sections are classified, their NeuroM coordinates are converted to NEURON section information for further use.

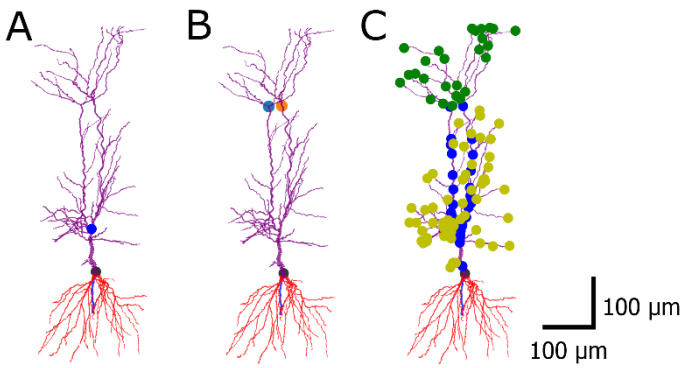

Figure 3.2: Classifying the apical dendrites of pyramidal cells. Morphological reconstruction made within the HBP at University College London (UCL). The soma is marked in black, the red dendrites underneath are the basal dendrites, apical dendrites are colored purple. (A) The original method of NeuroM finds a single apical point which is actually a bifurcation of the trunk. (B) Further developing the method, multiple apical points can be found. (C) The apical dendritic sections are classified. Blue: trunk, yellow: oblique dendrites, green: tuft sections. [Th1]

We note that this function can only be used for hoc models that load their morphologies from a separate morphology file (e.g., ASC, SWC) as NeuroM can only deal with morphologies provided in these standard formats. For models with NEURON morphologies implemented directly in the hoc language, the SectionLists required by a given test should be implemented within the model.

3.5 Models from literature

In this paper we demonstrate the utility of the HippoUnit validation test suite by applying its tests to validate and compare the behavior of several different detailed rat hippocampal CA1 pyramidal cell models available on ModelDB [18]. For this initial comparison we chose models published by several modeling groups worldwide that were originally developed for various purposes. The models compared were the following: the Golding et al., 2001 model [27] (ModelDB accession number: 64167), the Katz et al., 2009 model [68] (ModelDB accession number: 127351), the Migliore et al., 2011 model [110] (ModelDB accession number: 138205), the Poirazi et al., 2003 model [6], [79] (ModelDB accession number: 20212), the Bianchi et al., 2012 model [25] (ModelDB accession number: 143719), and the Gómez González et al., 2011 [111] model (ModelDB accession number: 144450).

Models from literature that are published on ModelDB typically implement their own simulations and plots to make it easier for users and readers to reproduce and visualize the results shown in the corresponding paper. Therefore, to be able to test the models described above using our test suite, we needed to create standalone versions of them. These standalone versions do not display any GUI, or contain any built-in simulations and run-time modifications, but otherwise their behavior should be identical to the published version of the models. We also added section lists of the radial oblique and the trunk dendritic sections to those models where this was not done yet, as some of the tests require these lists. To ensure that the standalone versions have the same properties as the original models, we checked their parameters after running their built-in simulations (in case they include any run-time modifications), and made sure they match the parameters of the standalone version. The modified models used for running validation tests are available in this GitHub repository: https://github.com/KaliLab/HippoUnit_demo.

DOI:10.15774/PPKE.ITK.2022.001

4. Results

4.1 The HippoUnit validation suite

HippoUnit (https://github.com/KaliLab/hippounit) is an open source test suite for the automatic and quantitative evaluation of the behavior of neural single cell models. The tests of HippoUnit automatically perform simulations that mimic common electrophysiological protocols on neuronal models to compare their behavior with quantitative experimental data using various feature-based error functions. Current validation tests cover somatic (subthreshold and spiking) behavior as well as signal propagation and integration in the dendrites. These tests were chosen because they collectively cover diverse functional aspects of cellular behavior that have been thoroughly investigated in experimental and modeling studies, and particularly because the necessary experimental data were available in sufficient quality and quantity. However, we note that the currently implemented tests, even in combination, probably do not fully constrain the behavior of the cell under all physiological conditions, and thus the test suite can be further improved by including additional tests and more experimental data. The tests were developed using data and models for rat hippocampal CA1 pyramidal cells. However, most of the tests are directly applicable to or can be adapted for other cell types if the necessary experimental data are available; examples of this will be presented in later sections.

HippoUnit is implemented in the Python programming language, and is based on the SciUnit [19] framework for testing scientific models. The current version of HippoUnit is capable of handling single cell models implemented in the NEURON simulator, provided that they do not apply any runtime modification, do not have a built-in graphical user interface, and do not automatically perform simulations. Meeting these conditions may require some modifications in the published code of the model. Once such a “standalone” version of the model is available, the tests of HippoUnit can be run by adapting and using the example Jupyter notebooks described in the Appendix, without any further coding required from the user. In principle, neural models developed using other software tools can also be tested by HippoUnit; however, this requires the re-implementation by the user of the interface functions that allow HippoUnit to run the necessary simulations and record their output (see the Methods section for more details).

In the current tests of HippoUnit, once all the necessary simulations have been performed and the responses of the model have been recorded, electrophysiological features are extracted from the voltage traces, and the discrepancy between the model’s behavior and the experiment is computed by comparing the feature values with those extracted from the experimental data (see Methods). Biological variability is taken into account by measuring the difference between the feature value for the model and the mean of the feature in the experiments

in units of the standard deviation for that particular feature observed in the experiments. For simplicity, we refer to the result of this comparison as the feature score; however, we note that there are many possible sources of such discrepancy including, among others, experimental artefacts and noise, shortcomings of the models, and differences between the conditions assumed by the models and those in the actual experiments (see the Discussion for more details). The final score of a given test achieved by a given model is given by the average (or, in some cases, the sum) of the feature scores for all the features evaluated by the test.

While the main output of the tests is the final score, which allows the quantitative comparison of the models' behavior to experimental data, it is important to emphasize that it should never be blindly accepted. A high final score does not necessarily mean that the model is bad – it may also indicate an issue with the data, a mismatch between experimental conditions and modeling assumptions, or some problem with the implementation of the test itself (see the Discussion for further details). For this reason, and also to provide more insight into how the scores were obtained, the tests of HippoUnit typically provide a number of other useful outputs (see Methods), including figures that visualize the model's behavior through traces and plot the feature and feature score values compared to the experimental data. It is always strongly recommended to look at the traces and other figures to get a fuller picture of the model's response to the stimuli, which helps with the correct interpretation of validation results. Such closer inspection also makes it possible to detect possible test failures, when the extraction of certain features does not work correctly for a given model.

HippoUnit can also take advantage of the parallel execution capabilities of modern computers. When tests require multiple simulations of the same model using different settings (e.g., different stimulation intensities or different stimulus locations in the cell), these simulations are run in parallel, which can make the validation process substantially faster, depending on the available computing resources.

One convenient way of running a test on a model is to use an interactive computational notebook, such as the Jupyter Notebook [112], which enables the combination of program codes to be run (we used Python code to access the functionality of HippoUnit), the resulting outputs (e.g. figures, tables, text) and commentary or explanatory text in a single document. Therefore, we demonstrate the usage of HippoUnit through this method (See Appendix and https://github.com/KaliLab/HippoUnit_demo).

DOI:10.15774/PPKE.ITK.2022.001

4.2 Comparison of the behavior of rat hippocampal CA1 pyramidal cell models selected from the literature

We selected six different publications containing models of rat hippocampal CA1 pyramidal cells whose implementations for the NEURON simulator were available in the ModelDB database. Our aim was to compare the behavior of every model to the experimental target data using the tests of HippoUnit, which also allowed us to compare the models to each other, and to test their generalization performance in paradigms that they were not originally designed to capture. These models differ in their complexity regarding the number and types of ion channels that they contain, and they were built for different purposes.

The Golding et al., 2001 model [27] was developed to show the dichotomy of the back-propagation efficacy and the amplitudes of the back-propagating action potentials at distal trunk regions in CA1 pyramidal cells and to make predictions on the possible causes of this behavior. It contains only the most important ion channels (Na, K_{DR}, K_A) needed to reproduce the generation and propagation of action potentials. [27] Three different versions of the model were tested. The one belonging to the Fig. 8 A of the corresponding paper shows weak action potential backpropagation. The Na, K_{DR} channels are uniformly distributed on its apical dendrites, while the density of the K_A channel increases linearly in the first 300 μm of the apical dendrites reaching a maximum density of four-fold higher than on the soma. Adding a slight positive gradient to the sodium channel density turned the model into strongly propagating. This model is shown in Fig. 8B of the paper. Decreasing the gradient of the K_A channel density while keeping the distribution of Na channels uniform, turned the original model into strongly propagating (Fig. 9B of Golding et al. 2001) [27].

The Katz et al., 2009 model [68] is based on the Golding et al. 2001 model (containing the same ion channels: Na, K_{DR}, K_A) and was built to investigate the functional consequences of the distribution of strength and density of synapses on the apical dendrites that they observed experimentally, for the mode of dendritic integration. In this model the Na and K_{DR} conductances are uniformly distributed in the dendrites, while the density of the K_A channel increases along the main apical dendrite, and uniformly distributed on the oblique dendrites with the value at their branching point [68].

The Migliore et al., 2011 model [110] was used to study schizophrenic behavior. It is based on earlier models of the same modeling group, which were used to investigate the initiation and propagation of action potentials in oblique dendrites, and have been validated against different electrophysiological data. The Na and K_{DR} ion channels are uniformly distributed in the dendrites of this model, while the density of the K_A and Ih conductances increase linearly with distance from the soma.

DOI:10.15774/PPKE.ITK.2022.001

The Poirazi et al., 2003 model [6], [79] was designed to clarify the issues about the integrative properties of thin apical dendrites that may arise from the different and sometimes conflicting interpretations of available experimental data. This is a quite complex model in the sense that it contains a large number of different types of ion channels and conductances (leak current, two kinds (somatic/axonic and dendritic) of Na, K_{DR} and two kinds (proximal, distal) of K_A currents, K_M and h-current, T-type, R-type and L-type Ca^{2+} and two types of Ca^{2+}-dependent potassium currents), whose properties were adjusted to fit in vitro experimental data. The model also contains four types of synaptic receptors.

The Bianchi et al., 2012 model [25] was designed to investigate the mechanisms behind depolarization block observed experimentally in the somatic spiking behavior of rat CA1 pyramidal cells. It was developed by combining and modifying the Shah et al., 2008 [113] and the Poirazi et al. 2003 models [6], [79]. The former of these was developed to show the significance of axonal M-type potassium channels, therefore the K_A and K_M currents are those whose kinetic properties and distribution were adapted from the Shah et al. model, while others were inherited from the Poirazi et al. model.

The Gómez González et al., 2011 [111] model is based on the Poirazi et al. 2003 model and it was modified to replicate the experimental data of [33] on the nonlinear signal integration of radial oblique dendrites when the inputs arrive in a short time window.

A common property of these models is that their parameters were set using manual procedures with the aim of reproducing the behavior of real rat CA1 PCs in one or a few specific paradigms. As some of them were built by modifying and further developing previous models, these share the same morphology (see Figure 4.1). On the other hand, the model of Gómez González et al. 2011 was adjusted to 5 different morphologies, which were all tested. In the case of the Golding et al. 2001 model, we tested three different versions (shown in Figs 8A, 8B and 9A of the corresponding paper [27]) that differ in the distribution of the sodium and the A-type potassium channels, and therefore the back-propagation efficacy of the action potentials. The morphologies and characteristic voltage responses of all the models used in this comparison are displayed in Figure 4.1.

DOI:10.15774/PPKE.ITK.2022.001

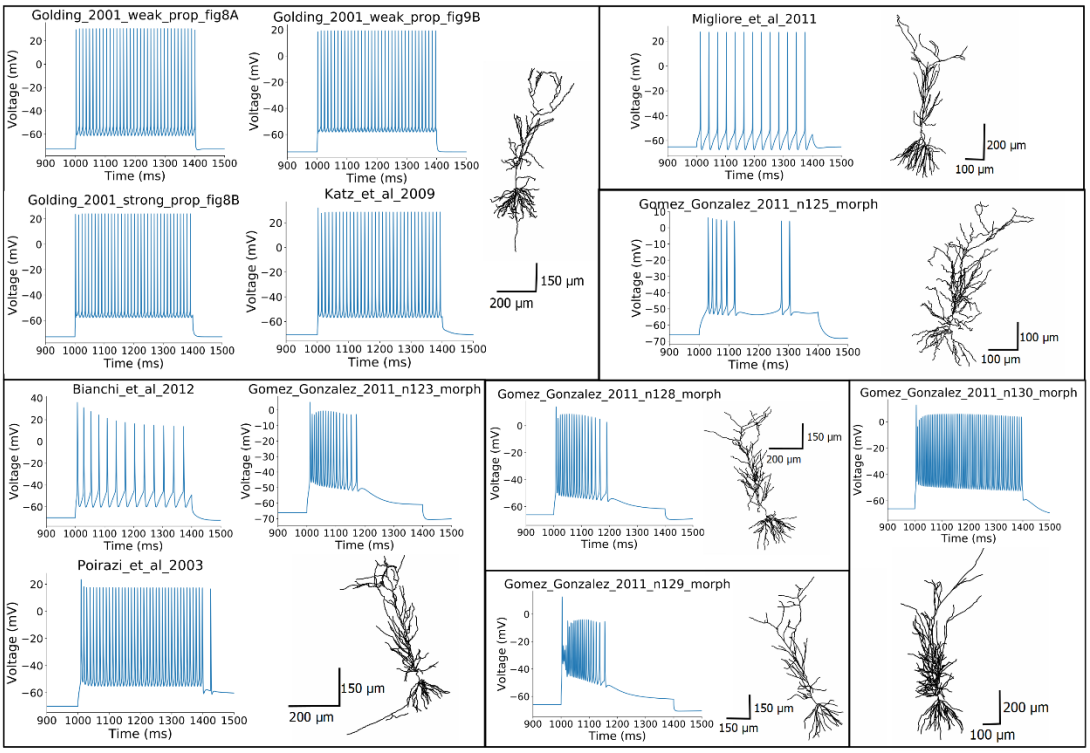

Figure 4.1: The morphologies of the different models tested and their voltage responses to a 400 ms somatic step current injection of 0.6 nA amplitude. (Some of the models share the same morphology, while the Gómez González et al. 2011 model was adjusted to five different morphologies.) [Th1]

Running the tests of HippoUnit on these models we took into account the original settings of the simulations of the models, and set the `v_init` (the initial voltage when the simulation starts), and the `celsius` (the temperature at which the simulation is done) variables accordingly. For the Bianchi et al 2012 model we used variable time step integration during all the simulations, as it was done in the original modeling study. For the other models a fixed time step were used (dt=0.025 ms).

4.2.1 Somatic Features Test

Using the Somatic Features Test of HippoUnit, we compared the behavior of the models to features extracted from the patch clamp dataset, as each of the tested models was apparently constructed using experimental data obtained from patch clamp recordings as a reference. After performing a review of the relevant literature, we concluded that the patch clamp dataset is in good agreement with experimental observations available in the literature (see Table 1 in Methods), and will be used as a representative example in this study.

In the patch clamp recordings, both the depolarizing and the hyperpolarizing current injections were 300 ms long and 0.05, 0.1, 0.15, 0.2, 0.25 nA in amplitude. Because during these recordings the cells were stimulated with relatively low amplitude current injections, some of

DOI:10.15774/PPKE.ITK.2022.001

the examined models (Migliore et al. 2011, Gómez González et al. 2011 n125 morphology) did not fire even for the highest amplitude tested. Some other models started to fire for higher current intensities than it was observed experimentally. In these cases the features that describe action potential shape or timing properties cannot be evaluated for the given model (for the current amplitudes affected). Therefore, besides the final score achieved by the models on this test (the average Z-score for the successfully evaluated features – see Methods for details) that shows the discrepancy of the models' behavior and the experimental observations regarding the successfully evaluated features, we also consider the proportion of the successfully evaluated features as an important measure of how closely the model matches this specific experimental dataset. This information, along with the names of the features that cannot be evaluated for the given model, are provided as outputs of the test, and should be considered when making conclusions on the model's performance. This is another example where looking at only the final score may not be enough to determine whether the model meets the requirements of the user, and shows how the other outputs of the tests can help the interpretation of the results.

Figure 4.2 shows how the extracted feature values of the somatic response traces of the different models fit the experimental values. It is clear that the behavior of the different models is very diverse. Each model captures some of the experimental features but shows a larger discrepancy for others.

DOI:10.15774/PPKE.ITK.2022.001

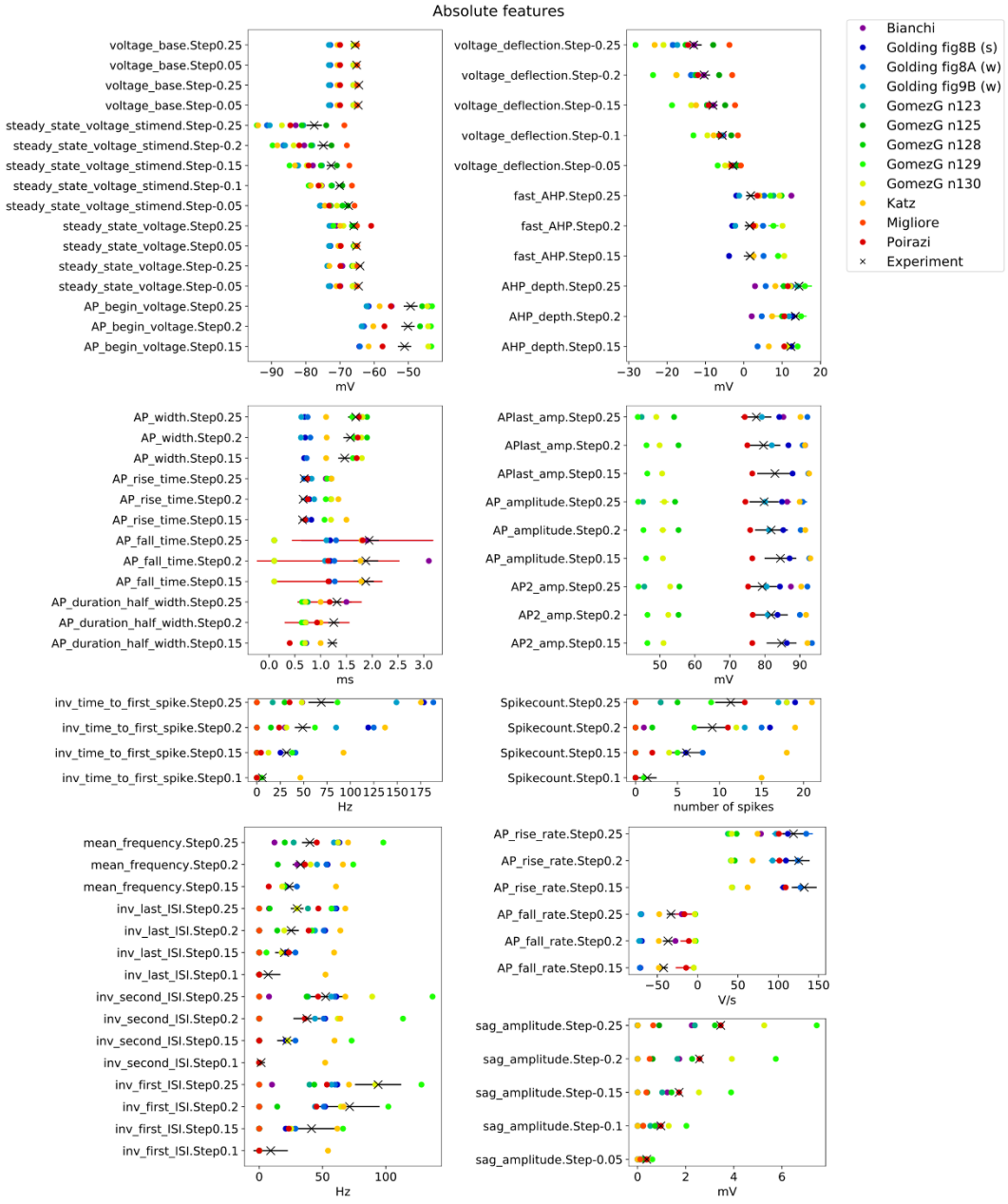

Figure 4.2: Feature values from the Somatic Features Test of HippoUnit applied to several published models. Absolute feature values extracted (using the electrophys Feature Extraction Library (eFEL)) from the voltage responses of the models to somatic current injections of varying amplitude, compared to mean experimental values (black X) that were extracted from the patch clamp dataset. Black solid, horizontal lines indicate the experimental standard deviation. Colored solid, horizontal lines typically show the standard deviation of spiking features of models, where the feature value of each action potential in the voltage trace is extracted and averaged. Feature names (y axis labels) are indicated as they are used in eFEL combined with the step current injection amplitude. Not all the evaluated features are shown here. (The (s) and (w) notations of the Golding et al. 2001 models in the legend indicate the strong and weak propagating versions of the model.) [Th1]

DOI:10.15774/PPKE.ITK.2022.001

The resting membrane potential (*voltage_base*) for all of the models was apparently adjusted to a more hyperpolarized value than in the experimental recordings we used for our comparison, and most of the models also return to a lower voltage value after the step stimuli (*steady_state_voltage*). An exception is the Poirazi et al. 2003 model, where the decay time constant after the stimulus is unusually high (this feature is not included in Figure 4.2, but the slow decay can be seen in the example trace in Figure 4.1, and detailed data are available here: https://github.com/KaliLab/HippoUnit_demo). The voltage threshold for action potential generation (*AP_begin_voltage*) is lower than the experimental value for most of the models (that were able to generate action potentials in response to the examined current intensities), but it is higher than the experimental value for most versions of the Gómez González et al. 2011 model. For negative current steps most of the models gets more hyperpolarized (*voltage_deflection*) (the most extreme is the Gómez González et al. 2011 model with the n129 morphology), while the Gómez González et al. 2011 model with the n125 morphology and the Migliore et al. 2011 model get less hyperpolarized than it was observed experimentally. The sag amplitudes are also quite high for the Gómez González et al. 2011 n129, and n130 models, while the Katz et al. 2009, and all versions of the Golding et al. 2001 models basically have no hyperpolarizing sag.

It is quite conspicuous how much the amplitude of the action potentials (*APlast_amp, AP_amplitude, AP2_amp*) differs in the Gómez González et al. 2011 models from the experimental values and from the other models as well. The Katz et al. 2009 and one of the versions ("Fig 8A") of the Golding et al. 2001 model have slightly too high action potential amplitudes, and these models have relatively small action potential width (*AP_width*). On the other hand, the rising phase (*AP_rise_time, AP_rise_rate*) of the Katz et al. 2009 model appears to be too slow.

Looking at the inverse interspike interval (*ISI*) values, it can be seen that the experimental spike trains show adaptation in the ISIs, meaning that the first ISI is smaller (the inverse ISI is higher) than the last ISI for the same current injection amplitude. This behavior can be observed in the case of the Katz et al. 2009 model, three versions (n128, n129, n130 morphology) of the Gómez González et al. 2011 model, but cannot really be seen in the Bianchi et al. 2011, the Poirazi et al. 2003 and the three versions of the Golding et al. 2001 models. At first look it may seem contradictory that in the case of the Gómez González et al. 2011 model version n129 morphology the spike counts are quite low, while the mean frequency and the inverse ISI values are high. This is because the soma of this model does not fire over the whole period of the stimulation, but starts firing at higher frequencies, then stops firing for rest of the stimulus (see Figure 4.1). The Katz et al. 2009 model fires quite a high number of action potentials (*Spikecount*) compared to the experimental data, at a high frequency.

In the experimental recordings there is a delay before the first action potential is generated, which becomes shorter with increasing current intensity (indicated by the

inv_time_to_first_spike feature that becomes larger with increasing input intensity). In most of the models this behavior can be observed, albeit to different degrees. The Katz et al. 2009 model has the shortest delays (highest *inv_time_to_first_spike* values), but the effect is still visible.

To quantify the difference between the experimental dataset and the simulated output of the models, these were compared using the feature-based error function (Z-Score) described above to calculate the feature score. Figure 4.3A shows the mean scores of the model features whose absolute values are illustrated in Figure 4.2 (averaged over the different current step amplitudes examined), while Figure 4.3B indicates the number of successfully evaluated features out of the number of features that were attempted to be evaluated. From Figure 4.3A it is even more clearly visible that each model fits some experimental features well but does not capture others. For example, it is quite noticeable in Figure 4.3A that most of the versions of the Gómez González et al. 2011 model (greenish dots) perform well for features describing action potential timing (upper part of the figure, e.g., *ISIs, mean_frequency*, *spikecount*), but get higher feature scores for features of action potential shape (lower part of the figure, e.g., *AP_rise_rate, AP_rise_time, AP_fall_rate, AP_fall_time, AP amplitudes*). Conversely, the Katz et al. 2009 model achieved better scores for AP shape features than for features describing AP timing. It is also worth noting that none of the feature scores for the model of Migliore et al. 2011 was higher than 4; however, looking at Figure 4.3B it can be seen that less than half of the experimental features were successfully evaluated in this model, which is because it does not fire action potentials for the current injection amplitudes examined here. As mentioned above the proportion of the successfully evaluated features is also an important measure of how well the behavior of the models fits the specific experimental observations, and should be taken into account.

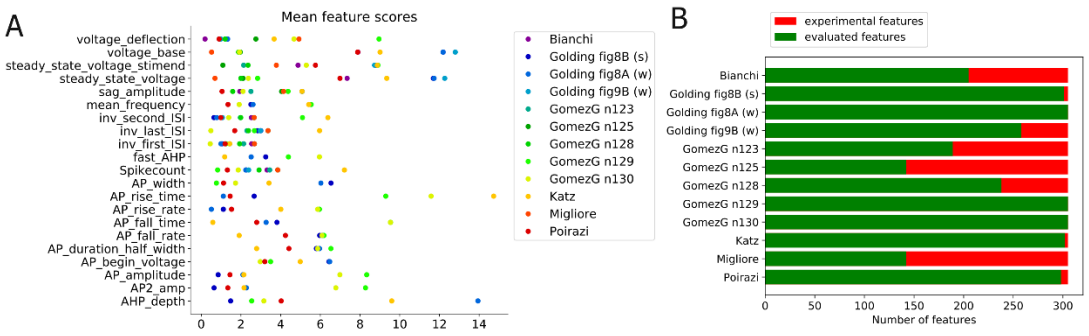

Figure 4.3: Evaluation of results from the Somatic Features Test of HippoUnit applied to published models. (A) Mean feature scores (the difference between the model's feature value and the experimental mean in units of the experimental SD) of the different models. Feature score values are averaged over the different input step amplitudes. (B) The bars represent the number of features that were attempted to be evaluated for the models (i.e., the number of features extracted from the experimental patch clamp dataset). The number of successfully evaluated features for the various models is shown in green, and the

DOI:10.15774/PPKE.ITK.2022.001

number of features that could not be evaluated for a particular model is shown in red. Features that are not evaluated successfully are most often spiking features at step amplitudes for which the tested model does not fire action potentials. [Th1]

Besides enabling the comparison of different models regarding how well they match a particular dataset, the tests of HippoUnit also allow one to determine the match between a particular model and several datasets of the same type. As experimental results can be heavily influenced by recording conditions and protocols, and also depend on factors such as the strain, age, and sex of the animal, it is important to find out whether the same model can simultaneously capture the outcome of different experiments, and if not, how closely it is able to match the different datasets. As a practically relevant example, we looked at how well the various published models that we were testing captured a different experimental dataset that also contained current clamp recordings from rat CA1 PCs, but which was obtained using sharp electrodes rather than the whole-cell patch clamp technique [3]. We therefore evaluated all the models with the Somatic Features Test of HippoUnit using both datasets, and then compared the results.

When we simply compared the raw outputs of the test for each model evaluated using the two different data sets (Fig 5A) we identified two factors that substantially bias the results. First, we found that the standard deviation values for the features extracted from the two datasets are very different in magnitude; more specifically, the patch clamp recording data set had much lower standard deviation values for most of the features. This results in relatively higher feature scores achieved by the models, as the difference of the model output from the experimental features is given in the unit of the experimental standard deviation. The other source of bias is that the two datasets were recorded not only using different recording methods – patch clamp and sharp electrode – but (partly as a consequence) also using different protocols (current amplitudes, current duration etc.), and therefore provide different sets of features. As an important example, voltage traces with and without action potentials clearly provide different types of features. Also note that the same electrophysiological parameter can often be extracted from multiple voltage traces, and these are all treated as separate features in the test, so a difference in the number of recorded traces automatically leads to a difference in the set of features. Consequently, the models are not compared to exactly the same set of features in the two cases. Mainly as a result of these two confounding factors, comparison of the raw scores of the models for the two data sets (Figure 4.4A) appears to indicate that most models fit the dataset obtained from sharp electrode recordings better, even though these models were typically built mostly based on patch clamp data.

DOI:10.15774/PPKE.ITK.2022.001

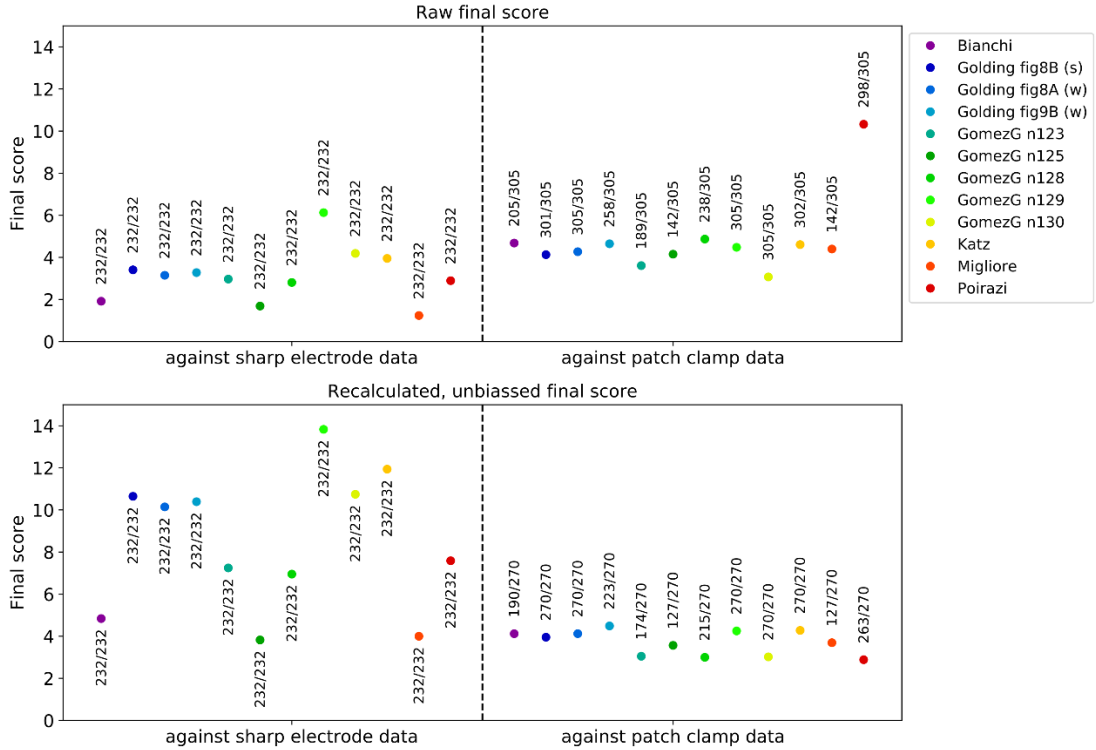

Figure 4.4: Comparison of the final scores achieved by the different models on the Somatic Features Test against validation data from two different datasets (sharp electrode data, patch clamp data). Final scores are calculated as the average of all the feature scores. In the upper panel (A) the raw output of the tests is shown, while in the lower panel (B) the feature scores and the final scores have been recalculated using standardized standard deviation values. Numbers above each data point show the proportion of the successfully evaluated features compared to the number of features attempted to be evaluated (successfully extracted from the data set). Note that while in the recalculated final scores (B) only those eFEL features were taken into account that could be extracted from both datasets, they are extracted for different current step amplitudes, which accounts for the difference in the number of observation features for the two datasets.

To overcome these issues and make unbiased comparisons of the models to the two datasets, the feature scores and the final scores were recalculated in the following way (Figure 4.4B). The new feature scores for the two different data sets were calculated as the difference of the model's feature value from the mean feature value of each dataset (as before), but divided by a common standard deviation value. This standardized SD value for each eFEL feature was the mean of the standard deviation values over the current steps in the patch clamp dataset (the results were qualitatively similar if we used the SD values from the sharp electrode dataset everywhere instead). Averaging the standard deviation values of the eFEL features over the current steps was required because the current step amplitudes were not the same in the two data sets, and we therefore needed to define SD values that were independent of the amplitude. To get rid of the second bias, only those eFEL features were used in the final score recalculation that are present in both observations (sharp electrode and patch clamp datasets) for at least one

DOI:10.15774/PPKE.ITK.2022.001

current step amplitude. (This change had the side effect of significantly decreasing the final score for the Poirazi et al. 2003 model because the feature *decay_time_constant_after_stim* was excluded here, as it could not be extracted from the sharp electrode data.) Now that the final scores are recalculated to get rid of most of the biasing factors, it becomes clear that the somatic behavior of every model fits the patch clamp data better (Figure 4.4B).

It is worth noting that one biasing factor still remains in the last comparison: as it has already been mentioned, not all the observation features can be evaluated for each of the models, especially when they are compared to the patch clamp data set, which uses smaller currents. To allow the assessment of the potential effect of this issue, the proportion of the successfully evaluated features relative to the number of features attempted to be evaluated (successfully extracted from the data set) for each model is also shown in Figure 4.4 next to each data point.

4.2.2 Depolarization Block Test

In the Depolarization Block Test three features are evaluated. Two of them examine the threshold current intensity to reach depolarization block. The *I_maxNumAP* feature is the current intensity at which the model fires the maximum number of action potentials, and the *I_below_depol_block* feature is the current intensity one step before the model enters depolarization block. Both are compared to the experimental I_{th} feature because, in the experiment [25], the number of spikes increased monotonically with increasing current intensity up to the current amplitude where the cell entered depolarization block during the stimulus, which led to a drop in the number of action potentials (see Figure 4.5A). By contrast, we experienced that some models started to fire fewer spikes for higher current intensities while still firing over the whole period of the current step stimulus, i.e., without entering depolarization block. Therefore, we introduced the two separate features for the threshold current. If these two feature values are not equal, a penalty is added to the score. The third evaluated feature is V_{eq}, the equilibrium potential during the depolarization block, which is calculated as the average of the membrane potential over the last 100 ms of a current pulse with amplitude 50 pA above *I_maxNumAP* (or 50 pA above *I_below_depol_block* if its value is not equal to *I_maxNumAP*). Each model has a value for the *I_maxNumAP* feature, while those models that do not enter depolarization block are not supposed to have a value for the *I_below_depol_block* feature and the *Veq* feature.

The results from applying the Depolarization Block Test to the models from ModelDB are shown in Figure 4.5. According to the test, four of the models entered depolarization block. However, by looking at the actual voltage traces provided by the test, it becomes apparent that only the Bianchi et al. 2011 model behaves correctly (which was developed to show this behavior). The other three models actually managed to “cheat” the test.

DOI:10.15774/PPKE.ITK.2022.001

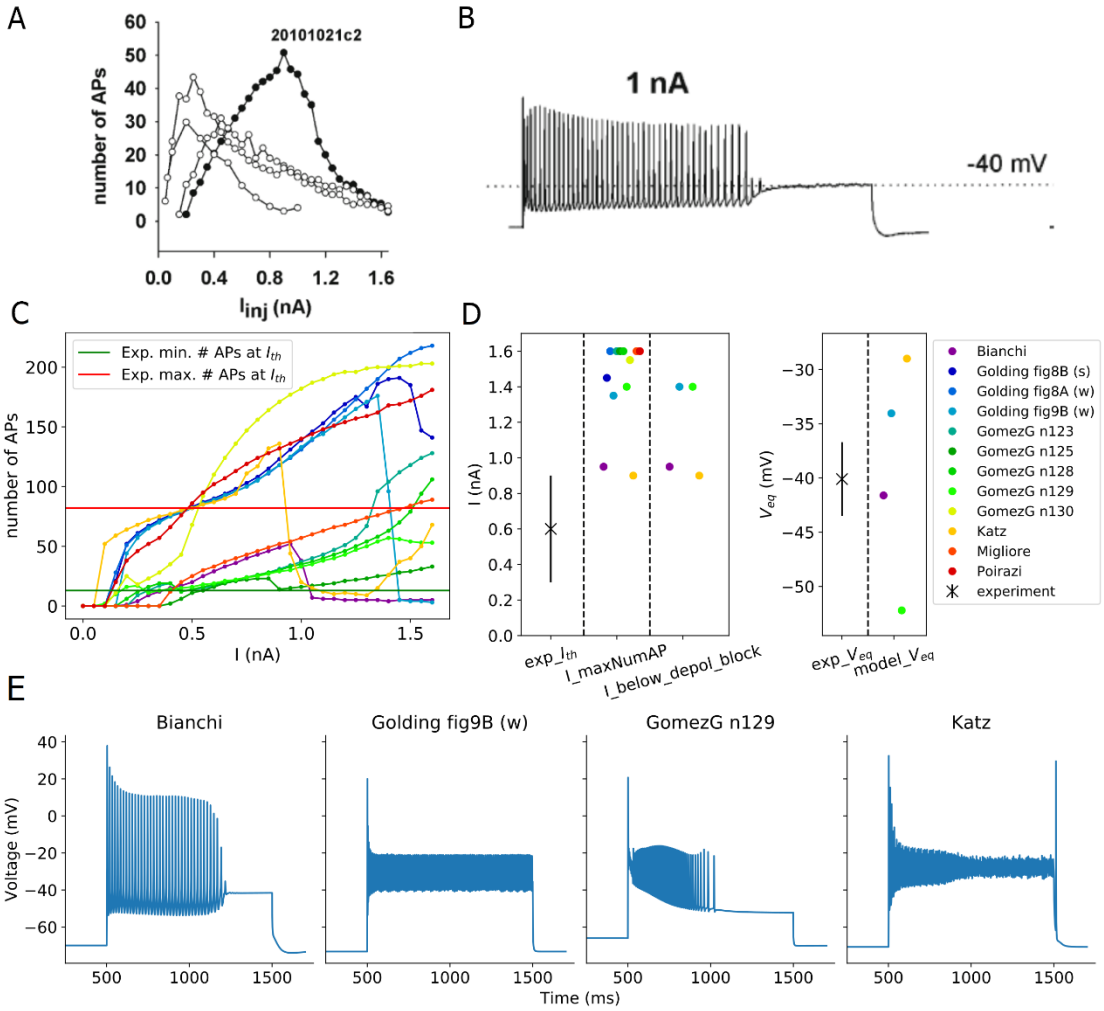

Figure 4.5: Results from the Depolarization Block Test of HippoUnit applied to published models. (A) Average number of action potentials from 4 cells (3 repetitions each) to 1 sec somatic current injection in the target experimental data. (B) Example voltage trace of a cell that entered depolarization block and reached an equilibrium potential of -40 mV in the target experiment. Panels (A) and (B) were adapted from Bianchi et al. 2012 [25]. (C) Number of APs fired by the models in response to 1 sec long somatic current injections of increasing intensity. (D) Depolarization block feature values extracted from the voltage responses of the models compared to the experimental observations. exp_I_{th} is the mean (SD is indicated with a solid line) of the experimentally observed threshold current amplitude to reach depolarization block. In the test two separate features are compared to the experimental threshold value: The I_maxNumAP feature is the current intensity at which the model fires the maximum number of action potentials, and the I_below_depol_block feature is the current intensity one step before the model enters depolarization block. According to the experimental observation, these two values are supposed to be the same, but for models, they may differ, in which case a penalty is added to the final score (see the text for more details). The V_{eq} is the equilibrium potential to which the somatic voltage settles after entering depolarization block. (E) Voltage traces of different models that were recognized by the test as

DOI:10.15774/PPKE.ITK.2022.001

depolarization block. Note that only the Bianchi et al. 2012 model actually entered depolarization block, the others "cheated" the test (see the main text for more details). [Th1]

In the case of the Katz et al. 2009 and the Golding et al. 2001 "Fig 9B" models, the APs get smaller and smaller with increasing stimulus amplitude until they get so small that they do not reach the threshold for action potential detection; therefore, these APs are not counted by the test and V_{eq} is also calculated. The Gómez González et al. 2011 model adjusted to the n129 morphology does not fire during the whole period of the current stimulation for a wide range of current amplitudes (see Figure 4.1). Increasing the intensity of the current injection it fires an increasing number of spikes, but always stops after a while before the end of the stimulus. On the other hand, there is a certain current intensity after which the model starts to fire fewer action potentials, and which is thus detected as *I_maxNumAP* by the test. Because no action potentials can be detected during the last 100 ms of the somatic response one step above the detected "threshold" current intensity, the model is declared to have entered depolarization block, and a V_{eq} value is also extracted.

In principle, it would be desirable to modify the test so that it correctly rejects the three models above. However, the models described above shows so similar behavior to depolarization block that is hard to distinguish using automatic methods. Furthermore, we have made substantial efforts to make the test more general and applicable to a wide variety of models with different behavior, and we are concerned that defining and adding further criteria to the test to deal with these specific cases would be an ad hoc solution, and would possibly cause further 'cheats' when applied to other models with unexpected behavior. These cases underline the importance of critically evaluating the full output (especially the figures of the recorded voltage traces) of the tests rather than blindly accepting the final scores provided.

4.2.3 Back-propagating Action Potential Test

This test first finds all the dendritic segments that belong to the main apical dendrite of the model and which are 50, 150, 250, 350 ± 20 μm from the soma, respectively. Then a train of action potentials of frequency around 15 Hz is triggered in the soma by injecting a step current of appropriate amplitude (as determined by the test), and the amplitudes of the first and last action potentials in the train are measured at the selected locations. In the Bianchi et al. 2012 and the Poirazi et al. 2003 models (which share the same morphology, see Figure 4.1) no suitable trunk locations could be found in the most proximal (50 ± 20 μm) and most distal (350 ± 20 μm) regions. This is because this morphology has quite long dendritic sections that are divided into a small number of segments. In particular, the first trunk section (apical_dendrite[0]) originates from the soma, is 102.66 μm long, and has only two segments. The center of one of them is 25.67 μm far from the soma, while the other is already 77 μm away from the soma.

DOI:10.15774/PPKE.ITK.2022.001

None of these segments belongs to the 50 ± 20 µm range, and therefore they are not selected by the test. The n123 morphology of the Gómez González et al. 2011 model has the same shape (Figure 4.1), but in this case the segments are different, and therefore it does not share the same problem.

At the remaining, successfully evaluated distance ranges in the apical trunk of the Bianchi et al. 2012 model, action potentials propagate very actively, barely attenuating. For the *AP1_amp* and *APlast_amp* features at these distances, this model has the highest feature score (Figure 4.6), while the Poirazi et al. 2003 model performs quite well.

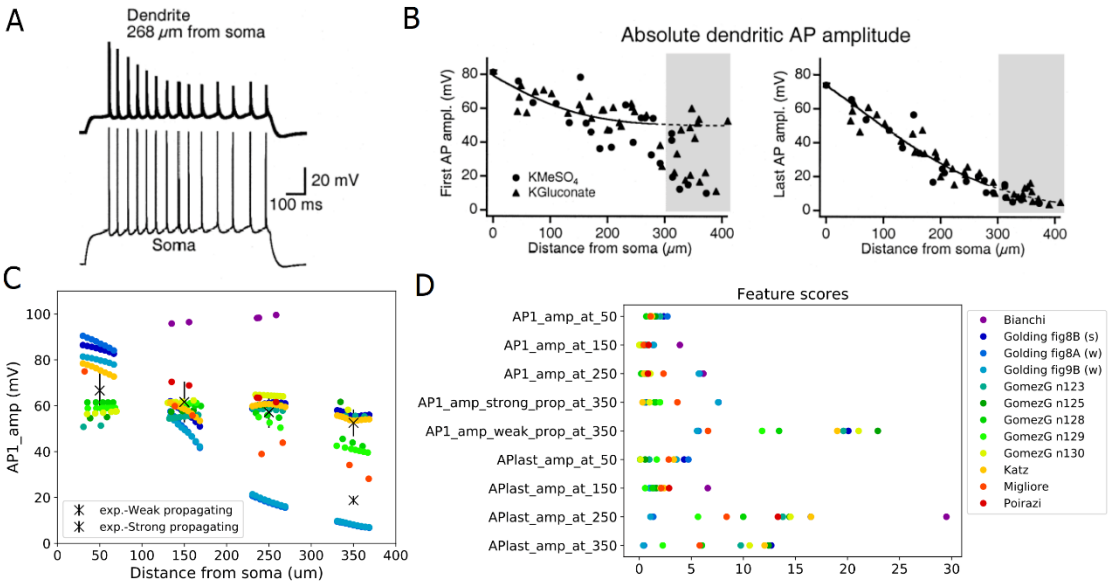

Figure 4.6: Results from the Back-propagating Action Potential Test of HippoUnit applied to published models. (A) Example experimental voltage traces triggered by somatic current injection and simultaneously recorded from the soma and the trunk. (B) The amplitude of the first (left) and last (right) back-propagating action potentials in a 10 to 20 Hz train triggered by somatic current injection as a function of the distance of the recording location from the soma in the target experiment. Panels (A) and (B) were adapted from Golding et al. 2001 [27]. (C) The amplitudes of the first back-propagating action potentials (in a train of spikes with frequency around 15 Hz evoked by somatic current injection) of the different models as a function of recording location distance from the soma. (D) Feature scores achieved by the different models on the Back-propagating AP Test. The amplitudes of the first and last back-propagating action potentials were averaged over the distance ranges of 50, 150, 250, 350 ± 20 µm and compared to the experimental features (see Methods for more details). [Th1]

The Golding et al. 2001 model was designed to investigate how the distribution of ion channels can affect the back-propagation efficacy in the trunk. The two versions of the Golding et al. 2001 model ("Fig 8A" and "Fig 9B" versions) which are supposed to be weakly propagating according to the corresponding paper [27], are also weakly propagating according to the test. However, the difference between their strongly and weakly propagating feature

DOI:10.15774/PPKE.ITK.2022.001

scores is not too large (Figure 4.6), which is probably caused by the much smaller standard deviation value of the experimental data for the weakly propagating case. Although the amplitudes of the first action potentials of these two models fit the experimental data relatively well, they start to decline slightly closer to the soma than it was observed experimentally, as the amplitudes are already very small at 250 ± 20 μm (Figure 4.6). (In Figure 4.6 the data corresponding to these two versions of the model are almost completely overlapping for more distal regions.) The amplitudes for the last action potential fit the data well, except in the most proximal regions (see the relatively high feature score in Figure 4.6D or the detailed results here: https://github.com/KaliLab/HippoUnit_demo). For all versions of the Golding et al. 2001 model, AP amplitudes are too high at the most proximal distance range. As for the strongly propagating version of the Golding et al. 2001 model ("Fig 8B" version), the amplitude of the first action potential is too high at the proximal locations, but further it fits the data well. The amplitude of the last action potential remains too high even at more distal locations. It is worth noting that, in the corresponding paper [27], they only examined a single action potential triggered by a 5 ms long input in their simulations, and did not examine or compare to their data the properties of the last action potential in a longer spike train. Finally, we note that in all versions of the Golding et al. 2001 model a spike train with frequency around 23 Hz was evoked and examined as it turned out to be difficult to set the frequency closer to 15 Hz.

The different versions of the Gómez González et al. 2011 model behave qualitatively similarly in this test, although there were smaller quantitative differences. In almost all versions the amplitudes of the first action potential in the dendrites are slightly too low at the most proximal locations but fit the experimental data better at further locations. The exceptions are the versions with the n128 and n129 morphologies, which have lower first action potential amplitudes at the furthest locations, but not low enough to be considered as weak propagating. The amplitudes for the last action potential are too high at the distal regions but fit better at the proximal ones. The only exception is the one with morphology n129, where the last action potential attenuates more at further locations and fits the data better.

In the case of the Katz et al. 2009 model, a spike train with frequency around 40 Hz was examined, as the firing frequency increases so suddenly with increasing current intensity in this model that no frequency closer to 15 Hz could be adjusted. In this model the last action potential propagates too strongly, while the dendritic amplitudes for the first action potential are close to the experimental values.

In the Migliore et al. 2011 model the amplitudes for the last action potential are too high, while the amplitude of the first back-propagating action potential is too low at locations in the 250 ± 20 μm and 350 ± 20 μm distance ranges.

DOI:10.15774/PPKE.ITK.2022.001

Finally, all the models that we examined were found to be strongly propagating by the test, with the exception of those versions of the Golding et al. 2001 model that were explicitly developed to be weakly propagating.

4.2.4 PSP Attenuation Test

In this test the extent of the attenuation of the amplitude of an excitatory post-synaptic potential (EPSP) is examined as it propagates towards the soma from different input locations in the apical trunk. The Katz et al. 2009, the Bianchi et al. 2012, and all versions of the Golding et al. 2001 models perform quite well in this test (Figure 4.7C). The various versions of the Golding et al. 2001 model are almost identical in this respect, which is not surprising as they differ only in the distribution of the sodium and A-type potassium channels. This shows that, as we would expect, these properties do not have much effect on the propagation of relatively low-amplitude signals such as unitary PSPs. Interestingly, the different versions of the Gómez González et al. 2011 model, with different morphologies, behave quite differently, which shows that this behavior can depend very much on the morphology of the dendritic tree.

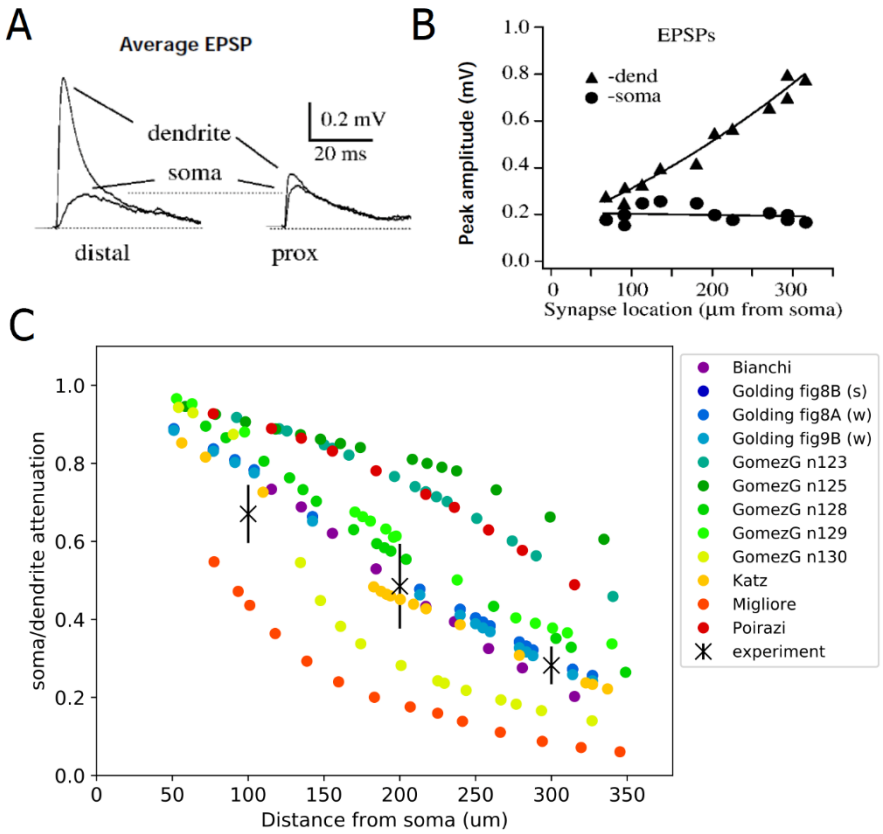

Figure 4.7: Results from the PSP Attenuation Test of HippoUnit applied to published models. (A) The experimental averages of the EPSPs recorded at the dendritic input site and the soma. (B) Mean peak amplitude of EPSPs measured simultaneously at the soma and the dendrite as a function of the synaptic

input distance from the soma in the target experiment. The soma/dendrite attenuation values that are used for the quantitative comparison were calculated from these data. Panels (A) and (B) were adapted from Magee and Cook 2000 [29]. (C) Soma/dendrite EPSP attenuation as a function of the synaptic input distance from the soma in the different models. [Th1]

4.2.5 Oblique Integration Test

This test probes the integration properties of the radial oblique dendrites of rat CA1 pyramidal cell models. The test is based on the experimental results described in [33]. In this study, the somatic voltage response was recorded while synaptic inputs in single oblique dendrites were activated in different spatio-temporal combinations using glutamate uncaging. The main finding was that a sufficiently high number of synchronously activated and spatially clustered inputs produced a supralinear response consisting of a fast (Na) and a slow (NMDA) component, while asynchronously activated inputs summed linearly or sublinearly.

This test selects all the radial oblique dendrites of the model that meet the experimental criteria: they are terminal dendrites (they have no child sections) and are at most 120 μm from the soma. Then the selected dendrites are stimulated in a proximal and in a distal region (separately) using an increasing number of clustered, synchronous or asynchronous synaptic inputs to get the voltage responses of the model, and extract the features of dendritic integration. The synaptic inputs are not unitary inputs, i.e., their strength is not equivalent to the strength of one synapse in the real cell; instead, the strength is adjusted in a way that 5 synchronous inputs are needed to trigger a dendritic action potential. The intensity of the laser used for glutamate uncaging was set in a similar way in the experiments [33]. Most of the features were extracted at this just-suprathreshold level of input. We noticed that in some cases the strength of the synapse is not set correctly by the test; for example, it may happen that an actual dendritic spike does not reach the spike detection threshold in amplitude, or sometimes the EPSP may reach the threshold for spike detection without actual spike generation. The user has the ability to set the threshold used by eFEL for spike detection, but sometimes a single threshold may not work even for the different oblique dendrites (and proximal and distal locations in the same dendrites) of a single model. For consistency, we used the same spike detection threshold of -20 mV for all the models.

The synaptic stimulus contains an AMPA and an NMDA receptor-mediated component. As the default synapse, HippoUnit uses the Exp2Syn double exponential synapse built into NEURON for the AMPA component, and its own built-in NMDA receptor model, whose parameters were set according to experimental data from the literature (see the Methods section for more details). In those models that originally do not have any synaptic component (the Bianchi et al 2011 model and all versions of the Golding et al. 2001 model) this default synapse

DOI:10.15774/PPKE.ITK.2022.001

was used. Both the Katz et al. 2009 and the Migliore et al. 2011 models used the Exp2Syn in their simulations, so in their case the time constants of this function were set to the values used in the original publications. As these models did not contain NMDA receptors, the default NMDA receptor model and the default AMPA/NMDA ratio of HippoUnit were used. The Gómez González et al 2011 and the Poirazi et al. 2003 models have their own AMPA and NMDA receptor models and their own AMPA/NMDA ratio values to be tested with.

As shown by the averaged "measured EPSP vs expected EPSP" curves in Figure 4.8E, all three versions of the Golding et al. 2001 model have a jump in the amplitude of the somatic response at the threshold input level, which is the result of the generation of dendritic spikes. However, in two of these models, even these larger average responses do not reach the supralinear region, as it would be expected according to the experimental observations [33]. The reason for this discrepancy is that a dendritic spike was generated in the simulations in only a subset of the stimulated dendrites; in the rest of the dendrites tested, the amplitude of the EPSPs went above the spike detection threshold during the adjustment of the synaptic weight without actually triggering a dendritic spike, which led to the corresponding synaptic strength being incorrectly set for that particular dendrite. Averaging over the results for locations with and without dendritic spikes led to an overall sublinear integration profile.

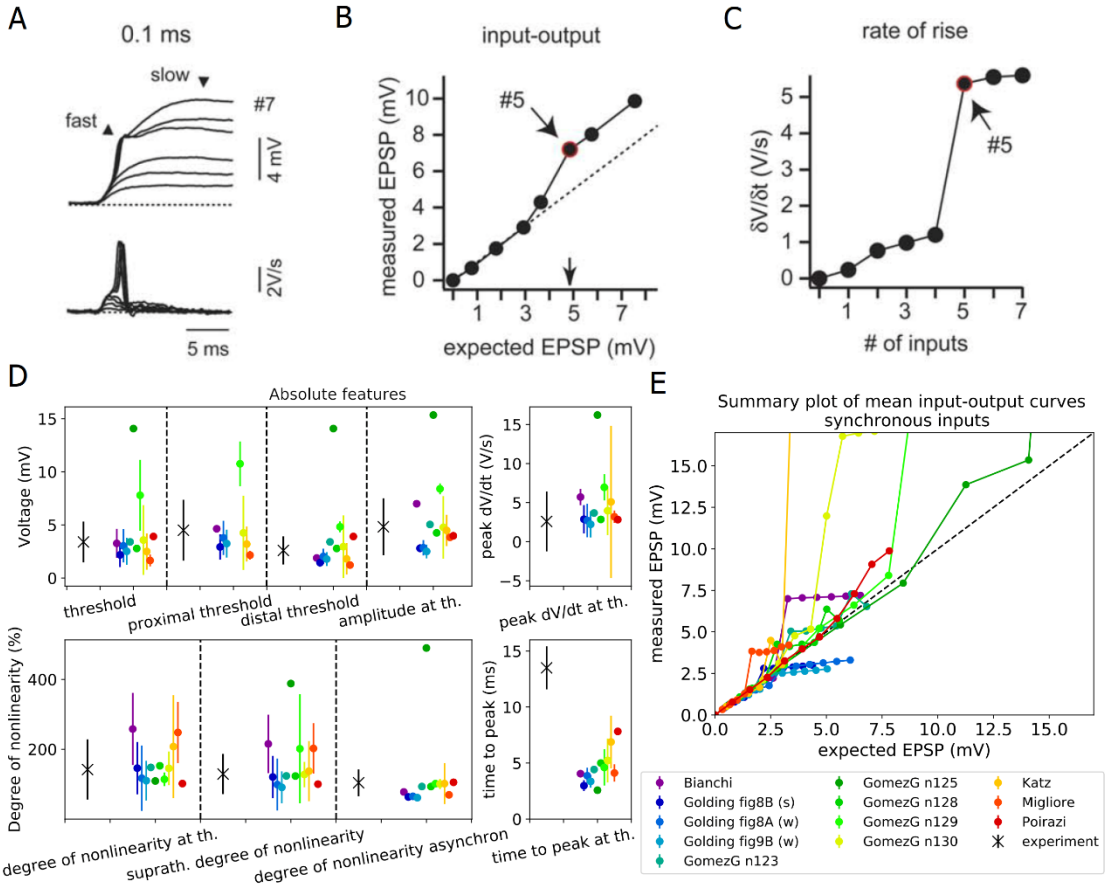

Figure 4.8: Results from the Oblique Integration Test of HippoUnit applied to published models. (A) Example experimental recording of somatic EPSPs to an increasing number of synchronous synaptic

DOI:10.15774/PPKE.ITK.2022.001

inputs showing the fast component that is the result of the generation of a sodium spike on the dendrite (top) and the first temporal derivatives of the same traces (bottom). (B) Experimental supralinear input-output curve of synchronous synaptic inputs to the oblique dendrites. (C) Peak derivative values versus the number of synchronous inputs in the target experiment showing a step increase at the input level of dendritic spike generation. Panels (A)-(C) were adapted from Losonczy and Magee 2006 [33] (D) Comparison of the responses of the models to experimental results (black X) according to features of dendritic integration. Features values are given as mean and standard deviation, as several dendritic locations of each model are tested. (E) The averaged input – output curves of all the dendritic locations of the models examined. EPSP amplitudes are measured at the soma. Dashed line shows linearity. In models whose curve goes above the dashed line, oblique dendrites integrate synaptic inputs that are spatially and temporally clustered supralinearly. [Th1]

The Migliore et al. 2011 model performs quite well on this test. In this case, seven dendrites could be tested out of the ten dendrites within the correct distance range because, in the others, the dendritic spike at the threshold input level also elicited a somatic action potential, and therefore these dendrites were excluded from further testing.

In the Katz et al. 2009 model all the selected dendritic locations could be tested, and in most of them the synaptic strength could be adjusted appropriately. For a few dendrites, some input levels higher than the threshold for dendritic spike generation also triggered somatic action potentials. This effect causes the high supralinearity in the “measured EPSP vs expected EPSP” curve, but has no effect on the extracted features.

In the Bianchi et al. 2012 model only one dendrite could be selected, in which very high amplitude dendritic spikes were evoked by the synaptic inputs, making the signal integration highly supralinear.

In the Poirazi et al. 2003 model also only one dendrite could be selected based on its distance from the soma; furthermore, only the distal location could be tested even in this dendrite, as at the proximal location the dendritic action potential at the threshold input level generated a somatic action potential. However, at the distal location, the synaptic strength could not be set correctly. For the synaptic strength chosen by the test, the actual threshold input level where a dendritic spike is first generated is at 4 inputs, but this dendritic AP is too small in amplitude to be detected, and the response to 5 inputs is recognized as the first dendritic spike instead. Therefore, the features that should be extracted at the threshold input level are instead extracted from the voltage response to 5 inputs. In this model this results in a reduced *supralinearity* value, as this feature is calculated one input level higher than the actual threshold. In addition, for even higher input levels dendritic bursts can be observed, which causes large *supralinearity* values in the “measured EPSP vs expected EPSP” curve in Figure 4.8E, but this does not affect the feature values.

DOI:10.15774/PPKE.ITK.2022.001

Models from Gómez González et al. 2011 were expected to be particularly relevant for this test, as these models were tuned to fit the same data set on which this test is based. However, we encountered an important issue when comparing our test results for these models to the results shown in the paper [111]. In particular, the paper clearly indicates which dendrites were examined, and it is stated that those are at maximum 150 μm from the soma. However, when we measured the distance of these locations from the soma by following the path along the dendrites (as it is done by the test of HippoUnit), we often found it to be larger than 150 μm. We note that when the distance was measured in 3D coordinates rather than along the dendrites, all the dendrites used by Gómez González et al. 2011 appeared to be within 150 μm of the soma, so we assume that this definition was used in the paper. As we consider the path distance to be more meaningful than Euclidean distance in this context, and this was also the criterion used in the experimental study, we consistently use path distance in HippoUnit to find the relevant dendritic segments. Nevertheless, this difference in the selection of dendrites should be kept in mind when the results of this validation for models of Gómez González et al. 2011 are evaluated.

In three versions of the Gómez González et al. 2011 model (those that were adjusted to the n123, n125 and n128 morphologies) only one oblique dendrite matched the experimental criteria and could therefore be selected, and these are not among those that were studied by the developers of the model. In each of these cases the dendritic spike at the proximal location at the input threshold level triggered a somatic action potential, and therefore only the distal location could be tested. In the case of the n125 morphology, the dendritic spikes that appear first for just-suprathreshold input are so small in amplitude that they do not reach the spike detection threshold (-20 mV), and are thus not detected. Therefore, the automatically adjusted synaptic weight is larger than the appropriate value would be, which results in larger somatic EPSPs than expected (see Figure 4.8E). With this synaptic weight, the first dendritic spike and therefore the jump to the supralinear region in the “measured EPSP vs expected EPSP” curve is for 4 synaptic inputs instead of 5. Similarly to the Poirazi et al. 2003 model, this results in a lower *degree of nonlinearity at threshold* feature value, than it would be if the feature were extracted at the actual threshold input level (4 inputs) instead of the one which the test attempted to adjust (5 inputs). The *suprathreshold nonlinearity* feature has a high value because at that input level (6 inputs), somatic action potentials are triggered.

In the version of the Gómez González et al. 2011 model that uses the n129 morphology, 10 oblique dendrites could be selected for testing (none of them is among those that its developers used) but only 2 could be tested because, for the rest, the dendritic spike at the threshold input level already elicits a somatic action potential. The synaptic weights required to set the threshold input level to 5 are not found correctly in most cases; the actual threshold input level is at 4 or 3. Suprathreshold nonlinearity is high, because at that input level (6 inputs) somatic action potentials are triggered for some of the examined dendritic locations.

DOI:10.15774/PPKE.ITK.2022.001

The version of the Gómez González et al. 2011 model that uses the n130 morphology achieves the best (lowest) final score on this test. In this model many oblique dendrites could be selected and tested, including two (179, 189) that the developers used in their simulations [111]. In most cases the synaptic weights are nicely found to set the threshold input level to 5 synapses. For some dendrites there are somatic action potentials at higher input levels, but that does not affect the features.

The value of the *time to peak* feature for each model is much smaller than the experimental value (Figure 4.8D). This is because in each of the models the maximum amplitude of the somatic EPSP is determined by the fast component, caused by the appearance of the dendritic sodium spikes, while in the experimental observation this is rather shaped by the slow NMDA component following the sodium spike.

4.2.6 Overall characterization and model comparison based on all tests of HippoUnit

In summary, using HippoUnit, we compared the behavior of several rat hippocampal CA1 pyramidal cell models available on ModelDB in several distinct domains, and found that all of these models match experimental results well in some domains (typically those that they were originally built to capture) but fit the experimental observations less precisely in others. Figure 4.9 summarizes the final scores achieved by the different models on the various tests (lower scores indicate a better match in all cases).

DOI:10.15774/PPKE.ITK.2022.001

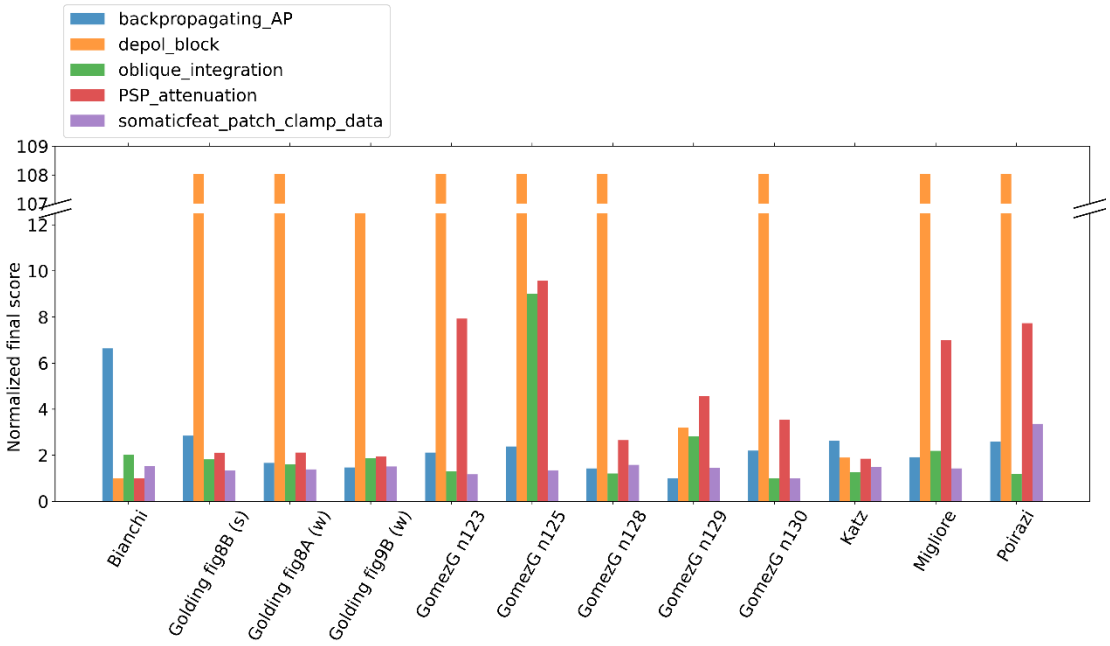

Figure 4.9: Normalized final scores achieved by the different published models on the various tests of HippoUnit. The final scores of each test are normalized by dividing the scores of each model by the best achieved score on the given test. [Th1]

Perhaps a bit surprisingly, the different versions of the Golding et al. 2001 model showed a good match to the experimental data in all of the tests (except for the Depolarization Block Test), even though these are the simplest ones among the models in the sense that they contain the smallest number of different types of ion channels. On the other hand, these models do not perform outstandingly well on the Back-propagating Action Potential Test, although they were developed to study the mechanisms behind (the dichotomy of) action potential back-propagation, which is evaluated by this test based on the data that were published together with these models [27]. The most probable reason for this surprising observation is that, in the original study [27], only a few features of the model's response were compared with the experimental results. HippoUnit tested the behavior of the model based on a larger set of experimental features from the original study, and was therefore able to uncover differences between the model's response and the experimental data on features for which the model was not evaluated in the source publication.

The Bianchi et al. 2012 model is the only one that can produce real depolarization block within the range of input strengths examined by the corresponding test. The success of this model in this test is not surprising because this is the only model that was tuned to reproduce this behavior; on the other hand, the failure of the other models in this respect clearly shows that proper depolarization block requires some combination of mechanisms that are at least partially distinct from those that allow good performance in the other tests. The Bianchi et al. 2012 model achieves a relatively high final score only on the Back-propagating Action Potential Test, as

action potentials seem to propagate too actively in its dendrites, leading to high AP amplitudes even in more distal compartments.

The Gómez González et al. 2011 models were developed to capture the same experimental observations on dendritic integration that are tested by the Oblique Integration Test of HippoUnit, but, somewhat surprisingly, some of its versions achieved quite high feature scores on this test, while others perform quite well. This is partly caused by the fact that HippoUnit often selects different dendritic sections for testing from those that were studied by the developers of these models (see above for details). The output of HippoUnit shows that the different oblique dendrites of these models can show quite diverse behavior, and beyond those studied in the corresponding paper [111], other oblique dendrites do not necessarily match the experimental observations. Some of its versions also perform relatively poorly on the PSP-Attenuation Test, similar to the Migliore et al. 2011 and the Poirazi et al. 2003 models. The Katz et al. 2009 model is not outstandingly good in any of the tests, but still achieves relatively good final scores everywhere (although its apparent good performance on the Depolarization Block Test is misleading - see detailed explanation above).

The model files that were used to test the models described above, the detailed validation results (all the output files of HippoUnit), and the Jupyter Notebooks that show how to run the tests of HippoUnit on these models are available in the following Github repository: https://github.com/KaliLab/HippoUnit_demo.

4.3 Application of HippoUnit to models built using automated parameter optimization within the Human Brain Project

Besides enabling a detailed comparison of published models, HippoUnit can also be used to monitor the performance of new models at various stages of model development. Here, we illustrate this by showing how we have used HippoUnit within the HBP to systematically validate detailed multi-compartmental models of hippocampal neurons developed using multi-objective parameter optimization methods implemented by the open source Blue Brain Python Optimization Library (BluePyOpt [16]). To this end, we extended HippoUnit to allow it to handle the output of optimization performed by BluePyOpt (see Methods).

Models of rat CA1 pyramidal cells were optimized using target feature data extracted from sharp electrode recordings [3]. Then, using the Somatic Features Test of HippoUnit, we compared the behavior of the models to features extracted from this sharp electrode dataset. However, while only a subset of the features extracted by eFEL was used in the optimization (mostly those that describe the rate and timing of the spikes; e.g., the different inter-spike interval (ISI), time to last/first spike, mean frequency features), we considered all the eFEL features that could be successfully extracted from the data during validation.

DOI:10.15774/PPKE.ITK.2022.001

In addition, sharp electrode measurements were also available for several types of interneurons in the rat hippocampal CA1 region, and models of these interneurons were also constructed using similar automated methods [3]. Using the appropriate observation file and the stimulus file belonging to it, the Somatic Features Test of HippoUnit can also be applied to these models to evaluate their somatic spiking features. The other tests of HippoUnit are currently not applicable to interneurons, mostly due to the lack of appropriate target data.

We applied the tests of HippoUnit to the version of the models published in [3], and to a later version (v4) described in Ecker et al. (2020)[114], which was intended to further improve the dendritic behavior of the models, as this is critical for their proper functioning in the network. The two sets of models were created using the same morphology files and similar optimization methods and protocols. These new optimizations differed mainly in the allowed range for the density of the sodium channels in the dendrites. For the pyramidal cell models a new feature was also introduced in the parameter optimization that constrains the amplitudes of back-propagating action potentials in the main apical dendrite. The new interneuron models also had an exponentially decreasing (rather than constant) density of Na channels, and A-type K channels with more hyperpolarized activation in their dendrites. For more details on the models, see the original publications ([3], [114]).

After running all the tests of HippoUnit on both sets of models generated by BluePyOpt, we performed a comparison of the old [3] and the new versions of the models by doing a statistical analysis of the final scores achieved by the models of the same cell type on the different tests. In Figure 4.10 the median, the interquartile range and the full range of the final scores achieved by the two versions of the model set are compared. According to the results of the Wilcoxon signed-rank test the new version of the models achieved significantly better scores on the Back-propagating Action Potential test ($p = 0.0046$), on the Oblique Integration Test ($p = 0.0033$), and on the PSP Attenuation Test ($p = 0.0107$), which is the result of reduced dendritic excitability. Moreover, in most of the other cases the behavior of the models improved slightly (but not significantly) with the new version. Only in the case of the Somatic Features test applied to bAC interneurons did the new models perform slightly worse (but still quite well), and this difference was not significant ($p = 0.75$).

These results show the importance of model validation performed against experimental findings, especially those not considered when building the model, in every iteration during the process of model development. This approach can greatly facilitate the construction of models that perform well in a variety of contexts, help avoid model regression, and guide the model building process towards a more robust and general implementation.

DOI:10.15774/PPKE.ITK.2022.001

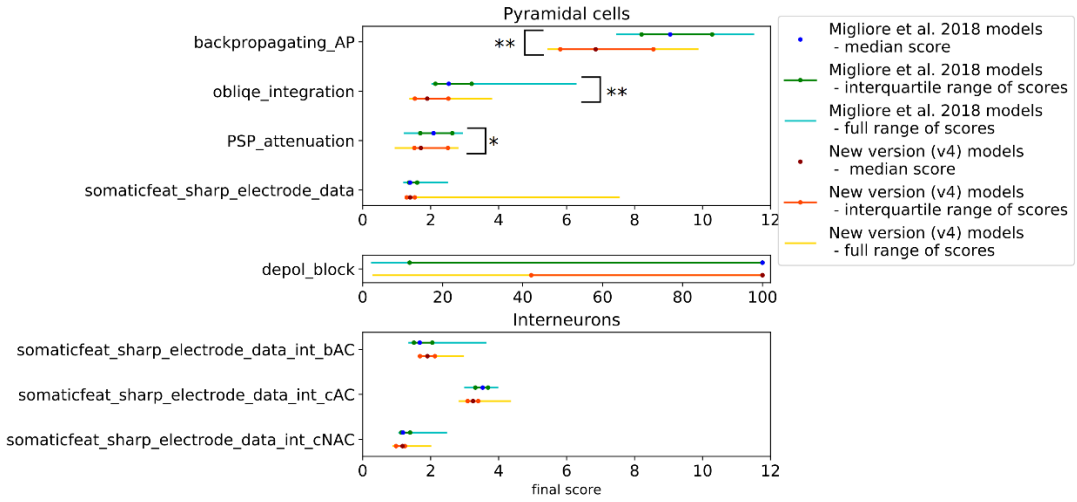

Figure 4.10: Employing the tests of HippoUnit to monitor the behavior of a set of detailed data-driven models of hippocampal neurons at different stages of model development. Models of four different cell types (pyramidal cells and continuous accommodating (int cAC), bursting accommodating (int bAC) and continuous non-accommodating (int cNAC) interneurons) of the rat hippocampal CA1 region were developed within the Human Brain Project by automated optimization using BluePyOpt. The tests of HippoUnit were used to evaluate and compare the behavior of the older (Migliore et al 2018) version and the new (v4) version of these models. The median, the interquartile range and the full range of the final scores achieved by the models of each cell type were calculated and the results of the two versions of the model set are compared. Asterisks indicate significant differences (*: $p<0.05$; **: $p<0.01$). [Th1]

Furthermore, testing the dendritic properties of these models, especially the attenuation of synaptically induced EPSPs (see Figure 4.11), we showed that the v4 version of these models are suitable for being used in the in silico study of synaptic physiology in the hippocampal CA1 region [114].

DOI:10.15774/PPKE.ITK.2022.001

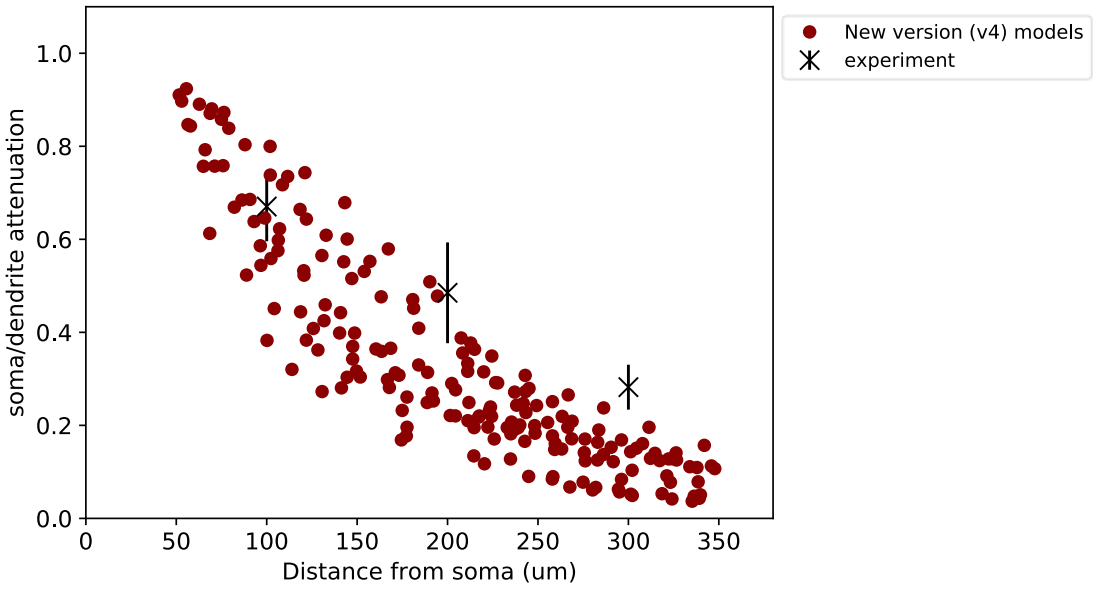

Figure 4.11: Results from the PSP Attenuation Test of HippoUnit applied to the new (v4) version of the BluePyOpt optimized models within the Human Brain Project. Soma/dendrite EPSP attenuation as a function of the synaptic input distance from the soma in the differen models. The plot shows that the attenuation of synaptic EPSPs is consistent with experimental data [29].

4.4 Integration of HippoUnit into the Validation Framework and the Brain Simulation Platform of the Human Brain Project

The HBP is developing scientific infrastructure to facilitate advances in neuroscience, medicine, and computing [115]. One component of this research infrastructure is the Brain Simulation Platform (https://bsp.humanbrainproject.eu), an online collaborative platform that supports the construction and simulation of neural models at various scales. As we argued above, systematic, automated validation of models is a critical prerequisite of collaborative model development. Accordingly, the Brain Simulation Platform includes a software framework for quantitative model validation and testing that explicitly supports applying a given validation test to different models and storing the results [116]. The framework consists of a web service, and a set of test suites, which are Python modules based on the SciUnit package. As we discussed earlier, SciUnit uses the concept of capabilities, which are standardized interfaces between the models to be tested and the validation tests. By defining the capabilities to which models must adhere, individual validation tests can be implemented independently of any specific model and used to validate any compatible model despite differences in their internal structures, the language and/or the simulator used. Each test must include a specification of the required model capabilities, the location of the reference (experimental) dataset, and data analysis code to transform the recorded variables (e.g., membrane potential) into feature values that allow the simulation results to be directly and quantitatively compared to the experimental data through

statistical analysis. The web services framework [116] supports the management of models, tests, and validation results. It is accessible via web apps within the HBP Collaboratory, and also through a Python client. The framework makes it possible to permanently record, examine and reproduce validation results, and enables tracking the evolution of models over time, as well as comparison against other models in the domain.

Every test of HippoUnit described in this paper has been individually registered in the Validation Framework. The JSON files containing the target experimental data for each test are stored (besides the HippoUnit_demo GitHub repository) in storage containers at the Swiss National Supercomputing Centre (CSCS), where they are publicly available. The location of the corresponding data file is associated with each registered test, so that the data are loaded automatically when the test is run on a model via the Validation Framework. As the Somatic Features Test of HippoUnit was used to compare models against five different data sets (data from sharp electrode measurements in pyramidal cells and interneurons belonging to three different electronic types, and data obtained from patch clamp recordings in pyramidal cells), these are considered to be and have been registered as five separate tests in the Validation Framework.

All the models that were tested and compared in this study (including the CA1 pyramidal cell models from the literature and the BluePyOpt optimized CA1 pyramidal cells and interneurons of the HBP) have been registered and are available in the Model Catalog of the Validation Framework with their locations in the CSCS storage linked to them. In addition to the modifications that were needed to make the models compatible with testing with HippoUnit (described in the section “Methods – Models from literature”), the versions of the models uploaded to the CSCS container also contain an __init__.py file. This file implements a python class that inherits all the functions of the ModelLoader class of HippoUnit without modification. Its role is to make the validation of these models via the Framework more straightforward by defining and setting the parameters of the ModelLoader class (such as the path to the HOC and NMODL files, the name of the section lists, etc.) that otherwise need to be set after instantiating the ModelLoader (see the HippoUnit_demo GitHub repository: https://github.com/KaliLab/HippoUnit_demo/tree/master/jupyter_notebooks).

The validation results discussed in this paper have also been registered in the Validation Framework, with all their related files (output figures and JSON files) linked to them. These can be accessed using the Model Validation app of the framework.

The Brain Simulation Platform of the HBP contains several online ‘Use Cases’, which are available on the platform and help the users to try and use the various established pipelines. The Use Case called ‘Hippocampus Single Cell Model Validation’ can be used to apply the tests of HippoUnit to models that were built using automated parameter optimization within the HBP.

The Brain Simulation Platform also hosts interactive "Live Paper" documents that refer to published papers related to the models or software tools on the Platform. Live Papers provide links that make it possible to visualize or download results and data discussed in the respective paper, and even to run the associated simulations on the Platform. We have created a Live Paper (https://humanbrainproject.github.io/hbp-bsp-live-papers/2021/saray_et_al_2021/saray_et_al_2021.html) showing the results of the study presented in this paper in more detail. This interactive document provides links to all the output figures and data files resulting from the validation of the models from literature discussed here. This provides a more detailed insight into their behavior individually. Moreover, as part of this Live Paper a HippoUnit Use Case is also available in the form of a Jupyter Notebook, which guides the user through running the validation tests of HippoUnit on the models from literature that are already registered in the Framework, and makes it possible to reproduce the results presented here.

4.5 Extending HippoUnit for other important cell types of the hippocampus

As in our research group we are also developing models of different hippocampal cell types other than CA1 pyramidal cells, we started to extend HippoUnit by adding new tests for the validation of these cell types. New validation tests cover signal propagation in dendrites of basket cells and CA3 pyramidal cells, and the propagation of action potentials in the axon of basket cells.

Models used for demonstrating the new validation tests were downloaded from ModelDB [18]:

The Tzilivaki et al. 2019 [117] (ModelDB: 237595) basket cell models were developed to show that fast spiking interneurons in the hippocampal circuit do not behave as point neurons, but their dendritic tree is able to sum incoming signals in different ways depending on the spatio-temporal pattern of the synaptic inputs. The model was adapted to five different morphologies.

The Hemond et al. 2008 [118] (ModelDB: 101629) CA3 pyramidal cell models were built to investigate the active mechanisms behind the different firing patterns of this cell type observed experimentally. Four different models were adapted to the four different firing patterns. In the following we will refer to them by the figure number in which they were presented in the corresponding paper [118]: Hemond_2008_fig9b – burst firing, Hemond_2008_fig9c – strongly adapting, Hemond_2008_fig9d – non-adapting, Hemond_2008_fig9e – delayed onset firing.

The new tests are not yet fully integrated into HippoUnit, but they are already available on GitHub as a branch to HippoUnit: https://github.com/sasaray/hippounit/tree/New_tests_for_other_cell_types.

The simplified versions of the above-mentioned literature models (that were used during validation), the target experimental data for the new tests, and Jupyter notebooks showing how to run the new tests, along with the detailed validation results, are also available on GitHub: https://github.com/sasaray/HippoUnit_demo/tree/New_tests_for_other_cell_types.

4.5.1 Back-propagating AP Test Basket Cell

This test evaluates the efficacy and shape of back-propagating action potentials at different locations on the basal and apical dendrites of basket cells. As the first step, a (user-specified) number of dendritic locations is selected on both the apical and the basal dendritic tree (if the model has both of them) in distance ranges of 50, 150 ± 50 µm on the apical and 20, 50 ± 15 µm on the basal dendrites from the soma. These values are read by the test from the stimulus JSON input file and were set according to how the experimental data were processed. The original random selection of HippoUnit has been modified to make it more general and useable for any of the main dendritic types (apical, tuft, trunk, oblique, basal) and also for the axon, based on section lists, depending on which one is given as an argument to the function.

Next, a 1 nA amplitude and 1 sec duration current step input is injected to the soma of the model, and the voltage responses are recorded at the selected dendritic locations. The amplitude, maximum rise slope and half-duration of the first and the last back-propagating action potentials in the 1 sec train are compared to data from Hu et al. (2010) [119]. In the current version of the test, these features are extracted using eFEL. As in the other tests of HippoUnit, the extracted feature values are first averaged at the different distance ranges, and then compared to experimental features to get the feature scores.

Figure 4.12D,E shows the results of this test on the Tzilivaki et al. 2019 basket cell models that share the same biophysical properties but have different morphologies. It can be seen that in these models the action potential back-propagation is more active than it was observed experimentally, as the AP amplitudes measured in the models are larger than the experimental data, while the AP rise slope of the first AP is lower (Figure 4.12D). The width of the action potentials (AP half-duration) seems to depend on the nature of the dendritic branch, as in most of these models its value falls into two separate groups. Although the 5 versions of the model behave similarly, the feature errors they achieve on the test are not identical (Figure 4.12 E), which shows that morphological properties play a role in action potential back-propagation.

DOI:10.15774/PPKE.ITK.2022.001

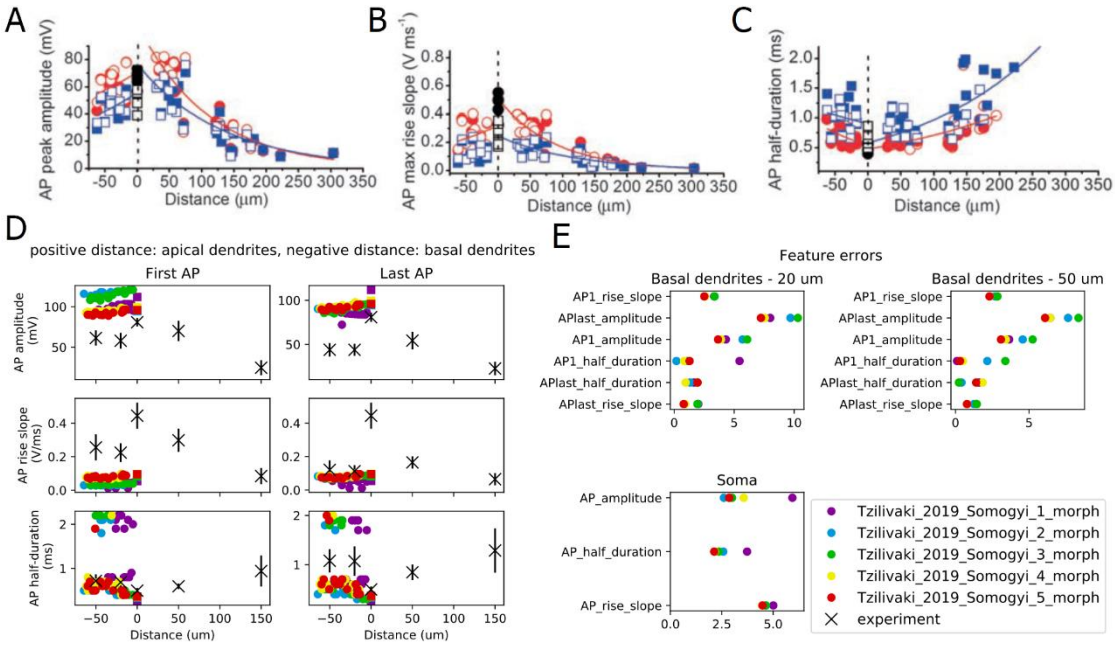

Figure 4.12: Results from the Back-propagating AP Test Basket Cell. (A) –(C) The target experimental data of the AP peak amplitude, maximal slope of the rise, and duration at half-maximal amplitude against recording distances from the soma (negative distances – basal, positive distances - apical dendrites). Solid symbols: somatic current injection; open symbols: dendritic current injection. Red: first AP; blue: last AP in a 1 sec train. Figures were adapted from Hu et al. 2010 [119]. (D) The properties of the 1st and last bAPs at different distances on the basal dendrites of the models (these models do not have apical dendrites). (E) The feature scores achieved by the models. (black X - experimental observation, squares of different colours at distance 0 indicate the somata of the different models).

4.5.2 AP Propagation Axon Test Basket Cell

This test is very similar to the previous one with the exception that here the properties of the propagating action potentials are investigated at the axon. Axonal locations are selected randomly in the distance ranges of 50, 100, 150, 200 ± 25 µm from the soma, and the voltage responses to a 1 nA, 1 sec long step somatic current injection are recorded at these locations. The amplitude and half-duration of the first and the last action potentials (extracted using eFEL) in the evoked spike train at different distances on the axon are compared to data from Hu et al. (2018) [120].

Similarly to the AP back-propagation on the dendrites, APs propagate with higher amplitude on the axon than shown by the experimental data (Figure 4.13E). As it can be seen from the different feature errors gained by the models with different morphologies (Figure 4.13F), anatomy also plays a role in AP propagation on the axon.

DOI:10.15774/PPKE.ITK.2022.001

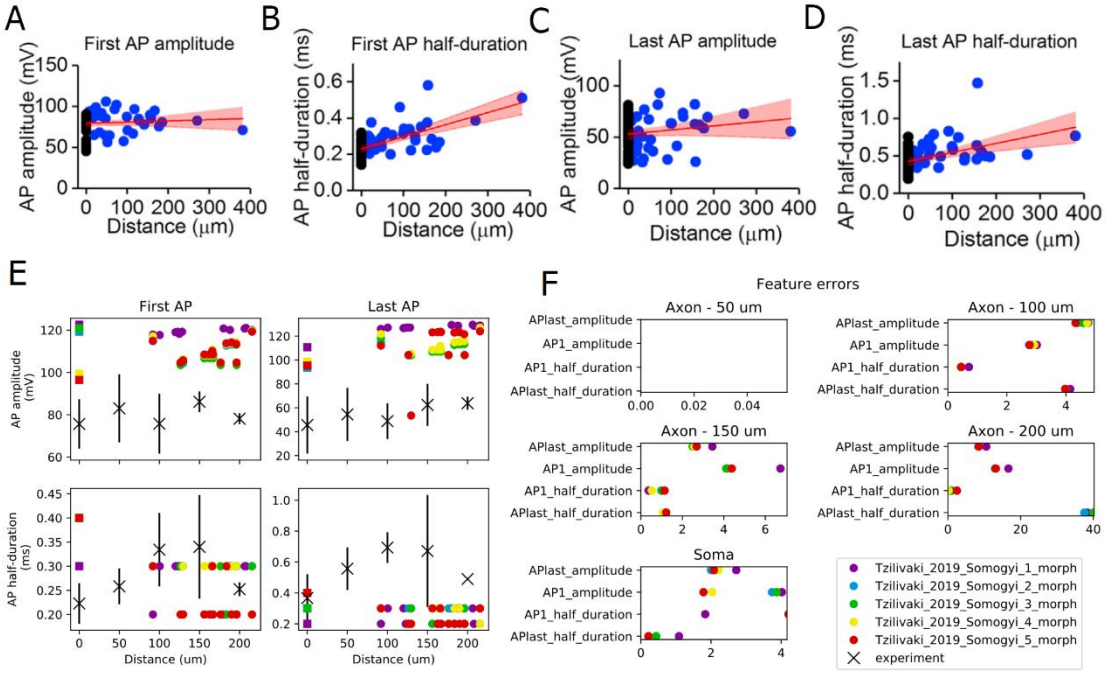

Figure 4.13: Results from the AP Propagation Axon Test Basket Cell. (A) –(D) Target experimental data for the first (A) and last (C) AP amplitude and the first (B) and last (D) AP half-duration against the distance of the axonal recording location from the soma. (black: somatic recordings; blue: axonal recordings). Figures were adapted from Hu et al. 2018 [120]. (E) The properties of the 1st and last APs at different distances on the axon of the different models. (F) The feature scores achieved by the models. (black X - experimental observation, squares of different colours at distance 0 indicate the somata of the different models).

4.5.3 Back-propagating AP Test CA3 PC

In this validation the efficacy and shape of back-propagating action potentials at different locations on the basal and apical dendrites of CA3 pyramidal cell models are tested. Action potentials are evoked by two different inputs: a long-lasting rheobase somatic current injection and short current pulses of different frequencies. The target experimental data are from Kim et al. (2012) [121].

After randomly selecting recording locations on the apical (at 100, 200, 300 ± 50μm from the soma) and basal (at 50 ± 25μm from the soma) dendritic tree of the model, the rheobase current intensity (defined as the smallest step current amplitude in response to which the soma fires an action potential) is automatically determined by a function implemented in the test for this purpose. The rheobase somatic current injection is then applied for 1 sec, and the amplitude and half-duration of the first back-propagating AP are extracted using eFEL at the different dendritic locations to be compared to the target data.

DOI:10.15774/PPKE.ITK.2022.001

For the short current pulse stimuli, a new capability function had to be implemented, that is capable of stimulating the cell with multiple current injections of the given amplitude and frequency. The frequencies (20, 50, 100 Hz) of the pulses, the duration of a single pulse (2 ms), the number of pulses (10), and the amplitude of the pulses (3.0 nA) are read from the stimulus input JSON file which is based on the experimental protocol of the target data. It may happen that not all the short pulses elicit an action potential, and therefore this is examined by the test. If there is a smaller number of AP-s in the train than pulses in the input, then the input amplitude is increased by 20% until the condition is met, but only up to five times. If this is still not enough, the features are not evaluated, which is noted in the output. On the other hand, it also may happen that the short but relatively high amplitude pulses generate high amplitude EPSP-s. Therefore, in this test the AP detection threshold of eFEL is set to 0 mV (in other tests it is usually -20 mV). From the voltage responses recorded at the dendritic locations the AP amplitude and the AP half-duration of the first and fifth APs are extracted using eFEL and the ratios of these features are calculated for the first and the fifth AP. As usual, the features are averaged over the distance ranges of interest and compared to the target experimental data to get the feature scores. The final score is yielded as the average of the feature scores.

From the validation results it can be seen that in the Hemond et al. 2008 models for the long rheobase current injection the action potentials propagate back to the basal and proximal apical dendrites with lower but to the more distal apical dendrites with higher amplitude compared to the target experimental data (Figure 4.14C). The AP duration of the back-propagating action potentials takes two different values depending on the dendritic location in some of the models (Figure 4.14C). As this phenomenon was observed also in the case of both tests of the basket cells, it may be a bug in the method used to extract this feature, which needs further investigation.

The ratios of the fifth and first APs for the short current pulses of different frequencies shows that in the models the action potential amplitude, in contrast to the experimental data, does not attenuate with distance on the dendrites, as this value remains close to 1 in each model. The AP half-duration also seems to remain nearly constant in the different distances, but this is in agreement with the target data. (See Figure 4.14D.)

Surprisingly, these models show quite similar behavior regarding the back-propagating action potentials, although they were tuned to show different somatic firing patterns [118]. It could be expected that the different mechanisms affecting somatic firing may affect AP back-propagation as well.

DOI:10.15774/PPKE.ITK.2022.001

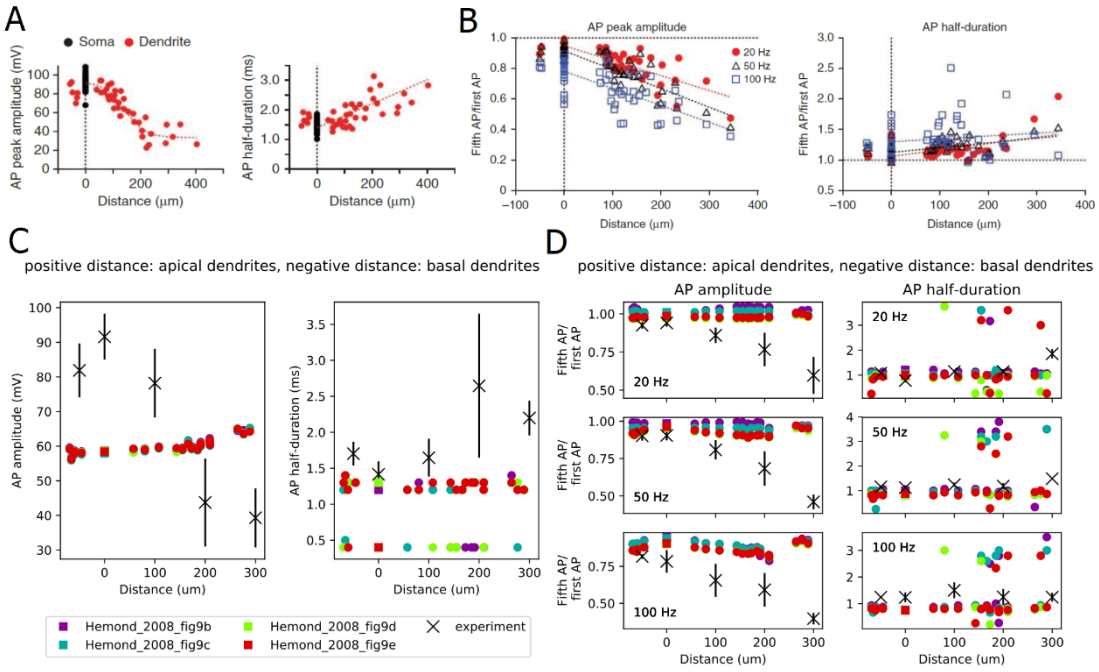

Figure 4.14: Results from the Back-propagating AP Test CA3 PC. (A) Target experimental data for the AP amplitude and AP half-duration to somatic rheobase current injection against the distance of the recording location from the soma (negative distances – basal, positive distances - apical dendrites). (B) Experimental ratio of the amplitude (left) and half-duration (right) of the 5th and 1st bAPs evoked by short somatic current pulses of different frequencies at different distances from the soma. Panels (A) and (B) were adapted from Kim et al. 2012 [121]. (C) The properties of the models' bAPs at different distances on the dendritic tree evoked by long rheobase somatic current injection. (D) The ratio of the amplitude and half-duration of the 5th and 1st bAPs evoked by short somatic current pulses at different distances from the soma. (black X - experimental observation, squares of different colours at distance 0 indicate the soma of the different models).

5 Discussion

5.1 Applications of the HippoUnit test suite

In this thesis, we have described the design, usage, and some initial applications of HippoUnit, a software tool that enables the automated comparison of the physiological properties of models of hippocampal neurons with the corresponding experimental results. HippoUnit, together with its possible extensions and other similar tools, allows the rapid, systematic evaluation and comparison of neuronal models in multiple domains. By providing the software tools and examples for effective model validation, we hope to encourage the modeling community to use more systematic testing during model development, with the aim of making the process of model building more efficient, reproducible and transparent.

DOI:10.15774/PPKE.ITK.2022.001

For anatomically and biophysically detailed data-driven neural models to be predictive, it is important that they are able to generalize beyond their original scope. However, most detailed biophysical models to date were built to capture only a few important or interesting properties of a given neuron type. Systematic testing and comparison of the behavior of these models is still rare, and thus it is often unknown how these models would behave when used under different circumstances, and to what extent they can be used to address different scientific questions. As a result, the modeling community still keeps building new models of the same cell type for various purposes, instead of reusing and further developing the already existing ones. On the other hand, in those cases when new models are based on previously published ones, model parameters are often adjusted to fit a new set of experimental data. These adjustments typically alter the ability of the model to capture the experimental data targeted by the original model, but this remains unrecognized because of the lack of comprehensive testing. As we have shown, an illustrative example of this regression issue is the Bianchi et al. 2012 model. This model was mainly based on the Poirazi et al. 2013 model, which was developed to show specific dendritic behaviors and was even tested using data on back-propagating action potentials during its development [79]. However, the test results presented above indicate that when the somatic behavior of this model was adjusted to reproduce experimental observations on depolarization block, it lost the ability to show realistic back-propagation of action potentials into the apical dendrite. In addition, some publications on neuronal models simply state that the model has been validated against electrophysiological data, but the details of these validations (such as the methods used, the experimental data considered or even the results) are usually not shared.

Therefore, one important use case for the application of HippoUnit is the evaluation and comparison of existing models. We demonstrated this by using HippoUnit to test and compare the behavior of several models of rat CA1 pyramidal neurons available on ModelDB in several distinct domains against electrophysiological data available in the literature (or shared by collaborators). Besides providing independent and standardized verification of the behavior of the models, the results also allow researchers to judge which existing models show a good match to the experimental data in the domains that they care about, and thus to decide whether they could re-use one of the existing models in their own research.

Besides enabling the comparison of different models regarding how well they match a particular dataset, the tests of HippoUnit also allow one to determine the match between a particular model and several datasets of the same type. As experimental results can be heavily influenced by recording conditions and protocols, and also depend on factors such as the strain, age, and sex of the animal, it is important to find out whether the same model can simultaneously capture the outcome of different experiments, and if not, how closely it is able to match the different datasets. As an example, we showed how the Somatic Features Test of HippoUnit can be used to compare the somatic behavior of a particular model to features extracted from both

DOI:10.15774/PPKE.ITK.2022.001

patch clamp and sharp electrode recordings and determine which of these is captured better by the model (see Figure 4.4).

HippoUnit is also a useful tool during model development. In a typical data-driven modeling scenario, researchers decide which aspects of model behavior are relevant for them, find experimental data that constrain these behaviors, then use some of these data to build the model, and use the rest of the data to validate the model. HippoUnit and similar test suites make it possible to define quantitative criteria for declaring a model valid (ideally before modeling starts), and to apply these criteria consistently throughout model development. We demonstrated this approach through the example of detailed single cell models of rat CA1 pyramidal cells and interneurons optimized within the HBP.

Furthermore, several authors have argued for the benefits of creating "community models" [122]–[126] through the iterative refinement of models in an open collaboration of multiple research teams. Such consensus models would aim to capture a wide range of experimental observations, and may be expected to generalize (within limits) to novel modeling scenarios. A prerequisite for this type of collaborative model development is an agreement on which experimental results will be used to constrain and validate the models. Automated test suites provide the means to systematically check models with respect to all the relevant experimental data, with the aim of tracking progress and avoiding "regression," whereby previously correct model behavior is corrupted by further tuning.

Although the primary goal of HippoUnit is the objective, quantitative comparison of the behavior of the models to experimental data in certain paradigms, its more creative application provides an opportunity to explore the mechanisms underlying the specific behavior. Rerunning the tests of HippoUnit on modified versions of the model (for example changing a kinetic parameter of an ion channel or eliminating it from the model) may answer the question whether the given ion channel or parameter has a role in the formation of the specific behavior.

However, it is important to note that it is possible that different models with significantly different parameter combinations show the experimentally experienced electrophysiological behavior with similarly good scores on the tests. In the case of CA1 pyramidal cell models developed by automatic parameter fitting in our research group (by Luca Tar), we experienced several times that the models are able to perform similarly well on each test with significantly different parameter combinations (even involving different types of ion channels). Therefore, we believe that there are indeed several solutions for developing a particular function.

Finally, the tests of HippoUnit have been integrated into the recently developed Validation Framework of the HBP, which makes it possible to collect neural models and validation tests, and supports the application of the registered tests to the registered models. Most importantly, it makes it possible to save the validation results and link them to the models

DOI:10.15774/PPKE.ITK.2022.001

in the Model Catalog, making them publicly available and traceable for the modeling community.

5.2 Interpreting the results of HippoUnit

It is important to emphasize that a high final score on a given validation test using a particular experimental dataset does not mean that the model is not good enough or cannot be useful for a variety of purposes (including the ones it was originally developed for). The discrepancy between the target data and the model's behavior, as quantified by the validation tests, may be due to several different reasons. First, all experimental data contain noise and may have systematic biases associated with the experimental methods employed. Sometimes the experimental protocol is not described in sufficient detail to allow its faithful reproduction in the simulations. It may also occur that a model is based on experimental data that were obtained under conditions that are substantially different from the conditions for the measurement of the validation target dataset. Using different recording techniques, such as sharp electrode or patch clamp recordings or the different circumstances of the experiments (e.g., the strain, age, and sex of the animal, or the temperature during measurement) can heavily affect the experimental results. Furthermore, the post-processing of the recorded electrophysiological data can also alter the results. For these reasons, probably no single model should be expected to achieve an arbitrarily low score on all of the validation tests developed for a particular cell type. Keeping this in mind, it is important that the modelers decide which properties of the cell type are relevant for them, and what experimental conditions they aim to mimic. Validation results should be interpreted or taken into account accordingly, and the tests themselves may need to be adapted. The interpretation of the results is aided by several additional outputs of the tests besides the final score. The traces, the extracted feature values as well as the feature scores are saved into output files and also plotted for visualization. This information is intended to help determine the strengths and weaknesses of the model and evaluate its usefulness according to the needs of the user.

The issue of neuronal variability also deserves consideration in this context. The morphology, biophysical parameters, and physiological behavior of neurons is known to be non-uniform, even within a single cell type, and this variability may be important for the proper functioning and robustness of neural circuits [11], [48], [127]. Recent models of neuronal networks have also started to take into account this variability [128]. The tests of HippoUnit account for experimental variability by measuring the distance of the feature values of the model from the experimental mean (the feature score) in units of the experimental standard deviation. This means that any feature score less than about 1 actually corresponds to behavior which may be considered "typical" in the experiments (within one standard deviation of the mean), and a

DOI:10.15774/PPKE.ITK.2022.001

feature score of 2 or 3 may still be considered acceptable for any single model. In fact, even higher values of the feature score may sometimes be consistent with the data if the experimental distribution is long-tailed rather than normal. However, such high values of the feature score certainly deserve attention as they signal a large deviation from the typical behavior observed in the experiments.

Furthermore, the acceptable feature score will generally depend on the goal of the modeling study. In particular, a study which intends to construct and examine a single model of typical experimental behavior should aim to keep all the relevant feature scores relatively low. On the other hand, when modeling entire populations of neurons, one should be prepared to accept a wider range of feature scores in some members of the model population, although the majority of the cells (corresponding to typical members of the experimental population) should still display relatively low scores. In fact, when modeling populations of neurons, one would ideally aim to match the actual distribution of neuronal features (including the mean, standard deviation, and possibly higher moments as well), and the distribution of feature scores (and actual feature values) from the relevant tests of HippoUnit actually provides the information that is necessary to compare the variability of the experimental and model cell populations.

5.3 Uniform model formats reduce the costs of validation

Although HippoUnit is built in a way that its tests are, in principle, model-agnostic, so that the implementation of the tests does not depend on model implementation, it still required a considerable effort to create the standalone versions of the models from literature to be tested, even though all of the selected models were developed for the NEURON simulator. This is because each model has a different file structure and internal logic that needs to be understood in order to create an equivalent standalone version. When the section lists of the main dendritic types do not exist, the user needs to create them by extensively analyzing the morphology and even doing some coding. In order to reduce the costs of systematic validation, models would need to be expressed in a format that is uniform and easy to test. As HippoUnit already has its capability functions implemented in a way that it is able to handle models developed in NEURON, the only requirement for such models is that they should contain a HOC file that describes the morphology (including the section lists for the main dendritic types of the dendritic tree) and all the biophysical parameters of the model, without any additional simulations, GUIs or run-time modifications. Currently, such a standalone version of the models is not made available routinely in publications or on-line databases, but could be added by the creators of the models with relatively little effort.

On the other hand, applying the tests of HippoUnit to models built in other languages requires the re-implementation of the capability functions that are responsible for running the

simulations on the model (see Methods). In order to save the user from this effort, it would be useful to publish neuronal models in a standard and uniform format that is simulator independent and allows general use in a variety of paradigms. This would allow an easier and more transparent process of community model development and validation, as it avoids the need of reimplementation of parts of software tools (such as validation suites), and the creation of new, (potentially) non-traced software versions. This approach is already initiated for neurons and neuronal networks by the developers of NeuroML [129], NineML [130], PyNN [131], Sonata [132], and Brian [19]. Once a large set of models becomes available in these standardized formats, it will be straightforward to extend HippoUnit (and other similar test suites) to handle these models.

5.4 Extensibility of HippoUnit

Although we were aiming to develop a test suite that is as comprehensive as possible, and that captures the most typical and basic properties of the rat hippocampal CA1 pyramidal cell, the list of features that can be tested by HippoUnit is far from complete. Upon availability of the appropriate quantitative experimental data, new tests addressing additional properties of the CA1 pyramidal cell could be included, for example, on the signal integration of the basal or the more distal apical dendrites (that are discussed in section 2.1.2.2.), or on action potential initiation and propagation in the axon. Therefore, we implemented HippoUnit in a way that makes it possible to extend it by adding new tests.

As HippoUnit is based on the SciUnit package [19] it inherits SciUnits's modular structure. This means that a test is usually composed of four main classes: the test class, the model class, the capabilities class and the score class (as described in more detail in the Methods section). Thanks to this structure it is easy to extend HippoUnit with new tests by implementing them in new test classes and adding the capabilities and scores needed. The methods of the new capabilities can be implemented in the ModelLoader class, which is a generalized Model class for models built in the NEURON simulator, or in a newly created Model class specific to the model to be tested.

Adding new tests to HippoUnit requires adding the corresponding target experimental data as well in the form of a JSON file. The way the JSON files are created depends on the nature and source of the experimental data. In some cases the data may be explicitly provided in the text of the papers (as for the Oblique Integration and the Depolarization Block tests), therefore their JSON files are easy to make manually. Most typically, the data have to be processed to get the desired feature mean and standard deviation values and create the JSON file. In these cases it is worth writing a script that does this automatically. Some examples on how this was done for the current tests of HippoUnit are available here:

https://github.com/sasaray/HippoUnit_demo/tree/master/target_features/Examples_on_creating_JSON_files/.

We have already started to develop a new test to examine the generation of Ca^{2+} spikes or plateau potentials in the distal apical dendrites of CA1 pyramidal cell models and the resulting complex spike burst firing pattern on the soma. In this test the stimulation of the models is done according to the experimental protocol of Takahashi & Magee, 2009 [32]. The examined features will be the duration of the dendritic plateau potentials and the somatic firing frequency.

As it is described in chapter 4.5, we recently started to extend HippoUnit by adding new tests for important hippocampal cell types, other than CA1 pyramidal cells. Furthermore, as HippoUnit is open-source and is shared on GitHub, it is possible for other developers, modelers or scientists to modify or extend the test suite working on their own forks of the repository. If they would like to directly contribute to HippoUnit, a 'pull request' can be created to the main repository.

5.5 Generalization possibilities of the tests of HippoUnit

In the current version of HippoUnit most of the validation tests can only be used to test models of rat hippocampal CA1 pyramidal cells, as the observation data come from electrophysiological measurements of this cell type and the tests were designed to follow the experimental protocols of the papers from which these data derive. However, with small modifications most of the tests can be used for other cell types, or with slightly different stimulation protocols, if there are experimental data available for the features or properties tested.

The Somatic Features Test can be used for any cell type and with any current step injection protocol even in its current form using the appropriate data and configuration files. These two files must be in agreement with each other; in particular, the configuration file should contain the parameters of the step current protocols (delay, duration, amplitude) used in the experiments from which the feature values in the data file derive. In this study this test was used with two different experimental protocols (sharp electrode measurements and patch clamp recordings that used different current step amplitudes and durations), and for testing four different cell types (rat hippocampal CA1 PC and interneurons).

In the current version of the Depolarization Block Test the properties of the stimulus (delay, duration, and amplitudes) are hard-coded to reproduce the experimental protocol used in a study of CA1 PCs [33]. However, the test could be easily modified to read these parameters from a configuration file like in the case of other tests, and then the test could be applied to other cell types if data from similar experimental measurements are available.

DOI:10.15774/PPKE.ITK.2022.001

As the Back-propagating AP Test examines the back-propagation efficacy of action potentials in the main apical dendrite (trunk), it is mainly suitable for testing pyramidal cell models; however, it can be used for PC models from other hippocampal or cortical regions, potentially using different distance ranges of the recording sites. If different distances are used, the feature names ('AP1_amp_X' and 'APlast_amp_X', where X is the recording distance) in the observation data file and the recording distances given in the stimuli file must be in agreement. Furthermore, it would also be possible to set a section list of other dendritic types instead of the trunk to be examined by the test. This way, models of other cell types (with dendritic trees qualitatively different from those of PCs) could also be tested. The frequency range of the spike train (10 – 20 Hz, preferring values closest to 15 Hz) is currently hard-coded in the function that automatically finds the appropriate current amplitude, but the implementation could be made more flexible in this case as well.

The PSP Attenuation Test is quite general. Both the distances and tolerance values that determine the stimulation locations on the dendrites and the properties of the synaptic stimuli are given using the configuration file. Here again the feature names in the observation data file ('attenuation_soma/dend_x_um', where x is the distance from the soma) must fit the distances of the stimulation locations in the configuration file when one uses the tests with data from a different cell type or experimental protocol. Similarly to the Back-propagating AP Test the PSP Attenuation Test also examines the main apical dendrite (trunk), but could be altered to use section lists of other dendritic types.

The Oblique Integration Test is very specific to the experimental protocol of [33]. There is no configuration file used here, but the synaptic parameters (of the ModelLoader class) and the number of synapses to which the model should first generate a dendritic spike ('threshold_index' parameter of the test class) can be adjusted by the user after instantiating the ModelLoader and the test classes respectively. The time intervals between the inputs (synchronous (0.3 ms), asynchronous (2.2 ms)) are currently hard-coded in the test.

HippoUnit has been used mainly to test models of rat hippocampal CA1 pyramidal cells as described above. However, having the appropriate observation data, most of its tests could easily be adapted to test models of different cell types, even in cases when the experimental protocol is slightly different from the currently implemented ones. The extent to which a test needs to be modified in order to test models of other cell types depends on how much the behavior of the new cell type differs from the behavior of rat CA1 pyramidal cells, and to what extent the protocol of the experiment differs from the ones we used as the bases of comparison in the current study. Examples for this are the tests presented in chapter 4.5. Although, they are similar to the Back-propagating AP Test of HippoUnit for the CA1 pyramidal cell, the experimental protocol and the features of the observation data for the CA3 pyramidal cell and the basket cell differed in such an extent, that new tests had to be implemented.

DOI:10.15774/PPKE.ITK.2022.001

6 Summary

In this section the new scientific results of the dissertation are summarized in the form of thesis points.

Thesis I: I proposed, elaborated and developed an open-source Python validation test suite (HippoUnit), which is the first test suite to make it possible to automatically and systematically test multiple properties of anatomically and biophysically detailed models of the hippocampal CA1 pyramidal cell by making quantitative comparisons between the models and electrophysiological data.

Corresponding publications: [Th1], [Th3-Th7], [Th13-Th16]

Thesis II: I demonstrated the utility of my validation test suite by applying its tests to compare the behavior of several different hippocampal CA1 pyramidal cell models from the ModelDB database against electrophysiological data available in the literature. This way I also compared the models to each other and tested their generalization performance in paradigms that they were not originally designed to capture. I concluded and showed that each of these models provide a good match to experimental results in some domains but not in others. Thus automated, systematic testing is needed to reveal the weaknesses and strengths of neural models available in the literature and to evaluate their usefulness according to the needs of the user.

Corresponding publications: [Th1], [Th10-Th12]

Thesis III: I employed the HippoUnit test suite to validate the dendritic properties of models of hippocampal CA1 neurons that were developed within the Human Brain Project using parameter optimization methods, but considering only somatic features. This way I showed that these models are suitable for studying synaptic properties.

Corresponding publication: [Th2], [Th7]

Thesis IV: I employed the test suite to aid the development of models of hippocampal neurons within the Human Brain Project by systematically validating and thus monitoring the performance of them at various stages of model development. Based on the validation results I proposed the direction in which they should be further developed and removed those models that did not meet our needs. These models were then used to build a network model of the hippocampal CA1 region.

Corresponding publications: [Th1], [Th2], [Th7]

Thesis V: HippoUnit was the first test suite to be integrated into the Validation Framework developed within the Human Brain Project, that makes it possible to permanently record, examine and reproduce validation results, and enables tracking the evolution of models over time, as well as comparison against other models in the domain. I also integrated the validation tests of HippoUnit into the Brain Simulation Platform of

the Human Brain Project and developed online Use Cases, that allow to run the tests on different models in a browser without the need of locally installing the required packages. By making these tools widely available I facilitated more reproducible and transparent model building in the neuroscience community.

Corresponding publications: [Th1], [Th9], [Th15], [Th16]

7 The Author's publications

7.1 Publications related to the theses:

7.1.1 Journal papers:

[Th1] Sára Sáray, Christian A. Rössert, Shailesh Appukuttan, Rosanna Migliore, Paola Vitale, Carmen A. Lupascu, Luca L. Bologna, Werner Van Geit, Armando Romani, Andrew P. Davison, Eilif Muller, Tamás F. Freund, Szabolcs Káli: HippoUnit: A software tool for the automated testing and systematic comparison of detailed models of hippocampal neurons based on electrophysiological data, PLOS Computational Biology; doi: https://doi.org/10.1371/journal.pcbi.1008114

[Th2] András Ecker, Armando Romani, Sára Sáray, Szabolcs Káli, Michele Migliore, Joanne Falck Sigrun Lange, Audrey Mercer, Alex M. Thomson, Eilif Muller, Michael W. Reimann Srikanth Ramaswamy: Data-driven integration of hippocampal CA1 synaptic physiology in silico, Hippocampus https://doi.org/10.1002/hipo.23220

7.1.2 Posters at international conferences:

[Th3] Sára Sáray, Péter Friedrich, Christian A. Rössert, Levente Kacz, Márk P. Török, Bence Bagi, Eilif Muller, Tamás F. Freund, Szabolcs Káli: Developing software tools for parameter fitting and validation of neuronal models, NeuroInformatics 2016 Conference, September 3-4, 2016, Reading, UK doi:10.3389/conf.fninf.2016.20.00076

[Th4] Sára Sáray, Péter Friedrich, Christian A. Rössert, Levente Kacz, Márk P. Török, Bence Bagi, Eilif Muller, Tamás F. Freund, Szabolcs Káli: Developing software tools for parameter fitting and validation of neuronal models, First Joint Conference of From Medicine to Bionics - 3rd European PhD Conference, November 17-20, 2016, Budapest, Hungary

[Th5] Sára Sáray, Péter Friedrich, Christian A. Rössert, Levente Kacz, Márk P. Török, Bence Bagi, Eilif Muller, Tamás F. Freund, Szabolcs Káli: Developing software tools for parameter fitting and validation of neuronal models, 1st HBP Student Conference, February 8-10, 2017, Vienna, Austria ISBN: 978-2-88945-421-1

[Th6] Sára Sáray, Shailesh Appukuttan, Bence Bagi, Pedro E. Garcia-Rodriguez, Péter Kovách, Carmen A. Lupascu, Máté Mohácsi, Christian A. Rössert, Luca Tar, Márk P. Török, Andrew Davison, Michele Migliore, Eilif Muller, Tamás F. Frend, Szabolcs Káli: Automated parameter fitting and testing of detailed neuronal models, Bernstein

Conference 2017, September, 12-15, 2017, Göttingen, Germany doi: 10.12751/nncn.bc2017.0134

[Th7] S Sáray, R Migliore, CA Lupascu, LL Bologna, CA Rössert, A Romani, J-D Courcol, S Antonel, W Van Geit, A Thomson, A Mercer, S Lange, J Falck, S Appukuttan, PE Garcia-Rodriguez, A Davison, E Muller, F Schürmann, M Migliore, TF Freund, S Káli: Systematic construction and validation of detailed models of hippocampal neurons using reproducible, collaborative workflows, 11th FENS Forum of Neuroscience Conference, July 7-11, 2018, Berlin, Germany

[Th8] Luca Tar, Sára Sáray, Tamás Freund, Szabolcs Káli: Developing a detailed model of CA1 pyramidal neurons using automated optimization and validation tools, 11th FENS Forum of Neuroscience Conference, July 7-11, 2018, Berlin, Germany

[Th9] S. Appukuttan, P. E. Garcia-Rodriguez, L. Sharma, S. Sáray, S. Káli, A. P. Davison; Systematic statistical validation of data-driven models in neuroscience, Society for Neuroscience (SfN) Meeting, 2018. (abstract available: https://www.abstractsonline.com/pp8/#!/4649/presentation/17769)

[Th10] Sára Sáray, Christian A. Rössert, Shailesh Appukuttan, Andrew P. Davison, Eilif Muller, Tamás F. Freund, Szabolcs Káli; Systematic automated validation of detailed models of hippocampal neurons against electrophysiological data, 28th Annual Computational Neuroscience Meeting (CNS*2019), July 13-17, 2019, Barcelona, Spain (https://doi.org/10.1186/s12868-019-0538-0)

[Th11] Sára Sáray, Christian A. Rössert, Shailesh Appukuttan, Andrew P. Davison, Eilif Muller, Tamás F. Freund, Szabolcs Káli: Systematic testing and validation of models of hippocampal neurons against electrophysiological data, IBRO Workshop, 29-30 January, 2020, Szeged, Hungary (Abstract available: https://www.mitt2020.hu/abstracts)

[Th12] Sára Sáray, Christian A. Rössert, Shailesh Appukuttan, Andrew P. Davison, Eilif Muller, Tamás F. Freund, Szabolcs Káli: Systematic testing and validation of models of hippocampal neurons against electrophysiological data, 29th Annual Computational Neuroscience Meeting July, 2020. Online. https://doi.org/10.1186/s12868-020-00593-1

7.1.3 Annual Proceedings of the PPCU Faculty of Information technology and Bionics Doctoral School:

[Th13] Sára Sáray, Developing software tools for parameter fitting and validation of detailed neuronal models. PhD Proceedings Annual Issues of the Doctoral School, Faculty of Information Technology and Bionics, Pázmány Péter Catholic University 11: pp. 85-88. (2016)

[Th14] Sára Sáray, Developing a general software framework for the automatized testing of neural models. PhD Proceedings Annual Issues of the Doctoral School, Faculty of Information Technology and Bionics, Pázmány Péter Catholic University12: pp. 89-92. (2017)

[Th15] Sára Sáray, HippoUnit: a Python test suite for the automatized validation of models of hippocampal neurons. PhD Proceedings Annual Issues of the Doctoral School, Faculty of Information Technology and Bionics, Pázmány Péter Catholic University13: pp. 86-89. (2018)

7.1.4 Workshop presentation

[Th16] Sára Sáray, Overview of HippoUnit, EBRAINS Infrastructure Training on Model Validation, 4–7 May 2021, Virtual Event (Invited talk) (https://www.humanbrainproject.eu/en/education/training-on-model-validation/)

7.2 Publications not related to the theses

7.2.1 Conference papers:

[Au1] Máté Mohácsi, Márk Patrik Török, Sára Sáray and Szabolcs Káli: A unified framework for the application and evaluation of different methods for neural parameter optimization, IEEE 2020 International Joint Conference on Neural Networks (IJCNN) 2020, 19-24th July 2020, Online, DOI: 10.1109/IJCNN48605.2020.9206692

7.2.2 Posters:

[Au2] Sára Sáray, Tamás F. Freund, Szabolcs Káli: Investigation of dendritic integration in CA1 pyramidal neurons using detailed biophysical models, Bernstein Conference, September 15-17, 2015, Heidelberg, Germany doi: 10.12751/nncn.bc2015.0056

[Au3] Sára Sáray, Christian A. Rössert, Tamás F. Freund, Szabolcs Káli: Systematic comparison and automatic validation of models of dendritic integration and somatic spiking in CA1 pyramidal cells, IBRO (International Brain Research Organization) Conference, January 20-21, 2016, Budapest, Hungary

[Au4] Sára Sáray, Christian A. Rössert, Tamás F. Freund, Szabolcs Káli: Systematic comparison and automatic validation of models of dendritic integration and somatic spiking in CA1 pyramidal cells, DENDRITES 2016 Workshop, June 18-21, 2016, Heraklion, Crete

[Au5] Luca Tar, Zsuzsanna Bengery, Sára Sáray, Tamás Freund, Szabolcs Káli; The contribution of dendritic spines to synaptic integration and plasticity in hippocampal pyramidal neurons, 28th Annual Computational Neuroscience Meeting (CNS*2019), July 13-17, 2019, Barcelona, Spain https://doi.org/10.1186/s12868-019-0538-0

[Au6] Máté Mohácsi, Márk Patrik Török, Sára Sáray, Tamás Freund, Szabolcs Káli; A unified framework for the application and evaluation of different methods for neural parameter optimization, NeuroInformatics 2019 Conference, September 1-2, 2019, Warsaw, Poland (Abstract available: https://www.neuroinformatics2019.org/wp-content/uploads/2019/09/NI2019_AbstractBook.pdf)

Acknowledgements

Foremost, I express my deep gratitude to Szabolcs Káli, my supervisor, for his guidance, patience, and valuable support and for his unbroken enthusiasm and encouragement in teaching me scientific research.

DOI:10.15774/PPKE.ITK.2022.001

I am grateful to Tamás Freund for his support and for giving me the opportunity to work in his research group.

Many thanks to my colleagues, Luca Tar and Máté Mohácsi, for their help and support both professionally and as friends.

I am grateful to Shailesh Appukuttan and Andrew Davison, who are members of the team developing the Validation Framework, for their support in making HippoUnit adaptable to the framework, and for their technical help in integrating all the tests, models, and validation results in the framework.

I would like to thank Christian Rössert, who was my supervisor during my internship at the Blue Brain Project, for his help in starting to develop the HippoUnit test suite and learning how to use Python as an interface to the NEURON simulator. I am also thankful for Werner Van Geit for his help in solving technical issues with programming and parallelization.

I gratefully acknowledge the help of Carmen Lupascu and Luca Bologna in the process of feature extraction.

I am very thankful to the leaders and members of the Pázmány Péter Catholic University, Faculty of Information Technology and Bionics and the Roska Tamás Doctoral School of Sciences and Technology for the opportunity to participate in the doctoral program, and Katinka Tivadarné Vida for her kind help and support. I also thank the work of the Dean's Office and the Financial Department.

I gratefully acknowledge the financial support of the following grants: the European Union's Horizon 2020 Framework Programme for Research and Innovation under Specific Grant Agreements No. 720270 and No. 785907 (Human Brain Project SGA1 and SGA2); the European Union, co-financed by the European Social Fund (EFOP-3.6.3-VEKOP- 16-2017-00002); the ÚNKP-19-3-III New National Excellence Program of the Ministry for Innovation and Technology (Hungary).

Last but certainly not least I am grateful to my family and friends who supported me in all possible ways.

List of Figures

Figure 2.1: Structure of the hippocampal formation. Original drawing of Santiago Ramón y Cajal (1911) of the subregions of the hippocampal formation showing the main cell types and axonal pathways. Inset shows the flow of information in the hippocampus. 7

Figure 2.2: The morphology, inputs and outputs of CA1 pyramidal neurons. Drawing of a CA1 pyramidal neuron reconstructed using Camera lucida. The soma is shown in the stratum pyramidale (s.p.), at its base the basal dendrites can be found in the stratum

DOI:10.15774/PPKE.ITK.2022.001

oriens (s.o.), the bifurcating two-branch trunk and the oblique dendrites are in the stratum radiatum (s.r.), and the tuft dendrites are in the stratum lacunosum-moleculare (s.l.m.). The major excitatory inputs of each layer are also indicated along with the most important intra- and extrahippocampal targets of the axonal branches. Extrahippocampal targets depend on the location of the neuron along the septo-temporal axis, which is also indicated on the figure. The figure was adapted from The Hippocampus Book [47]..... 13

Figure 4.1: The morphologies of the different models tested and their voltage responses to a 400 ms somatic step current injection of 0.6 nA amplitude. (Some of the models share the same morphology, while the Gómez González et al. 2011 model was adjusted to five different morphologies.) [Th1]..... 49

Figure 4.2: Feature values from the Somatic Features Test of HippoUnit applied to several published models. Absolute feature values extracted (using the electrophys Feature Extraction Library (eFEL)) from the voltage responses of the models to somatic current injections of varying amplitude, compared to mean experimental values (black X) that were extracted from the patch clamp dataset. Black solid, horizontal lines indicate the experimental standard deviation. Colored solid, horizontal lines typically show the standard deviation of spiking features of models, where the feature value of each action potential in the voltage trace is extracted and averaged. Feature names (y axis labels) are indicated as they are used in eFEL combined with the step current injection amplitude. Not all the evaluated features are shown here. (The (s) and (w) notations of the Golding et al. 2001 models in the legend indicate the strong and weak propagating versions of the model.) [Th1] 51

Figure 4.3: Evaluation of results from the Somatic Features Test of HippoUnit applied to published models. (A) Mean feature scores (the difference between the model's feature value and the experimental mean in units of the experimental SD) of the different models. Feature score values are averaged over the different input step amplitudes. (B) The bars represent the number of features that were attempted to be evaluated for the models (i.e., the number of features extracted from the experimental patch clamp dataset). The number of successfully evaluated features for the various models is shown in green, and the number of features that could not be evaluated for a particular model is shown in red. Features that are not evaluated successfully are most often spiking features at step amplitudes for which the tested model does not fire action potentials. [Th1] 53

Figure 4.4: Comparison of the final scores achieved by the different models on the Somatic Features Test against validation data from two different datasets (sharp electrode data, patch clamp data). Final scores are calculated as the average of all the feature

scores. In the upper panel (A) the raw output of the tests is shown, while in the lower panel (B) the feature scores and the final scores have been recalculated using standardized standard deviation values. Numbers above each data point show the proportion of the successfully evaluated features compared to the number of features attempted to be evaluated (successfully extracted from the data set). Note that while in the recalculated final scores (B) only those eFEL features were taken into account that could be extracted from both datasets, they are extracted for different current step amplitudes, which accounts for the difference in the number of observation features for the two datasets. 55

Figure 4.5: Results from the Depolarization Block Test of HippoUnit applied to published models. (A) Average number of action potentials from 4 cells (3 repetitions each) to 1 sec somatic current injection in the target experimental data. (B) Example voltage trace of a cell that entered depolarization block and reached an equilibrium potential of -40 mV in the target experiment. Panels (A) and (B) were adapted from Bianchi et al. 2012 [25]. (C) Number of APs fired by the models in response to 1 sec long somatic current injections of increasing intensity. (D) Depolarization block feature values extracted from the voltage responses of the models compared to the experimental observations. exp_I_{th} is the mean (SD is indicated with a solid line) of the experimentally observed threshold current amplitude to reach depolarization block. In the test two separate features are compared to the experimental threshold value: The I_maxNumAP feature is the current intensity at which the model fires the maximum number of action potentials, and the I_below_depol_block feature is the current intensity one step before the model enters depolarization block. According to the experimental observation, these two values are supposed to be the same, but for models, they may differ, in which case a penalty is added to the final score (see the text for more details). The V_{eq} is the equilibrium potential to which the somatic voltage settles after entering depolarization block. (E) Voltage traces of different models that were recognized by the test as depolarization block. Note that only the Bianchi et al. 2012 model actually entered depolarization block, the others “cheated” the test (see the main text for more details). [Th1].....57

Figure 4.6: Results from the Back-propagating Action Potential Test of HippoUnit applied to published models. (A) Example experimental voltage traces triggered by somatic current injection and simultaneously recorded from the soma and the trunk. (B) The amplitude of the first (left) and last (right) back-propagating action potentials in a 10 to 20 Hz train triggered by somatic current injection as a function of the distance of the recording location from the soma in the target experiment. Panels (A) and (B) were adapted from Golding et al. 2001 [27]. (C) The amplitudes of the first back-

DOI:10.15774/PPKE.ITK.2022.001

propagating action potentials (in a train of spikes with frequency around 15 Hz evoked by somatic current injection) of the different models as a function of recording location distance from the soma. (D) Feature scores achieved by the different models on the Back-propagating AP Test. The amplitudes of the first and last back-propagating action potentials were averaged over the distance ranges of 50, 150, 250, 350 ± 20 μm and compared to the experimental features (see Methods for more details). [Th1] 59

Figure 4.7: Results from the PSP Attenuation Test of HippoUnit applied to published models. (A) The experimental averages of the EPSPs recorded at the dendritic input site and the soma. (B) Mean peak amplitude of EPSPs measured simultaneously at the soma and the dendrite as a function of the synaptic input distance from the soma in the target experiment. The soma/dendrite attenuation values that are used for the quantitative comparison were calculated from these data. Panels (A) and (B) were adapted from Magee and Cook 2000 [29]. (C) Soma/dendrite EPSP attenuation as a function of the synaptic input distance from the soma in the different models. [Th1] 61

Figure 4.8: Results from the Oblique Integration Test of HippoUnit applied to published models. (A) Example experimental recording of somatic EPSPs to an increasing number of synchronous synaptic inputs showing the fast component that is the result of the generation of a sodium spike on the dendrite (top) and the first temporal derivatives of the same traces (bottom). (B) Experimental supralinear input-output curve of synchronous synaptic inputs to the oblique dendrites. (C) Peak derivative values versus the number of synchronous inputs in the target experiment showing a step increase at the input level of dendritic spike generation. Panels (A)-(C) were adapted from Losonczy and Magee 2006 [33] (D) Comparison of the responses of the models to experimental results (black X) according to features of dendritic integration. Features values are given as mean and standard deviation, as several dendritic locations of each model are tested. (E) The averaged input – output curves of all the dendritic locations of the models examined. EPSP amplitudes are measured at the soma. Dashed line shows linearity. In models whose curve goes above the dashed line, oblique dendrites integrate synaptic inputs that are spatially and temporally clustered supralinearly. [Th1] 63

Figure 4.9: Normalized final scores achieved by the different published models on the various tests of HippoUnit. The final scores of each test are normalized by dividing the scores of each model by the best achieved score on the given test. [Th1] 67

Figure 4.10: Employing the tests of HippoUnit to monitor the behavior of a set of detailed data-driven models of hippocampal neurons at different stages of model development.

DOI:10.15774/PPKE.ITK.2022.001

Models of four different cell types (pyramidal cells and continuous accommodating (int cAC), bursting accommodating (int bAC) and continuous non-accommodating (int cNAC) interneurons) of the rat hippocampal CA1 region were developed within the Human Brain Project by automated optimization using BluePyOpt. The tests of HippoUnit were used to evaluate and compare the behavior of the older (Migliore et al 2018) version and the new (v4) version of these models. The median, the interquartile range and the full range of the final scores achieved by the models of each cell type were calculated and the results of the two versions of the model set are compared. Asterisks indicate significant differences (*: $p<0.05$; **: $p<0.01$). [Th1].....70

Figure 4.11: Results from the PSP Attenuation Test of HippoUnit applied to the new (v4) version of the BluePyOpt optimized models within the Human Brain Project. Soma/dendrite EPSP attenuation as a function of the synaptic input distance from the soma in the differen models. The plot shows that the attenuation of synaptic EPSPs is consistent with experimental data [29].....71

Figure 4.12: Results from the Back-propagating AP Test Basket Cell. (A) –(C) The target experimental data of the AP peak amplitude, maximal slope of the rise, and duration at half-maximal amplitude against recording distances from the soma (negative distances – basal, positive distances - apical dendrites). Solid symbols: somatic current injection; open symbols: dendritic current injection. Red: first AP; blue: last AP in a 1 sec train. Figures were adapted from Hu et al. 2010 [119]. (D) The properties of the 1st and last bAPs at different distances on the basal dendrites of the models (these models do not have apical dendrites). (E) The feature scores achieved by the models. (black X - experimental observation, squares of different colours at distance 0 indicate the somata of the different models). 75

Figure 4.13: Results from the AP Propagation Axon Test Basket Cell. (A) –(D) Target experimental data for the first (A) and last (C) AP amplitude and the first (B) and last (D) AP half-duration against the distance of the axonal recording location from the soma. (black: somatic recordings; blue: axonal recordings). Figures were adapted from Hu et al. 2018 [120]. (E) The properties of the 1st and last APs at different distances on the axon of the different models. (F) The feature scores achieved by the models. (black X - experimental observation, squares of different colours at distance 0 indicate the somata of the different models). 76

Figure 4.14: Results from the Back-propagating AP Test CA3 PC. (A) Target experimental data for the AP amplitude and AP half-duration to somatic rheobase current injection against the distance of the recording location from the soma (negative distances – basal, positive distances - apical dendrites). (B) Experimental ratio of the amplitude

(left) and half-duration (right) of the 5th and 1st bAPs evoked by short somatic current pulses of different frequencies at different distances from the soma. Panels (A) and (B) were adapted from Kim et al. 2012 [121]. (C) The properties of the models' bAPs at different distances on the dendritic tree evoked by long rheobase somatic current injection. (D) The ratio of the amplitude and half-duration of the 5th and 1st bAPs evoked by short somatic current pulses at different distances from the soma. (black X - experimental observation, squares of different colours at distance 0 indicate the soma of the different models). 78

List of Tables

Table 2.1: Summary of the most important physiological properties of the hippocampal CA1 pyramidal cell, and the main mechanisms underlying them..... 26

Table 3.1: Comparison of the most important somatic features extracted using eFEL from the patch clamp dataset (used as target data in the Somatic Features Test) to results from patch clamp recordings available in the literature. [Th1] 36

Bibliography

[1] G. T. Einevoll *et al.*, "The Scientific Case for Brain Simulations," *Neuron*, vol. 102, no. 4, pp. 735–744, 2019, doi: 10.1016/j.neuron.2019.03.027.

[2] S. Káli and T. F. Freund, "Distinct properties of two major excitatory inputs to hippocampal pyramidal cells: A computational study," *European Journal of Neuroscience*, vol. 22, no. 8, pp. 2027–2048, 2005, doi: 10.1111/j.1460-9568.2005.04406.x.

[3] R. Migliore *et al.*, "The physiological variability of channel density in hippocampal CA1 pyramidal cells and interneurons explored using a unified data-driven modeling workflow," *PLoS Computational Biology*, vol. 14, no. 9, pp. 1–25, 2018, doi: 10.1371/journal.pcbi.1006423.

[4] E. Hay, S. Hill, F. Schürmann, H. Markram, and I. Segev, "Models of neocortical layer 5b pyramidal cells capturing a wide range of dendritic and perisomatic active properties," *PLoS Computational Biology*, vol. 7, no. 7, 2011, doi: 10.1371/journal.pcbi.1002107.

[5] A. V. M. Herz, T. Gollisch, C. K. Machens, and D. Jaeger, “Modeling single-neuron dynamics and computations: A balance of detail and abstraction,” *Science*, vol. 314, no. 5796, pp. 80–85, 2006, doi: 10.1126/science.1127240.

[6] P. Poirazi, T. Brannon, and B. W. Mel, “Pyramidal neuron as two-layer neural network,” *Neuron*, vol. 37, no. 6, pp. 989–999, 2003, doi: 10.1016/S0896-6273(03)00149-1.

[7] J. M. Bower, “The 40-year history of modeling active dendrites in cerebellar purkinje cells: Emergence of the first single cell ‘community model,’” *Frontiers in Computational Neuroscience*, vol. 9, no. 129, pp. 1–18, 2015, doi: 10.3389/fncom.2015.00129.

[8] R. D. Traub, R. K. S. Wong, R. Miles, and H. Michelson, “A model of a CA3 hippocampal pyramidal neuron incorporating voltage-clamp data on intrinsic conductances,” *Journal of Neurophysiology*, vol. 66, no. 2, pp. 635–650, 1991, doi: 10.1152/jn.1991.66.2.635.

[9] M. Almog and A. Korngreen, “A quantitative description of dendritic conductances and its application to dendritic excitation in layer 5 pyramidal neurons,” *Journal of Neuroscience*, vol. 34, no. 1, pp. 182–196, 2014, doi: 10.1523/JNEUROSCI.2896-13.2014.

[10] M. Almog and A. Korngreen, “Is realistic neuronal modeling realistic?,” *Journal of Neurophysiology*, vol. 116, no. 5, pp. 2180–2209, 2016, doi: 10.1152/jn.00360.2016.

[11] H. Markram *et al.*, “Reconstruction and Simulation of Neocortical Microcircuitry,” *Cell*, vol. 163, no. 2, pp. 456–492, 2015, doi: 10.1016/j.cell.2015.09.029.

[12] R. D. Traub *et al.*, “Single-column thalamocortical network model exhibiting gamma oscillations, sleep spindles, and epileptogenic bursts,” *Journal of Neurophysiology*, vol. 93, no. 4, pp. 2194–2232, 2005, doi: 10.1152/jn.00983.2004.

[13] C. J. Schneider, M. Bezaire, and I. Soltesz, “Toward a full-scale computational model of the rat dentate gyrus,” *Frontiers in Neural Circuits*, vol. 6, no. 83, pp. 1–8, 2012, doi: 10.3389/fncir.2012.00083.

[14] M. J. Bezaire, I. Raikov, K. Burk, D. Vyas, and I. Soltesz, “Interneuronal mechanisms of hippocampal theta oscillations in a full-scale model of the rodent CA1 circuit,” *eLife*, vol. 5, pp. 1–106, 2016, doi: 10.7554/eLife.18566.

[15] P. Friedrich, M. Vella, A. I. Gulyás, T. F. Freund, and S. Káli, “A flexible, interactive software tool for fitting the parameters of neuronal models,” *Frontiers in Neuroinformatics*, vol. 8, no. 63, pp. 1–19, 2014, doi: 10.3389/fninf.2014.00063.

[16] W. van Geit *et al.*, “BluePyOpt: Leveraging open source software and cloud infrastructure to optimise model parameters in neuroscience,” *Frontiers in Neuroinformatics*, vol. 10, no. 17, pp. 1–18, 2016, doi: 10.3389/fninf.2016.00017.

[17] M. C. Vanier and J. M. Bower, “A comparative survey of automated parameter-search methods for compartmental neural models,” *Journal of Computational Neuroscience*, vol. 7, no. 2, pp. 149–171, 1999, doi: 10.1023/A:1008972005316.

[18] R. A. McDougal *et al.*, “Twenty years of ModelDB and beyond: building essential modeling tools for the future of neuroscience,” *Journal of Computational Neuroscience*, vol. 42, no. 1, pp. 1–10, 2017, doi: 10.1007/s10827-016-0623-7.

[19] C. Omar, J. Aldrich, and R. C. Gerkin, “Collaborative infrastructure for test-driven scientific model validation,” *36th International Conference on Software Engineering, ICSE Companion 2014 - Proceedings*, pp. 524–527, 2014, doi: 10.1145/2591062.2591129.

[20] R. Gerkin and C. Omar, “NeuroUnit: Validation Tests for Neuroscience Models,” 2013. doi: 10.3389/conf.fninf.2013.09.00013.

[21] S. Appukuttan, P. E. Garcia, and A. P. Davison, “MorphoUnit.” Zenodo, 2020. doi: https://doi.org/10.5281/zenodo.3862936.

[22] S. Appukuttan, J. Dainauskas, and A. P. Davison, “SynapseUnit.” Zenodo, 2020. doi: http://doi.org/10.5281/zenodo.3862944.

[23] P. E. Garcia and A. P. Davison, “HippoNetworkUnit.” Zenodo, 2020. doi: http://doi.org/10.5281/zenodo.3886484.

[24] B. L. Sharma and A. P. Davison, “CerebUnit.” Zenodo, 2020. doi: http://doi.org/10.5281/zenodo.3885673.

[25] D. Bianchi *et al.*, “On the mechanisms underlying the depolarization block in the spiking dynamics of CA1 pyramidal neurons,” *Journal of Computational Neuroscience*, vol. 33, no. 2, pp. 207–225, 2012, doi: 10.1007/s10827-012-0383-y.

[26] N. Spruston, Y. Schiller, G. Stuart, and B. Sakmann, “Activity-Dependent Action Potential Invasion and Calcium Influx into Hippocampal CA1 Dendrites,” *Science*, vol. 268, no. 5208, pp. 297–300, 1995, doi: 10.1126/science.7716524.

[27] N. L. Golding, W. L. Kath, and N. Spruston, “Dichotomy of action-potential backpropagation in CA1 pyramidal neuron dendrites,” *Journal of Neurophysiology*, vol. 86, no. 6, pp. 2998–3010, 2001, doi: 10.1152/jn.2001.86.6.2998.

[28] S. Gasparini, A. Losonczy, X. Chen, D. Johnston, and J. C. Magee, “Associative pairing enhances action potential back-propagation in radial oblique branches of CA1 pyramidal neurons,” *Journal of Physiology*, vol. 580, no. 3, pp. 787–800, 2007, doi: 10.1113/jphysiol.2006.121343.

[29] J. C. Magee and E. P. Cook, “Somatic EPSP amplitude is independent of synapse location in hippocampal pyramidal neurons,” *Nature Neuroscience*, vol. 3, no. 9, pp. 895–903, 2000, doi: 10.1038/78800.

[30] S. Gasparini and J. C. Magee, “State-dependent dendritic computation in hippocampal CA1 pyramidal neurons,” *Journal of Neuroscience*, vol. 26, no. 7, pp. 2088–2100, 2006, doi: 10.1523/JNEUROSCI.4428-05.2006.

[31] G. Ariav, A. Polsky, and J. Schiller, “Submillisecond precision of the input-output transformation function mediated by fast sodium dendritic spikes in basal dendrites of CA1 pyramidal neurons,” *Journal of Neuroscience*, vol. 23, no. 21, pp. 7750–7758, 2003, doi: 10.1523/jneurosci.23-21-07750.2003.

[32] H. Takahashi and J. C. Magee, “Pathway Interactions and Synaptic Plasticity in the Dendritic Tuft Regions of CA1 Pyramidal Neurons,” *Neuron*, vol. 62, no. 1, pp. 102–111, 2009, doi: 10.1016/j.neuron.2009.03.007.

[33] A. Losonczy and J. C. Magee, “Integrative Properties of Radial Oblique Dendrites in Hippocampal CA1 Pyramidal Neurons,” *Neuron*, vol. 50, no. 2, pp. 291–307, 2006, doi: 10.1016/j.neuron.2006.03.016.

[34] O. J. Ahmed and M. R. Mehta, “The hippocampal rate code: anatomy, physiology and theory,” *Trends in Neurosciences*, vol. 32, no. 6, pp. 329–338, 2009, doi: 10.1016/j.tins.2009.01.009.

[35] D. G. Amaral and M. P. Witter, “The three-dimensional organization of the hippocampal formation: A review of anatomical data,” *Neuroscience*, vol. 31, no. 3, pp. 571–591, 1989, doi: 10.1016/0306-4522(89)90424-7.

[36] T. F. Freund and G. Buzsáki, “Interneurons of the Hippocampus,” *Hippocampus*, vol. 6, no. 4, pp. 347–470, 1996, doi: 10.1002/(sici)1098-1063(1996)6:4<347::aid-hipo1>3.0.co;2-i.

[37] N. L. M. Cappaert, N. M. van Strien, and M. P. Witter, *Hippocampal Formation*, Fourth Edi. Elsevier Inc., 2015. doi: 10.1016/B978-0-12-374245-2.00020-6.

[38] W. B. Scoville and B. Milner, “Loss of recent memory after bilateral hippocampal lesions,” *Journal of Neurology, Neurosurgery and Psychiatry*, vol. 20, no. 11, pp. 11–21, 1957, doi: 10.1136/jnnp.20.1.11.

[39] S. Corkin, D. G. Amaral, R. Gilberto González, K. A. Johnson, and B. T. Hyman, “H. M.’s Medial temporal lobe lesion: Findings from magnetic resonance imaging,” *Journal of Neuroscience*, vol. 17, no. 10, pp. 3964–3979, 1997, doi: 10.1523/jneurosci.17-10-03964.1997.

[40] J. Annese *et al.*, “Postmortem examination of patient H.M.’s brain based on histological sectioning and digital 3D reconstruction,” *Nature Communications*, vol. 5, pp. 1–9, 2014, doi: 10.1038/ncomms4122.

[41] G. Buzsáki, “Two-stage model of memory trace formation: A role for ‘noisy’ brain states,” *Neuroscience*, vol. 31, no. 3, pp. 551–570, 1989, doi: 10.1016/0306-4522(89)90423-5.

[42] J. O'Keefe, J. Dostrovsky, and J. D. J. O'Keefe, "Short Communications The hippocampus as a spatial map . Preliminary evidence from unit activity in the freely-moving rat," *Brain Research*, vol. 34, no. 1, pp. 171–175, 1971, [Online]. Available: http://www.ncbi.nlm.nih.gov/pubmed/5124915

[43] E. I. Moser, E. Kropff, and M. B. Moser, "Place cells, grid cells, and the brain's spatial representation system," *Annual Review of Neuroscience*, vol. 31, pp. 69–89, 2008, doi: 10.1146/annurev.neuro.31.061307.090723.

[44] N. J. Bannister and A. U. Larkman, "Dendritic morphology of CA1 pyramidal neurones from the rat hippocampus: I. Branching patterns," *Journal of Comparative Neurology*, vol. 360, no. 1, pp. 150–160, 1995, doi: 10.1002/cne.903600111.

[45] N. J. Bannister and A. U. Larkman, "Dendritic Morphology of CAl Pyramidal Neurones From the Rat Hippocampus: II. Spine Distributions," *Journal of Comparative Neurology*, vol. 360, no. 1, pp. 161–171, 1995, doi: 10.1002/cne.903600112.

[46] M. Megías, Z. Emri, T. F. Freund, and A. I. Gulyás, "Total number and distribution of inhibitory and excitatory synapses on hippocampal CA1 pyramidal cells," *Neuroscience*, vol. 102, no. 3, pp. 527–540, 2001, doi: 10.1016/S0306-4522(00)00496-6.

[47] N. Spruston and C. McBain, "Structural and Functional Properties of the Hippocampal Neurons," P. Andersen, R. Morris, D. Amaral, T. Bliss, and J. O'Keefe, Eds. Oxford University Press, 2007, pp. 133–203.

[48] I. Aradi and I. Soltesz, "Modulation of network behaviour by changes in variance in interneuronal properties," *Journal of Physiology*, vol. 538, no. 1, pp. 227–251, 2002, doi: 10.1113/jphysiol.2001.013054.

[49] N. P. Staff, H. Y. Jung, T. Thiagarajan, M. Yao, and N. Spruston, "Resting and active properties of pyramidal neurons in subiculum and CA1 of rat hippocampus," *Journal of Neurophysiology*, vol. 84, no. 5, pp. 2398–2408, 2000, doi: 10.1152/jn.2000.84.5.2398.

[50] B. N. Routh, D. Johnston, K. Harris, and R. A. Chitwood, "Anatomical and electrophysiological comparison of CA1 pyramidal neurons of the rat and mouse," *Journal of Neurophysiology*, vol. 102, no. 4, pp. 2288–2302, 2009, doi: 10.1152/jn.00082.2009.

[51] K. A. Dougherty, T. Islam, and D. Johnston, "Intrinsic excitability of CA1 pyramidal neurones from the rat dorsal and ventral hippocampus," *Journal of Physiology*, vol. 590, no. 22, pp. 5707–5722, 2012, doi: 10.1113/jphysiol.2012.242693.

[52] R. Malik, K. A. Dougherty, K. Parikh, C. Byrne, and D. Johnston, "Mapping the electrophysiological and morphological properties of CA1 pyramidal neurons along the longitudinal hippocampal axis," *Hippocampus*, vol. 26, no. 3, pp. 341–361, 2016, doi: 10.1002/hipo.22526.

[53] S. Gasparini, M. Migliore, and J. C. Magee, “On the initiation and propagation of dendritic spikes in CA1 pyramidal neurons,” *Journal of Neuroscience*, vol. 24, no. 49, pp. 11046–11056, 2004, doi: 10.1523/JNEUROSCI.2520-04.2004.

[54] C. M. McDermott, M. N. Hardy, N. G. Bazan, and J. C. Magee, “Sleep deprivation-induced alterations in excitatory synaptic transmission in the CA1 region of the rat hippocampus,” *Journal of Physiology*, vol. 570, no. 3, pp. 553–565, 2006, doi: 10.1113/jphysiol.2005.093781.

[55] J. F. Storm, “An after-hyperpolarization of medium duration in rat hippocampal pyramidal cells.,” *The Journal of Physiology*, vol. 409, no. 1, pp. 171–190, 1989, doi: 10.1113/jphysiol.1989.sp017491.

[56] J. F. Storm, “Action potential repolarization and a fast after-hyperpolarization in rat hippocampal pyramidal cells,” *Journal of Physiology*, vol. 385, pp. 733–759, 1987.

[57] N. Gu, K. Vervaeke, H. Hu, and J. F. Storm, “Kv7/KCNQ/M and HCN/h, but not KCa2/SK channels, contribute to the somatic medium after-hyperpolarization and excitability control in CA1 hippocampal pyramidal cells,” *Journal of Physiology*, vol. 566, no. 3, pp. 689–715, 2005, doi: 10.1113/jphysiol.2005.086835.

[58] B. King *et al.*, “IKCa channels are a critical determinant of the slow AHP in CA1 pyramidal neurons,” *Cell Reports*, vol. 11, no. 2, pp. 175–182, 2015, doi: 10.1016/j.celrep.2015.03.026.

[59] R. W. Turner *et al.*, “Assessing the role of IKCa channels in generating the sAHP of CA1 hippocampal pyramidal cells,” *Channels*, vol. 10, no. 4, pp. 313–319, 2016, doi: 10.1080/19336950.2016.1161988.

[60] E. C. McKiernan and D. F. Marrone, “CA1 pyramidal cells have diverse biophysical properties, affected by development, experience, and aging,” *PeerJ*, vol. 2017, no. 9, pp. 1–47, 2017, doi: 10.7717/peerj.3836.

[61] H. Y. Chu, Q. Gu, G. Z. Jin, G. Y. Hu, and X. Zhen, “Electrophysiological effects of SKF83959 on hippocampal CA1 pyramidal neurons: Potential mechanisms for the drug’s neuroprotective effects,” *PLoS ONE*, vol. 5, no. 10, pp. 1–9, 2010, doi: 10.1371/journal.pone.0013118.

[62] A. E. Metz, T. Jarsky, M. Martina, and N. Spruston, “R-type calcium channels contribute to afterdepolarization and bursting in hippocampal CA1 pyramidal neurons,” *Journal of Neuroscience*, vol. 25, no. 24, pp. 5763–5773, 2005, doi: 10.1523/JNEUROSCI.0624-05.2005.

[63] D. v Madison and R. A. Nicoll, “Control of the Repetitive discharge of rat CA1 pyramidal neurons in vitro,” *Journal of Physiology*, vol. 354, pp. 319–331, 1984.

[64] B. Knauer and M. Yoshida, “Switching between persistent firing and depolarization block in individual rat CA1 pyramidal neurons,” *Hippocampus*, vol. 29, no. 9, pp. 817–835, 2019, doi: 10.1002/hipo.23078.

[65] J. C. Magee and M. Carruth, “Dendritic voltage-gated ion channels regulate the action potential firing mode of hippocampal CA1 pyramidal neurons,” *Journal of Neurophysiology*, vol. 82, no. 4, pp. 1895–1901, 1999, doi: 10.1152/jn.1999.82.4.1895.

[66] N. Spruston, “Pyramidal neurons: Dendritic structure and synaptic integration,” *Nature Reviews Neuroscience*, vol. 9, no. 3, pp. 206–221, 2008, doi: 10.1038/nrn2286.

[67] K. Sidiropoulou, E. K. Pissadaki, and P. Poirazi, “Inside the brain of a neuron,” *EMBO Reports*, vol. 7, no. 9, pp. 886–892, 2006, doi: 10.1038/sj.embor.7400789.

[68] Y. Katz, V. Menon, D. A. Nicholson, Y. Geinisman, W. L. Kath, and N. Spruston, “Synapse Distribution Suggests a Two-Stage Model of Dendritic Integration in CA1 Pyramidal Neurons,” *Neuron*, vol. 63, no. 2, pp. 171–177, 2009, doi: 10.1016/j.neuron.2009.06.023.

[69] D. A. Nicholson, R. Trana, Y. Katz, W. L. Kath, N. Spruston, and Y. Geinisman, “Distance-Dependent Differences in Synapse Number and AMPA Receptor Expression in Hippocampal CA1 Pyramidal Neurons,” *Neuron*, vol. 50, no. 3, pp. 431–442, 2006, doi: 10.1016/j.neuron.2006.03.022.

[70] D. S. Wei, Y. A. Mei, A. Bagal, J. P. Y. Kao, S. M. Thompson, and C. M. Tang, “Compartmentalized and binary behavior of terminal dendrites in hippocampal pyramidal neurons,” *Science*, vol. 293, no. 5538, pp. 2272–2275, 2001, doi: 10.1126/science.1061198.

[71] D. A. Hoffman, J. C. Magee, C. M. Colbert, and D. Johnston, “K+ channel regulation of signal propagation in dendrites of hippocampal pyramidal neurons,” *Nature*, vol. 387, no. 6636, pp. 869–875, 1997, doi: 10.1038/43119.

[72] H. Y. Jung, T. Mickus, and N. Spruston, “Prolonged sodium channel inactivation contributes to dendritic action potential attenuation in hippocampal pyramidal neurons,” *Journal of Neuroscience*, vol. 17, no. 17, pp. 6639–6646, 1997, doi: 10.1523/jneurosci.17-17-06639.1997.

[73] N. L. Golding and N. Spruston, “Dendritic sodium spikes are variable triggers of axonal action potentials in hippocampal CA1 pyramidal neurons,” *Neuron*, vol. 21, no. 5, pp. 1189–1200, 1998, doi: 10.1016/S0896-6273(00)80635-2.

[74] N. L. Golding, H. Y. Jung, T. Mickus, and N. Spruston, “Dendritic calcium spike initiation and repolarization are controlled by distinct potassium channel subtypes in CA1 pyramidal neurons,” *Journal of Neuroscience*, vol. 19, no. 20, pp. 8789–8798, 1999, doi: 10.1523/jneurosci.19-20-08789.1999.

[75] G. J. Stuart and N. Spruston, “Dendritic integration: 60 years of progress,” *Nature Neuroscience*, vol. 18, no. 12, pp. 1713–1721, 2015, doi: 10.1038/nn.4157.

[76] C. Grienberger, X. Chen, and A. Konnerth, “NMDA receptor-dependent multidendrite Ca2+ spikes required for hippocampal burst firing invivo,” *Neuron*, vol. 81, no. 6, pp. 1274–1281, 2014, doi: 10.1016/j.neuron.2014.01.014.

[77] G. Buzsáki, M. Penttonen, Z. Nádasdy, and A. Bragin, “Pattern and inhibition-dependent invasion of pyramidal cell dendrites by fast spikes in the hippocampus in vivo,” *Proceedings of the National Academy of Sciences of the United States of America*, vol. 93, no. 18, pp. 9921–9925, 1996, doi: 10.1073/pnas.93.18.9921.

[78] S. Yang, V. Emiliani, and C. M. Tang, “The kinetics of multibranch integration on the dendritic arbor of CA1 pyramidal neurons,” *Frontiers in Cellular Neuroscience*, vol. 8, no. MAY, pp. 1–11, 2014, doi: 10.3389/fncel.2014.00127.

[79] P. Poirazi, T. Brannon, and B. W. Mel, “Arithmetic of subthreshold synaptic summation in a model CA1 pyramidal cell,” *Neuron*, vol. 37, no. 6, pp. 977–987, 2003, doi: 10.1016/S0896-6273(03)00148-X.

[80] Y. Kim, C. L. Hsu, M. S. Cembrowski, B. D. Mensh, and N. Spruston, “Dendritic sodium spikes are required for long-term potentiation at distal synapses on hippocampal pyramidal neurons,” *eLife*, vol. 4, no. AUGUST2015, pp. 1–30, 2015, doi: 10.7554/eLife.06414.

[81] N. L. Golding, N. P. Staff, and N. Spruston, “Dendritic spikes as a mechanism for cooperative long-term potentiation,” *Nature*, vol. 418, no. 6895, pp. 326–331, 2002, doi: 10.1038/nature00854.

[82] A. Losonczy, J. K. Makara, and J. C. Magee, “Compartmentalized dendritic plasticity and input feature storage in neurons,” *Nature*, vol. 452, no. 7186, pp. 436–441, 2008, doi: 10.1038/nature06725.

[83] J. K. Makara, A. Losonczy, Q. Wen, and J. C. Magee, “Experience-dependent compartmentalized dendritic plasticity in rat hippocampal CA1 pyramidal neurons,” *Nature Neuroscience*, vol. 12, no. 12, pp. 1485–1487, 2009, doi: 10.1038/nn.2428.

[84] S. Remy, J. Csicsvari, and H. Beck, “Activity-Dependent Control of Neuronal Output by Local and Global Dendritic Spike Attenuation,” *Neuron*, vol. 61, no. 6, pp. 906–916, 2009, doi: 10.1016/j.neuron.2009.01.032.

[85] T. Jarsky, A. Roxin, W. L. Kath, and N. Spruston, “Conditional dendritic spike propagation following distal synaptic activation of hippocampal CA1 pyramidal neurons,” *Nature Neuroscience*, vol. 8, no. 12, pp. 1667–1676, 2005, doi: 10.1038/nn1599.

[86] M. E. Sheffield and D. A. Dombeck, “Dendritic mechanisms of hippocampal place field formation,” *Current Opinion in Neurobiology*, vol. 54, pp. 1–11, 2019, doi: 10.1016/j.conb.2018.07.004.

[87] K. C. Bittner, A. D. Milstein, C. Grienberger, S. Romani, and J. C. Magee, “Behavioral time scale synaptic plasticity underlies CA1 place fields,” *Science*, vol. 357, no. 6355, pp. 1033–1036, 2017, doi: 10.1126/science.aan3846.

[88] P. Dayan and L. F. Abott, *Theoretical Neuroscience: Computational and Mathematical Modeling of Neural Systems*. The MIT Press, 2001.

[89] M. L. Hines and N. T. Carnevale, “The NEURON Simulation Environment,” *Neural Computation*, vol. 9, no. 6, pp. 1179–1209, 1997, doi: https://doi.org/10.1162/neco.1997.9.6.1179.

[90] M. L. Hines, A. P. Davison, and E. Muller, “NEURON and Python,” *Frontiers in Neuroinformatics*, vol. 3, no. JAN, pp. 1–12, 2009, doi: 10.3389/neuro.11.001.2009.

[91] M. Migliore, “Modeling the attenuation and failure of action potentials in the dendrites of hippocampal neurons,” *Biophysical Journal*, vol. 71, no. 5, pp. 2394–2403, 1996, doi: 10.1016/S0006-3495(96)79433-X.

[92] R. D. Traub and R. Llinas, “Hippocampal pyramidal cells: Significance of dendritic ionic conductances for neuronal function and epileptogenesis,” *Journal of Neurophysiology*, vol. 42, no. 2, pp. 476–496, 1979, doi: 10.1152/jn.1979.42.2.476.

[93] M. Kim *et al.*, “Colocalization of protein kinase a with adenylyl cyclase enhances protein kinase a activity during induction of Long-Lasting Long-Term-Potentiation,” *PLoS Computational Biology*, vol. 7, no. 6, 2011, doi: 10.1371/journal.pcbi.1002084.

[94] J. Jędrzejewska-Szmek, V. Luczak, T. Abel, and K. T. Blackwell, *β-adrenergic signaling broadly contributes to LTP induction*, vol. 13, no. 7. 2017. doi: 10.1371/journal.pcbi.1005657.

[95] T. Shuman *et al.*, “Breakdown of spatial coding and interneuron synchronization in epileptic mice,” *Nature Neuroscience*, vol. 23, no. 2, pp. 229–238, 2020, doi: 10.1038/s41593-019-0559-0.

[96] D. Bianchi *et al.*, “Effects of increasing CREB-dependent transcription on the storage and recall processes in a hippocampal CA1 microcircuit,” *Hippocampus*, vol. 24, no. 2, pp. 165–177, 2014, doi: 10.1002/hipo.22212.

[97] G. F. Turi *et al.*, “Vasoactive Intestinal Polypeptide-Expressing Interneurons in the Hippocampus Support Goal-Oriented Spatial Learning,” *Neuron*, vol. 101, no. 6, pp. 1150-1165.e8, 2019, doi: 10.1016/j.neuron.2019.01.009.

[98] S. Druckmann, Y. Banitt, A. Gidon, F. Schrümann, H. Markram, and I. Segev, “A novel multiple objective optimization framework for constraining conductance-based neuron

models by experimental data," *Frontiers in Neuroscience*, vol. 1, no. 1, pp. 7–18, 2007, doi: 10.3389/neuro.01.1.1.001.2007.

[99] W. van Geit, R. Moor, R. Ranjan, C. Roessert, and L. Riquelme, "Electrophys Feature Extraction Library." 2020. [Online]. Available: https://github.com/BlueBrain/eFEL

[100] S. J. Tripathy, J. Savitskaya, S. D. Burton, N. N. Urban, and R. C. Gerkin, "NeuroElectro: A window to the world's neuron electrophysiology data," *Frontiers in Neuroinformatics*, vol. 8, no. 40, pp. 1–11, 2014, doi: 10.3389/fninf.2014.00040.

[101] D. W. Wheeler, C. M. White, C. L. Rees, A. O. Komendantov, D. J. Hamilton, and G. A. Ascoli, "Hippocampome.org: A knowledge base of neuron types in the rodent hippocampus," *eLife*, vol. 4, pp. 1–28, 2015, doi: 10.7554/eLife.09960.

[102] A. R. Graves, S. J. Moore, E. B. Bloss, B. D. Mensh, W. L. Kath, and N. Spruston, "Hippocampal Pyramidal Neurons Comprise Two Distinct Cell Types that Are Countermodulated by Metabotropic Receptors," *Neuron*, vol. 76, no. 4, pp. 776–789, 2012, doi: 10.1016/j.neuron.2012.09.036.

[103] N. L. Golding, T. J. Mickus, Y. Katz, W. L. Kath, and N. Spruston, "Factors mediating powerful voltage attenuation along CA1 pyramidal neuron dendrites," *Journal of Physiology*, vol. 568, no. 1, pp. 69–82, 2005, doi: 10.1113/jphysiol.2005.086793.

[104] C. Roessert, D. Tanguy, and W. van Geit, "BluePyEfe: Blue Brain Python E-feature extraction." Zenodo, 2020. doi: 10.5281/zenodo.3728192.

[105] I. Bormann, "DigitizeIt: Digitizer software - digitize a scanned graph or chart into (x,y)-data." 2020. [Online]. Available: https://www.digitizeit.de/

[106] C. E. Jahr and C. F. Stevens, "Voltage dependence of NMDA-activated macroscopic conductances predicted by single-channel kinetics," *Journal of Neuroscience*, vol. 10, no. 9, pp. 3178–3182, 1990, doi: 10.1523/jneurosci.10-09-03178.1990.

[107] S. Hestrin, R. A. Nicoll, D. J. Perkel, and P. Sah, "Analysis of excitatory synaptic action in pyramidal cells using whole-cell recording from rat hippocampal slices," *Physiology*, no. 422, pp. 203–225, 1990, doi: 10.1113/jphysiol.1990.sp017980.

[108] M. Korinek, M. Sedlacek, O. Cais, I. Dittert, and L. Vyklicky, "Temperature dependence of N-methyl-d-aspartate receptor channels and N-methyl-d-aspartate receptor excitatory postsynaptic currents," *Neuroscience*, vol. 165, no. 3, pp. 736–748, 2010, doi: 10.1016/j.neuroscience.2009.10.058.

[109] M. Gevaert, L. Kanari, J. Palacios, E. Zisis, and B. Coste, "NeuroM." 2020. [Online]. Available: https://github.com/BlueBrain/NeuroM

[110] M. Migliore, I. de Blasi, D. Tegolo, and R. Migliore, "A modeling study suggesting how a reduction in the context-dependent input on CA1 pyramidal neurons could generate schizophrenic behavior," *Neural Networks*, vol. 24, no. 6, pp. 552–559, 2011, doi: 10.1016/j.neunet.2011.01.001.

[111] J. F. Gómez González, B. W. Mel, and P. Poirazi, “Distinguishing linear vs. non-linear integration in CA1 radial oblique dendrites: It’s about time,” *Frontiers in Computational Neuroscience*, vol. 5, no. November, pp. 1–12, 2011, doi: 10.3389/fncom.2011.00044.

[112] Jeffrey M. Perkel, “Why Jupyter is data scientists’ computational notebook of choice,” *Nature*, pp. 5–6, 2018, [Online]. Available: https://www.nature.com/articles/d41586-018-07196-1

[113] M. M. Shah, M. Migliore, I. Valencia, E. C. Cooper, and D. A. Brown, “Functional significance of axonal Kv7 channels in hippocampal pyramidal neurons,” *Proceedings of the National Academy of Sciences of the United States of America*, vol. 105, no. 22, pp. 7869–7874, 2008, doi: 10.1073/pnas.0802805105.

[114] A. Ecker *et al.*, “Data-driven integration of hippocampal CA1 synapse physiology in silico,” *Hippocampus*, 2020, doi: 10.1002/hipo.23220.

[115] K. A. Id *et al.*, “The Human Brain Project — Synergy between neuroscience , computing , informatics , and brain-inspired technologies,” pp. 1–7, 2019.

[116] H. Fragnaud, J. Gonin, J. Duperrier, E. Legouee, A. P. Davison, and S. Appukuttan, “hbp-validation-framework.” Zenodo, 2020. doi: http://doi.org/10.5281/zenodo.3888123.

[117] A. Tzilivaki, G. Kastellakis, and P. Poirazi, “Challenging the point neuron dogma: FS basket cells as 2-stage nonlinear integrators,” *Nature Communications*, vol. 10, no. 1, 2019, doi: 10.1038/s41467-019-11537-7.

[118] P. Hemond, D. Epstein, A. Boley, M. Migliore, G. A. Ascoli, and D. B. Jaffe, “Distinct classes of pyramidal cells exhibit mutually exclusive firing patterns in hippocampal area CA3b,” vol. 18, no. 4, pp. 411–424, 2008, doi: 10.1002/hipo.20404.Distinct.

[119] H. Hu, M. Martina, and P. Jonas, “Dendritic mechanisms underlying rapid synaptic activation of fast-spiking hippocampal interneurons,” *Science*, vol. 327, no. 5961, pp. 52–58, 2010, doi: 10.1126/science.1177876.

[120] H. Hu, F. C. Roth, D. Vandael, and P. Jonas, “Complementary Tuning of Na+ and K+ Channel Gating Underlies Fast and Energy-Efficient Action Potentials in GABAergic Interneuron Axons,” *Neuron*, vol. 98, no. 1, pp. 156-165.e6, 2018, doi: 10.1016/j.neuron.2018.02.024.

[121] S. Kim, S. J. Guzman, H. Hu, and P. Jonas, “Active dendrites support efficient initiation of dendritic spikes in hippocampal CA3 pyramidal neurons,” *Nature Neuroscience*, vol. 15, no. 4, pp. 600–606, 2012, doi: 10.1038/nn.3060.

[122] E. Marder and J. M. Goaillard, “Variability, compensation and homeostasis in neuron and network function,” *Nature Reviews Neuroscience*, vol. 7, no. 7, pp. 563–574, 2006, doi: 10.1038/nrn1949.

[123] E. Marder and A. L. Taylor, “Multiple models to capture the variability in biological neurons and networks,” *Nature Neuroscience*, vol. 14, no. 2, pp. 133–138, 2011, doi: 10.1038/nn.2735.

[124] E. Marder, M. L. Goeritz, and A. G. Otopalik, “Robust circuit rhythms in small circuits arise from variable circuit components and mechanisms,” *Current Opinion in Neurobiology*, vol. 31, pp. 156–163, 2015, doi: 10.1016/j.conb.2014.10.012.

[125] J. L. Ransdel, S. S. Nair, and D. J. Schulz, “Neurons within the same network independently achieve conserved output by differentially balancing variable conductance magnitudes,” *Journal of Neuroscience*, vol. 33, no. 24, pp. 9950–9956, 2013, doi: 10.1523/JNEUROSCI.1095-13.2013.

[126] J. Golowasch, M. S. Goldman, L. F. Abbott, and E. Marder, “Failure of averaging in the construction of a conductance-based neuron model,” *Journal of Neurophysiology*, vol. 87, no. 2, pp. 1129–1131, 2002, doi: 10.1152/jn.00412.2001.

[127] J. J. J. Hjorth *et al.*, “The microcircuits of striatum in silico,” *Proceedings of the National Academy of Sciences of the United States of America*, vol. 117, no. 17, pp. 9554–9565, 2020, doi: 10.1073/pnas.2000671117.

[128] P. Gleeson *et al.*, “NeuroML: A language for describing data driven models of neurons and networks with a high degree of biological detail,” *PLoS Computational Biology*, vol. 6, no. 6, pp. 1–19, 2010, doi: 10.1371/journal.pcbi.1000815.

[129] I. Raikov, “NineML – a description language for spiking neuron network modeling: the abstraction layer,” *BMC Neuroscience*, vol. 11, no. S1, p. 2202, 2010, doi: 10.1186/1471-2202-11-s1-p66.

[130] A. P. Davison *et al.*, “PyNN: A common interface for neuronal network simulators,” *Frontiers in Neuroinformatics*, vol. 2, no. 11, pp. 1–10, 2009, doi: 10.3389/neuro.11.011.2008.

[131] K. Dai *et al.*, “The SONATA Data Format for Efficient Description of Large-Scale Network Models,” *PLoS Computational Biology*, vol. 16, pp. 1–24, 2019, doi: 10.2139/ssrn.3387685.

[132] M. Stimberg, R. Brette, and D. F. M. Goodman, “Brian 2, an intuitive and efficient neural simulator,” *eLife*, vol. 8, pp. 1–41, 2019, doi: 10.7554/eLife.47314.

DOI:10.15774/PPKE.ITK.2022.001

Appendix

Example of running the SomaticFeaturesTest of HippoUnit using a Jupyter notebook

As the first step HippoUnit's test classes and `ModelLoader` class, along with a few additional Python packages must be imported:

```
1.  from __future__ import print_function #needed only in Python 2
2.  % matplotlib inline
3.
4.  from hippounit.utils import ModelLoader
5.  from hippounit import tests
6.
7.  import pkg_resources
8.  import json
9.  import collections
10. import numpy
```

Then the path to external mechanisms used by the Neuron implementation of the model (NMODL files) needs to be provided, which will be an argument to the `ModelLoader` class, so that the NMODL files can be compiled when the `ModelLoader` class is instantiated (if they are not compiled yet). Next, the variables related to the model are set. The initial voltage (`v_init`) and temperature (`celsius`) values specific to the model need to be set; otherwise, the default value in the corresponding capability method of the `ModelLoader` will be used. Setting the `cvode_active` boolean parameter to `True` or `False`, the user can decide to run the simulations using variable or fixed time step, respectively.

```
# path to NMODL files
mod_files_path = "/home/saray/published_models/Ca1_Bianchi_2012/experiment/"

#all the outputs will be saved here. It will be an argument to the test.
base_directory = '/mnt/csoport31-2/Modellezo_csapat/Sara/published_models_validation_results/'

#Load cell model
model = ModelLoader(mod_files_path = mod_files_path )

# outputs will be saved in subfolders named like this:
model.name="Bianchi_et_al_2012"

# path to hoc file
# the model must not display any GUI!!
model.hocpath = "/home/saray/published_models/Ca1_Bianchi_2012/experiment/main_model.hoc"

# If the hoc file doesn't contain a template, this must be None (the default value is None)
model.template_name = None

# model.SomaSecList_name should be None, if there is no Section List in the model for the soma, or if the name of the soma section is given by setting model.soma (the default value is None)
model.SomaSecList_name = None
# if the soma is not in a section list or to use a specific somatic section, add its name here:
model.soma = 'soma[0]'

# For the PSP Attenuation Test, and Back-propagating AP Test a section list containing the trunk sections is needed
model.TrunkSecList_name = 'apical_trunk_list'
# For the Oblique Integration Test a section list containing the oblique dendritic sections is needed
model.ObliqueSecList_name = 'oblique_dendrites'
```

```
# This will be argument to those tests, where dendritic locations are selected according to distances. If not set, the end of the above given soma section will be used as reference point for distance determination
trunk_origin = ['soma[0]', 1]

model.v_init = -70
model.celsius = 34

# It is possible to run the simulations using variable time step (default for this is False)
model.cvode_active = True
```

The target experimental data and the configuration file are loaded from the JSON files to the *observation* and *config* dictionaries, which are arguments of the test class:

```
# Load target data
with open('/home/saray/target_features/feat_CA1_pyr_cACpyr_more_features.json') as f:
    observation  = json.load(f, object_pairs_hook=collections.OrderedDict)

# Load stimuli file
ttype = "CA1_pyr_cACpyr"

stim_file = pkg_resources.resource_filename("hippounit", "tests/stimuli/somafeat_stim/stim_" + ttype + ".json")
with open(stim_file, 'r') as f:
    config = json.load(f, object_pairs_hook=collections.OrderedDict)
```

Then the test class is instantiated, and its `judge()` function (inherited from SciUnit) is called to run the test. The number of parallel processes to be used can be controlled by the user by setting the `test.npool` parameter.

```
# Instantiate test class
test = tests.SomaticFeaturesTest(observation=observation, config=config, force_run=False, show_plot=True, save_all = True, base_directory=base_directory)

# test.specify_data_set is added to the name of the subdirectory (somaticfeat), so test runs using different data sets can be saved into different directories
```

```
61. test.specify_data_set = 'UCL_data'
62.
63. # Number of parallel processes
64. test.npool = 30
65. #Run the test
66. score = test.judge(model)
67. #Summarize and print the score achieved by the model on the test using SciUnit's summa
    rize function
68. score.summarize()
```

For further details on how to run the different tests of HippoUnit for the different models, see the Jupyter Notebooks available here: https://github.com/KaliLab/HippoUnit_demo/tree/master/jupyter_notebooks.